

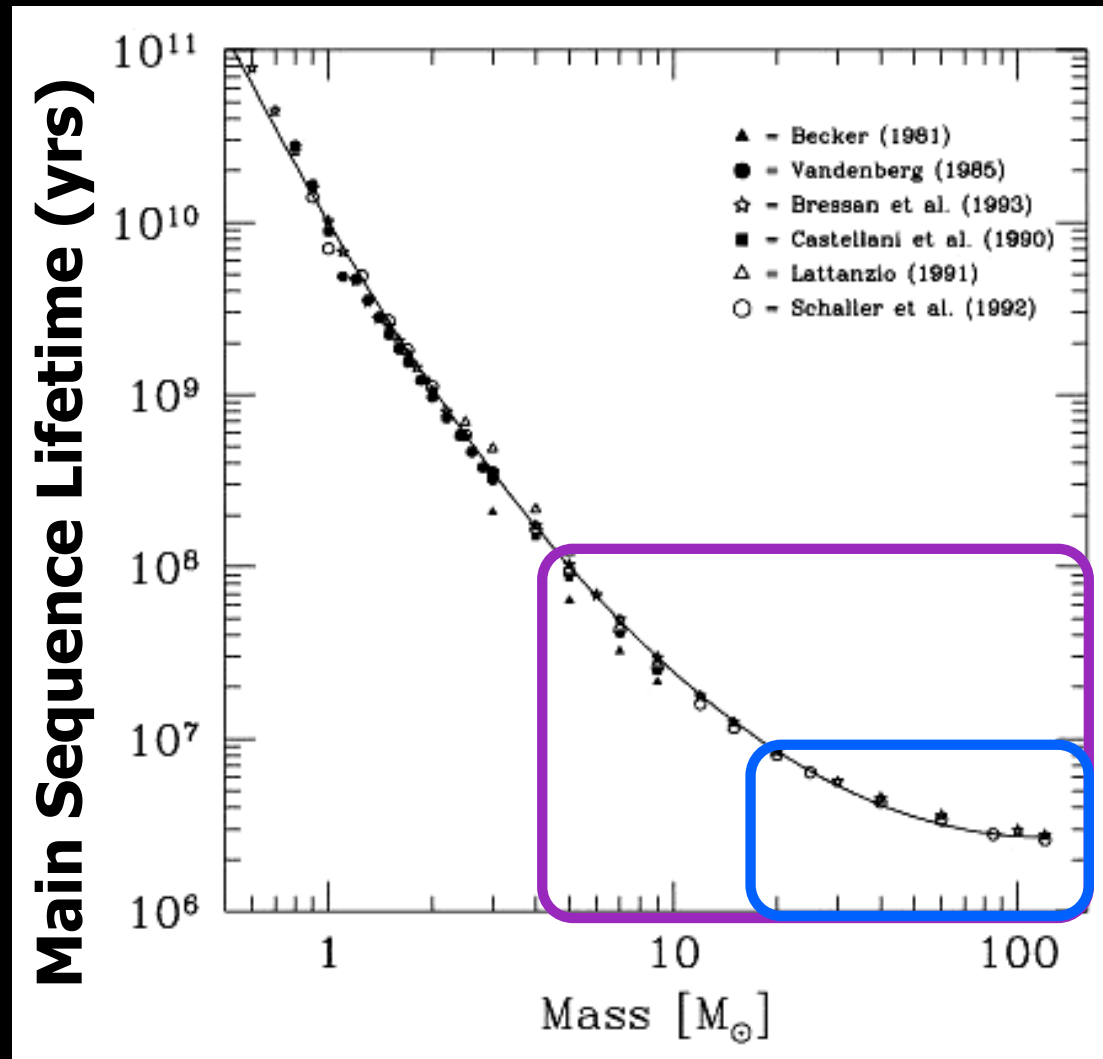
How do we infer star formation rates?

# Why is measuring SFR important?

- Converting gas into stars is a major evolutionary pathway
- SFR affects SN feedback, production of metals, state of the ISM, galaxy luminosity and color...basically everything!
- Should evolve with redshift
  - Need many indicators that work in different redshift regimes, and that can be checked against each other

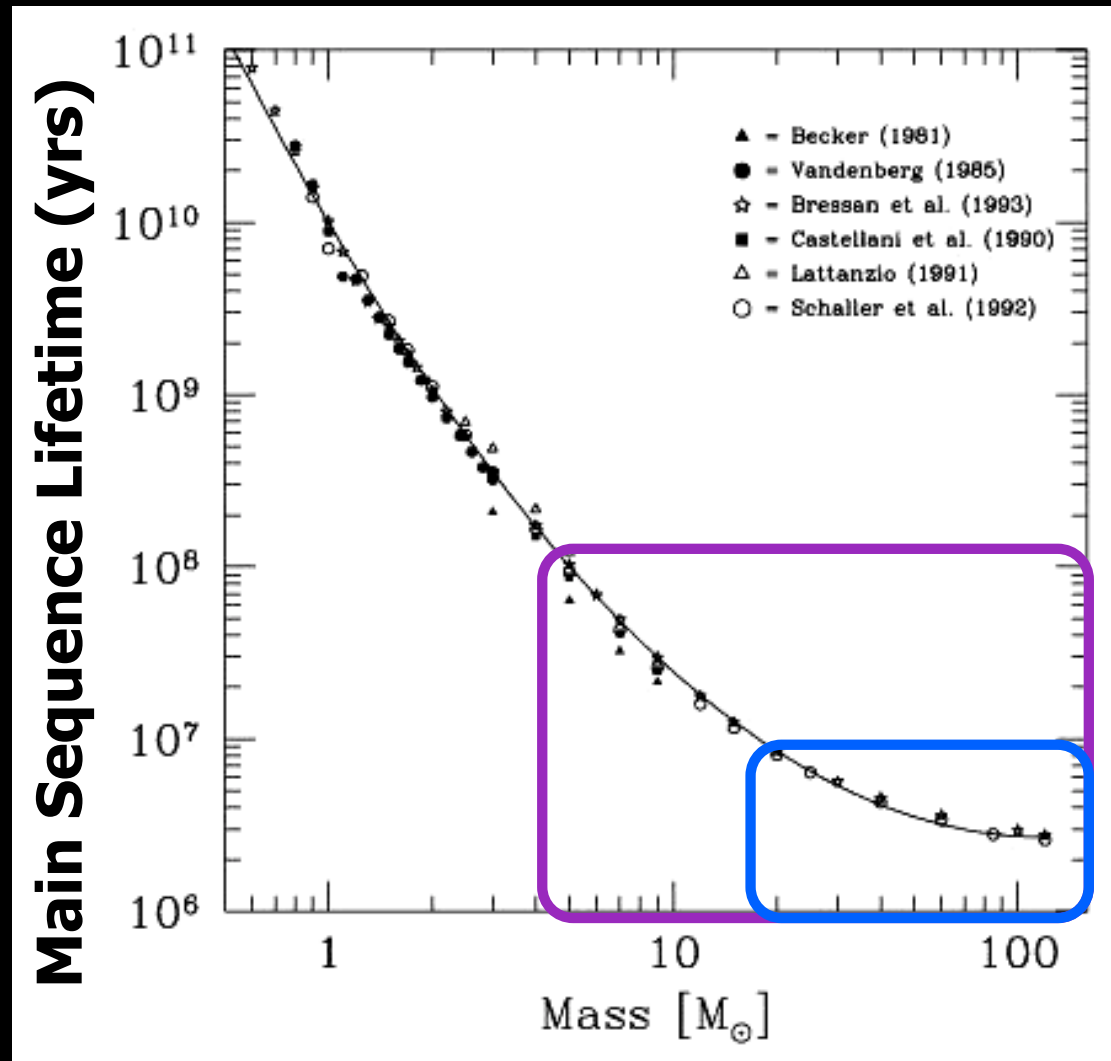
# Basic Principles

# Measuring the “instantaneous” SFR



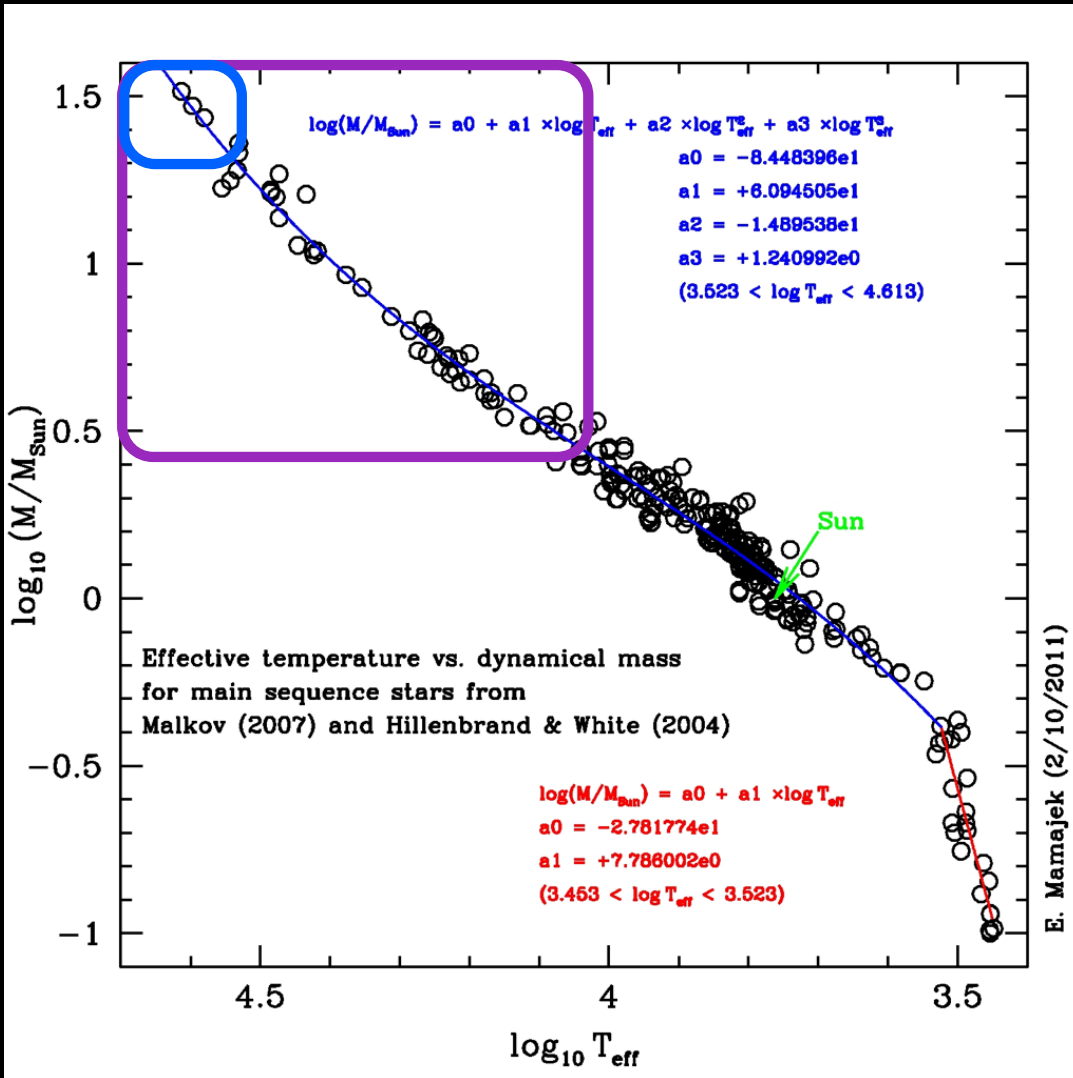
Define “instantaneous” to be <10-100 Myr

# Measuring the “instantaneous” SFR



Find tracers of  $>4-20 M_{\odot}$  (B & O) stars

# Measuring the “instantaneous” SFR



10-100Myr

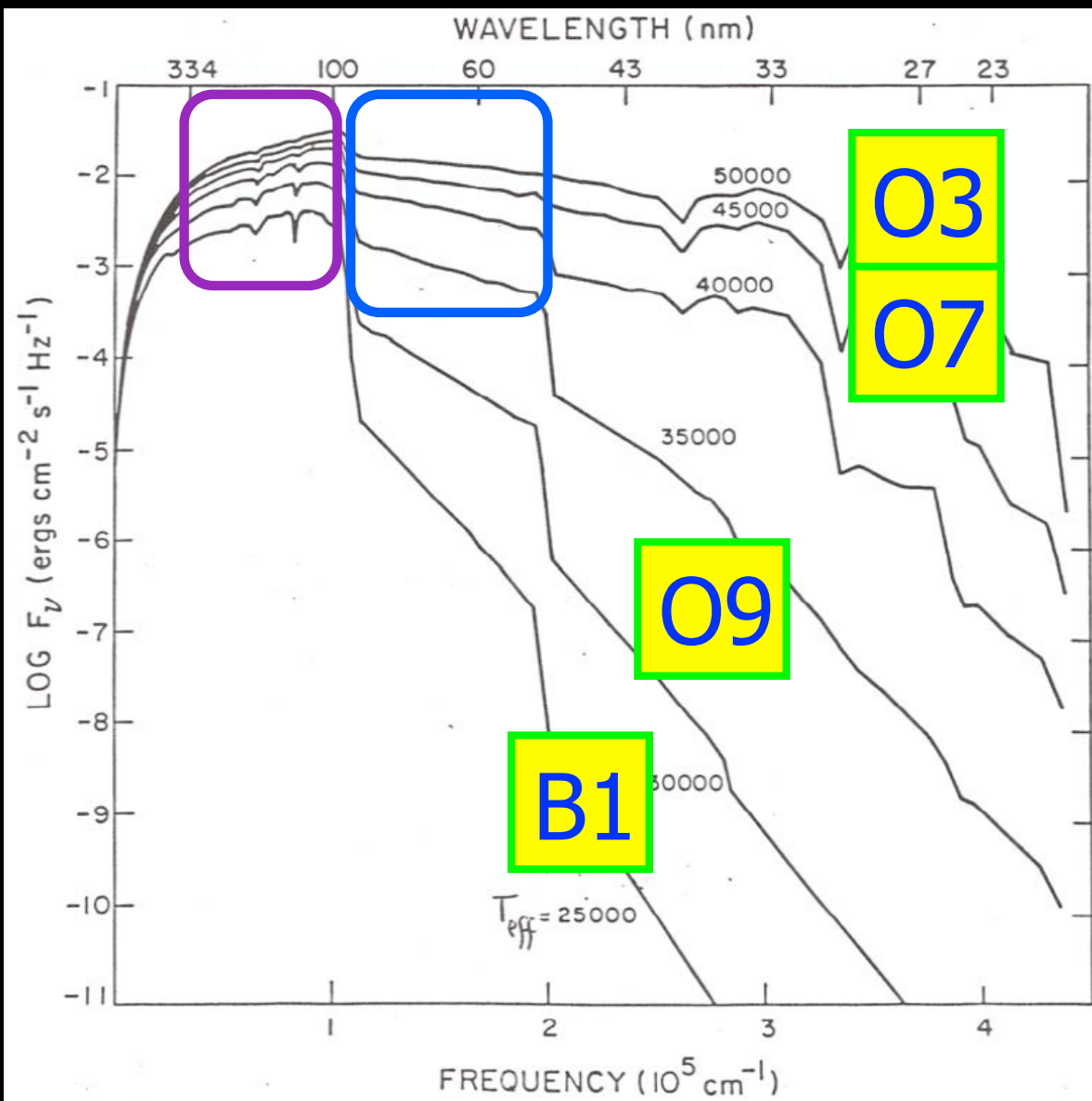
4-20  $M_{\odot}$

$T_{\text{eff}} > 11,000-35,000\text{K}$

# Signatures of >10,000-35,000K stars:

near- &  
far-UV  
flux

<100Myr



ionizing  
radiation

<10 Myr

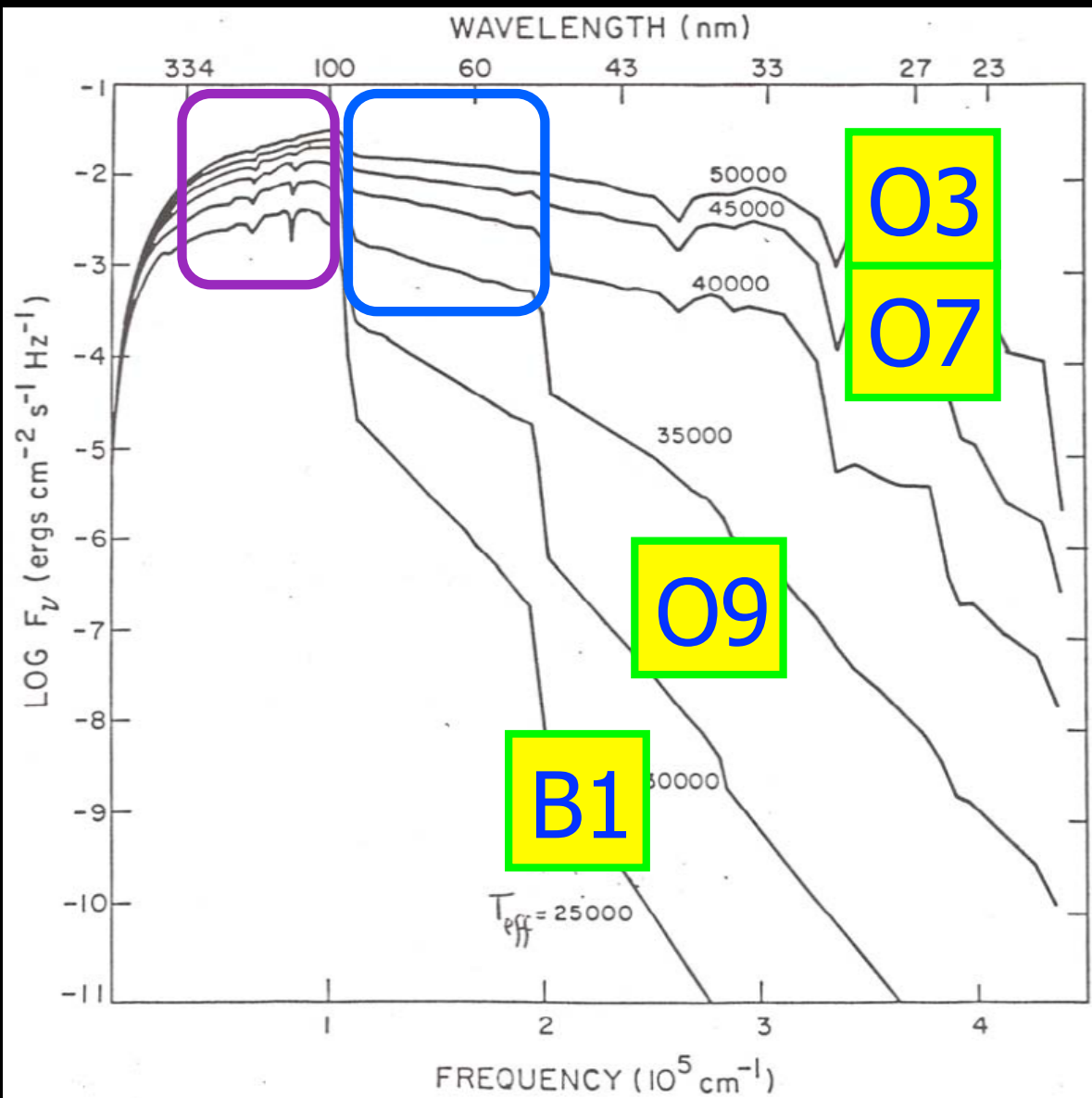
# Current SFR Tracers:

near- &  
far-UV  
flux

<100Myr

Ionizing  
radiation

<10 Myr



All amount to looking for UV flux or signs of ionized gas

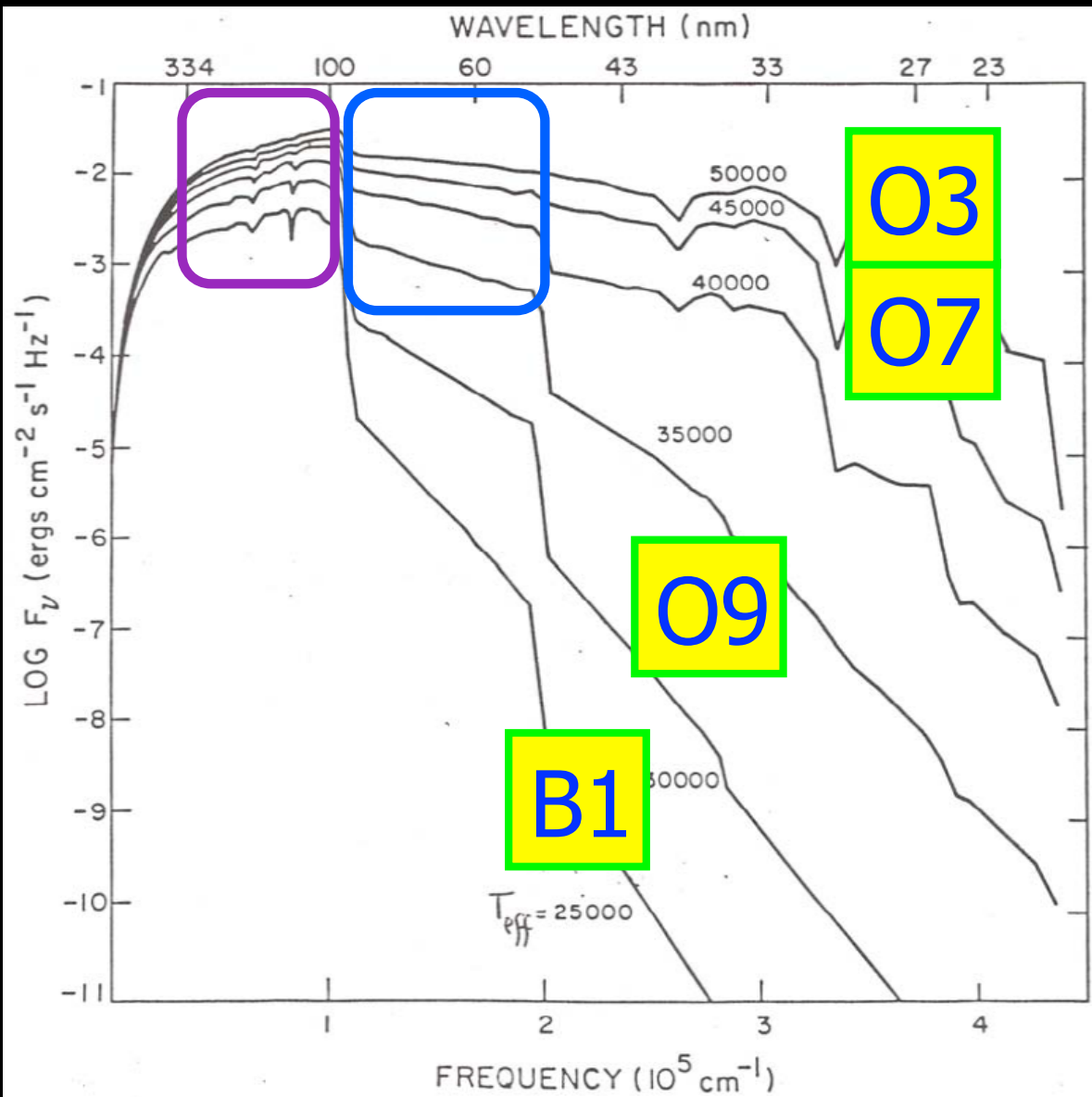
# Current SFR Tracers:

near- &  
far-UV  
flux

<100Myr

Ionizing  
radiation

<10 Myr



Rate of massive  
star production

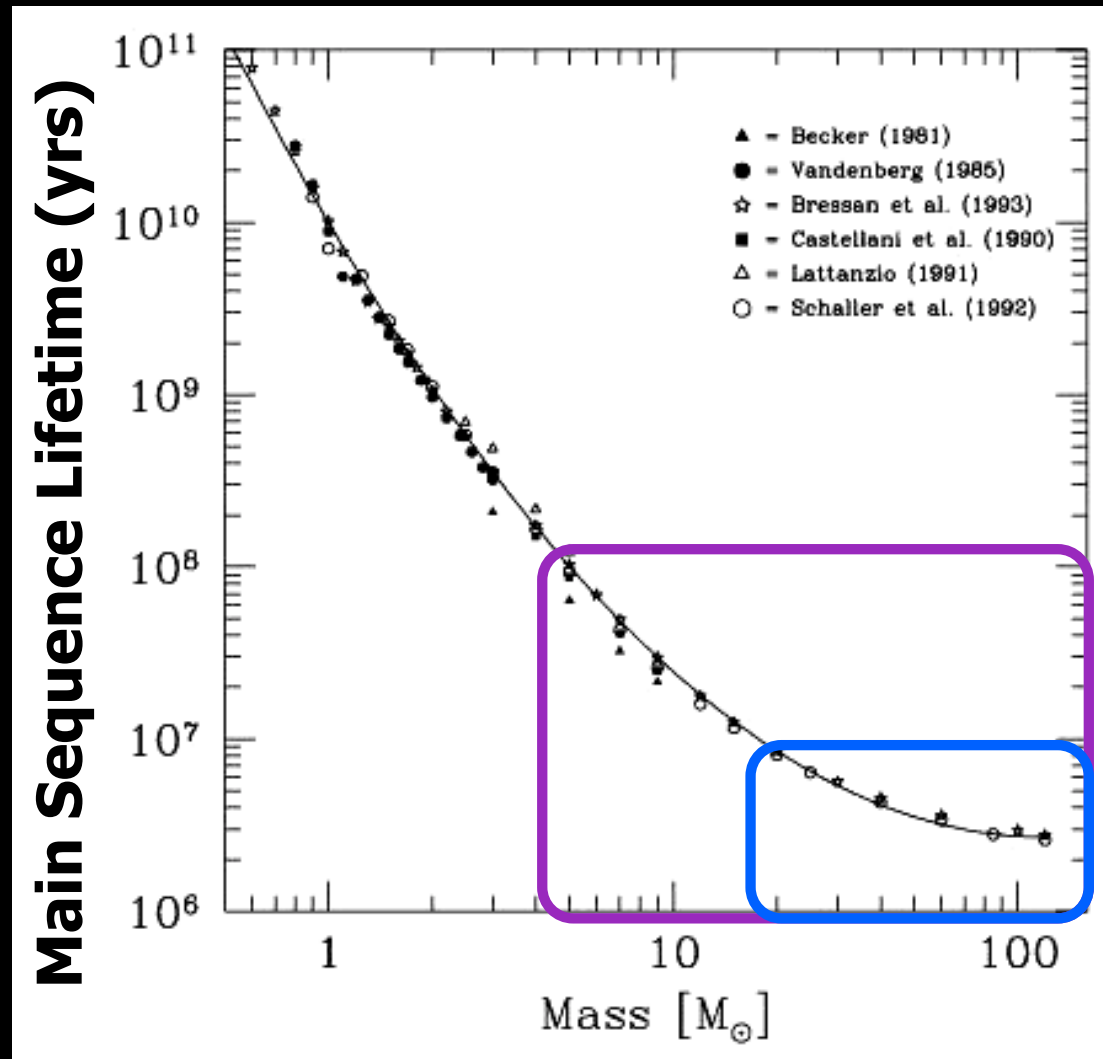
$$= \frac{\# \text{ of massive stars}}{\text{lifetime of massive stars}}$$

How do we link the presence of O & B stars to the *total* mass of young stars?

Rate of producing  
massive stars

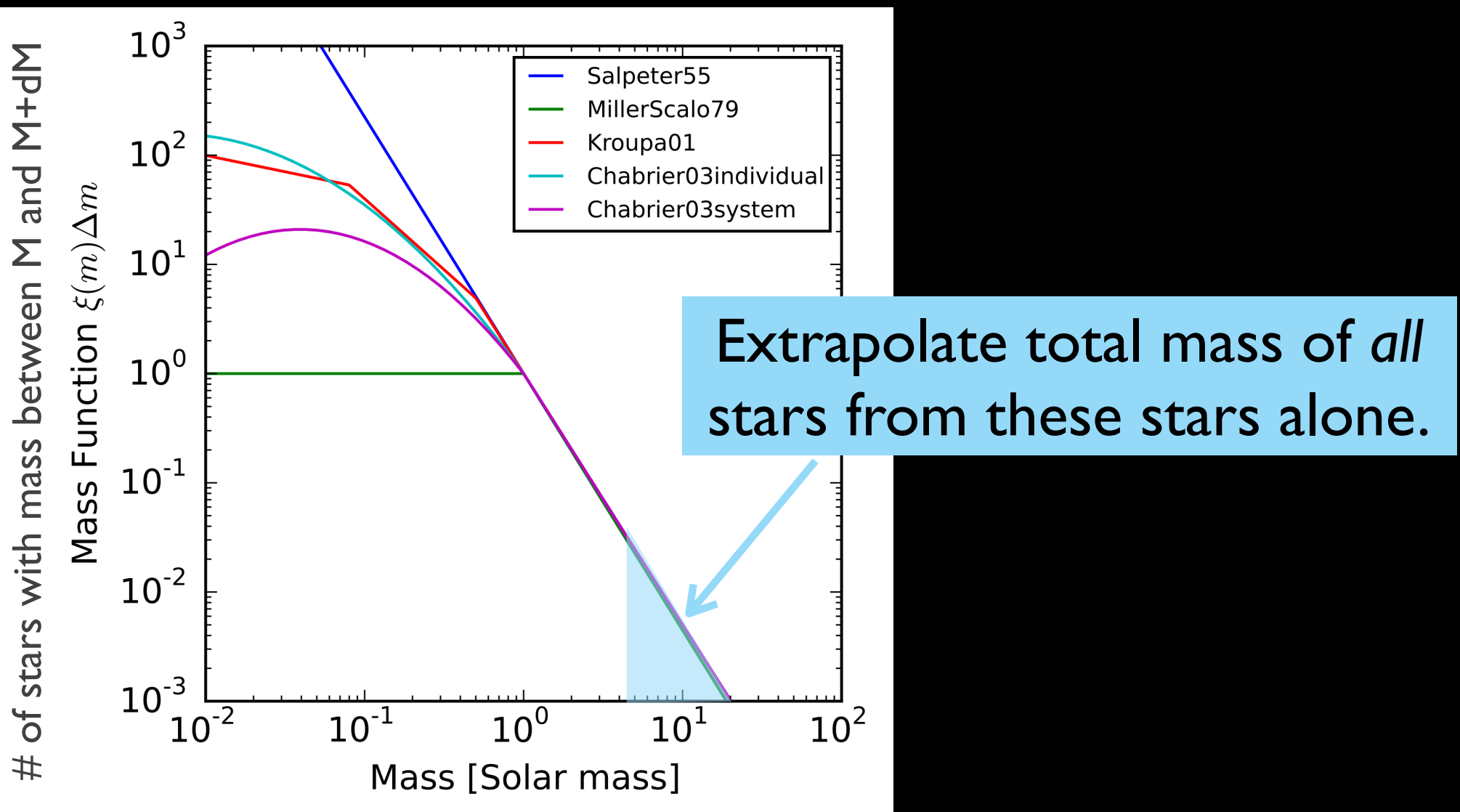
Rate of producing  
new stars

$\propto$



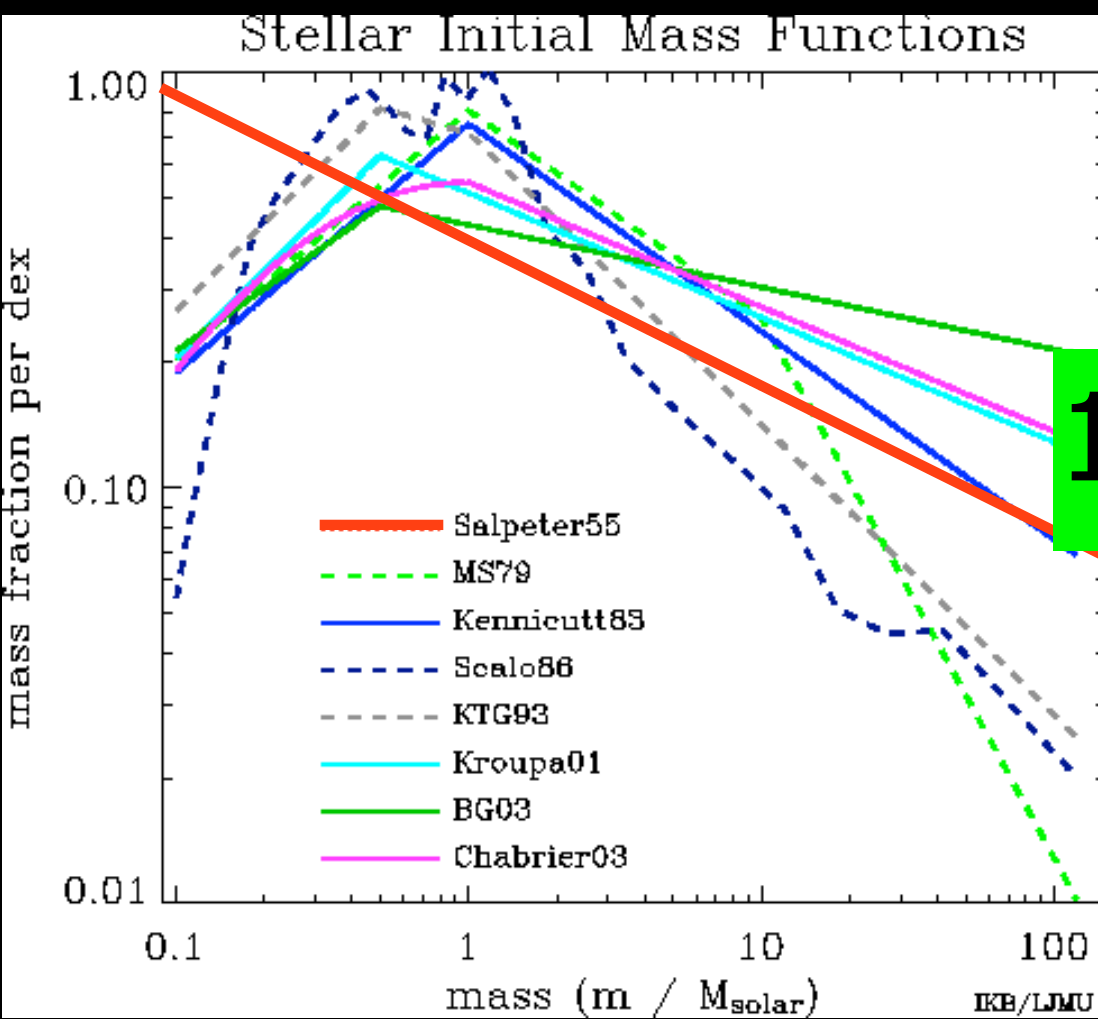
Extrapolate from high mass to *all* stellar masses

# The relative #'s of high and low mass stars is controlled by the “Initial Mass Function (IMF)”



# The Initial Mass Function (IMF):

$$\# \text{stars with } M \rightarrow M + dM = N_0 \xi(M) dM$$



where  $N_0$  sets the size of the burst, and the IMF  $\xi(M)$  is normalized such that

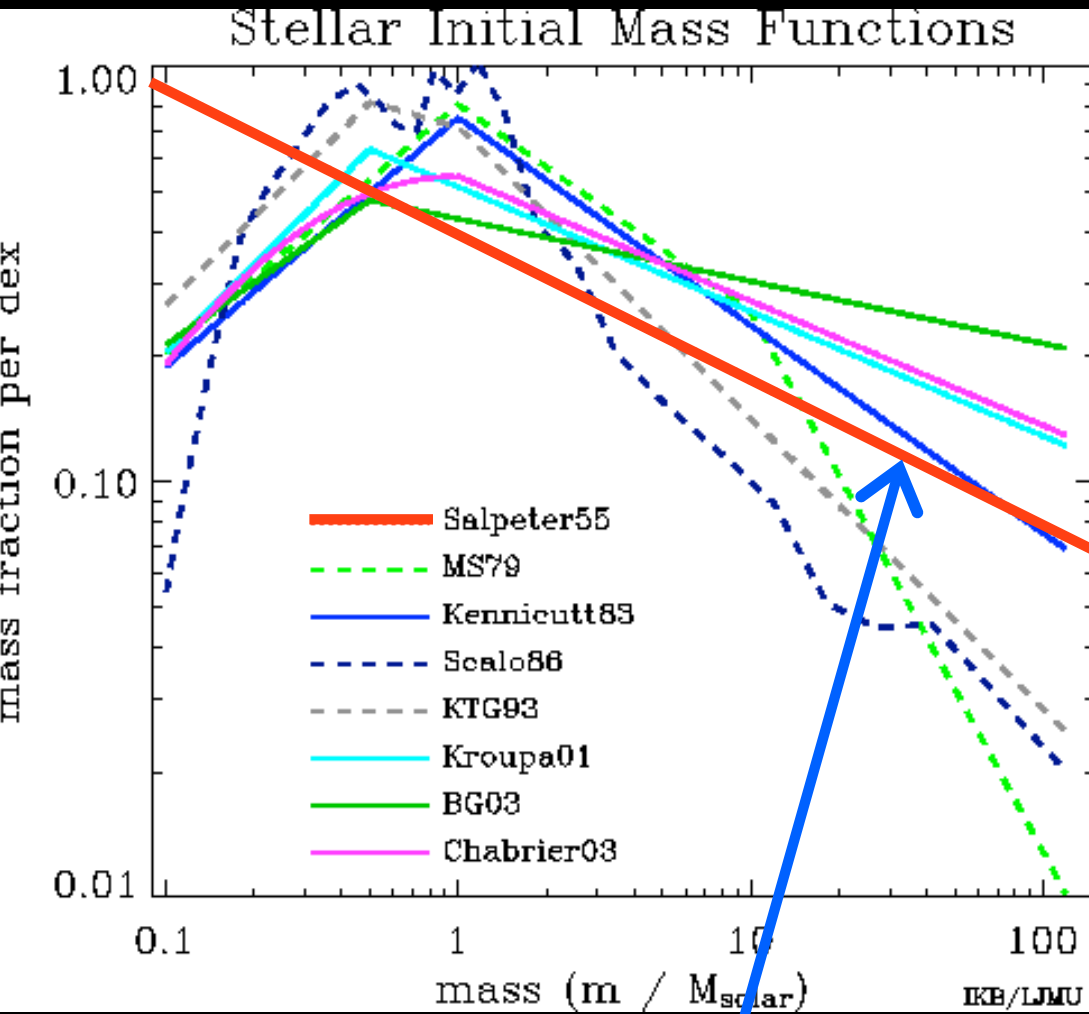
$$1M_{\odot} = \int M \xi(M) dM$$

or, so that  $\xi(M)$  is a probability distribution

KTG93=Kroupa et al 1993

MS79=Miller & Scalo 1979

BG03=Baldry & Glazebrook 2003



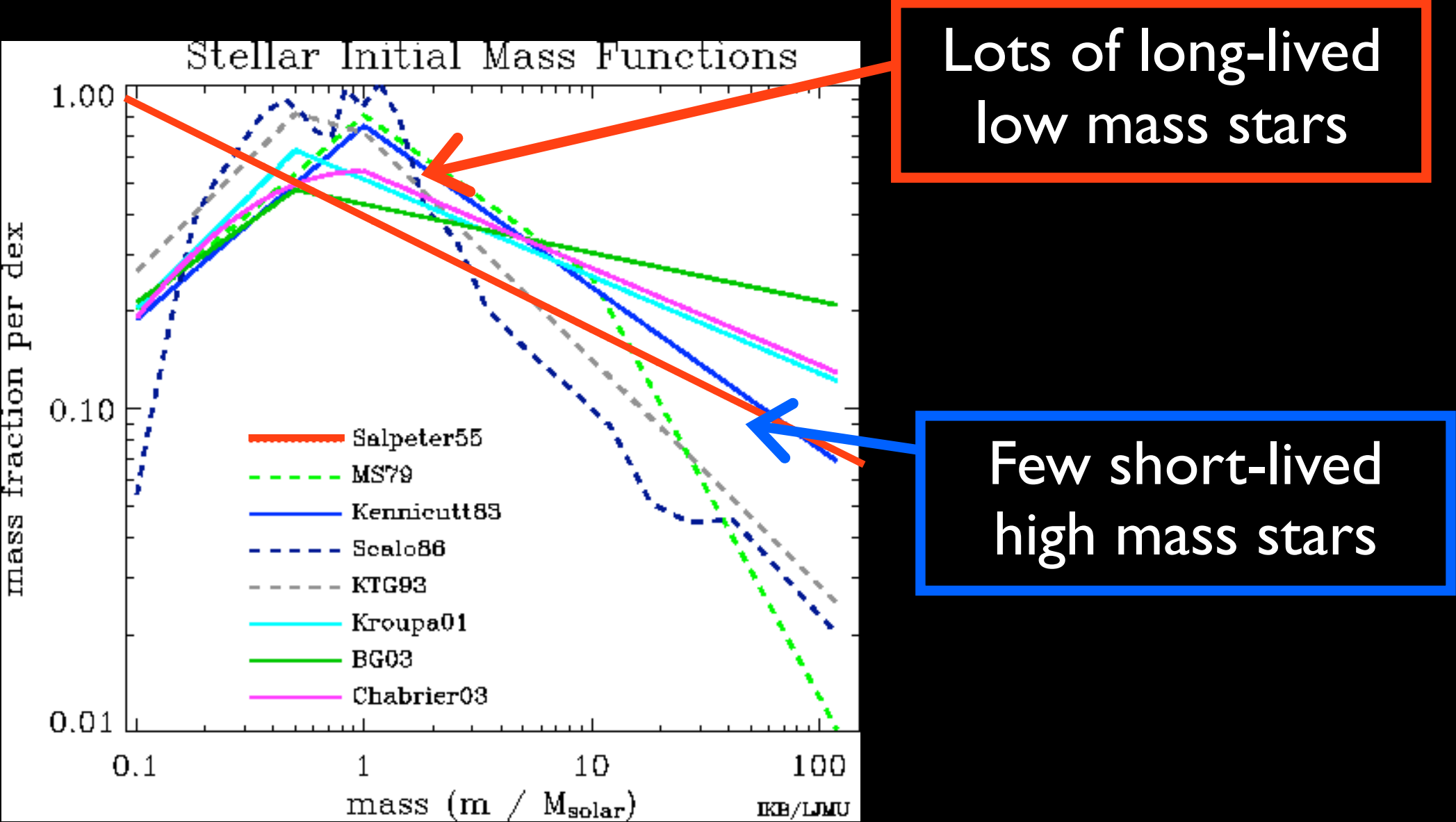
IMF is frequently approximated as a power law\*

$$\xi(M) \propto M^{-(1+x)}$$

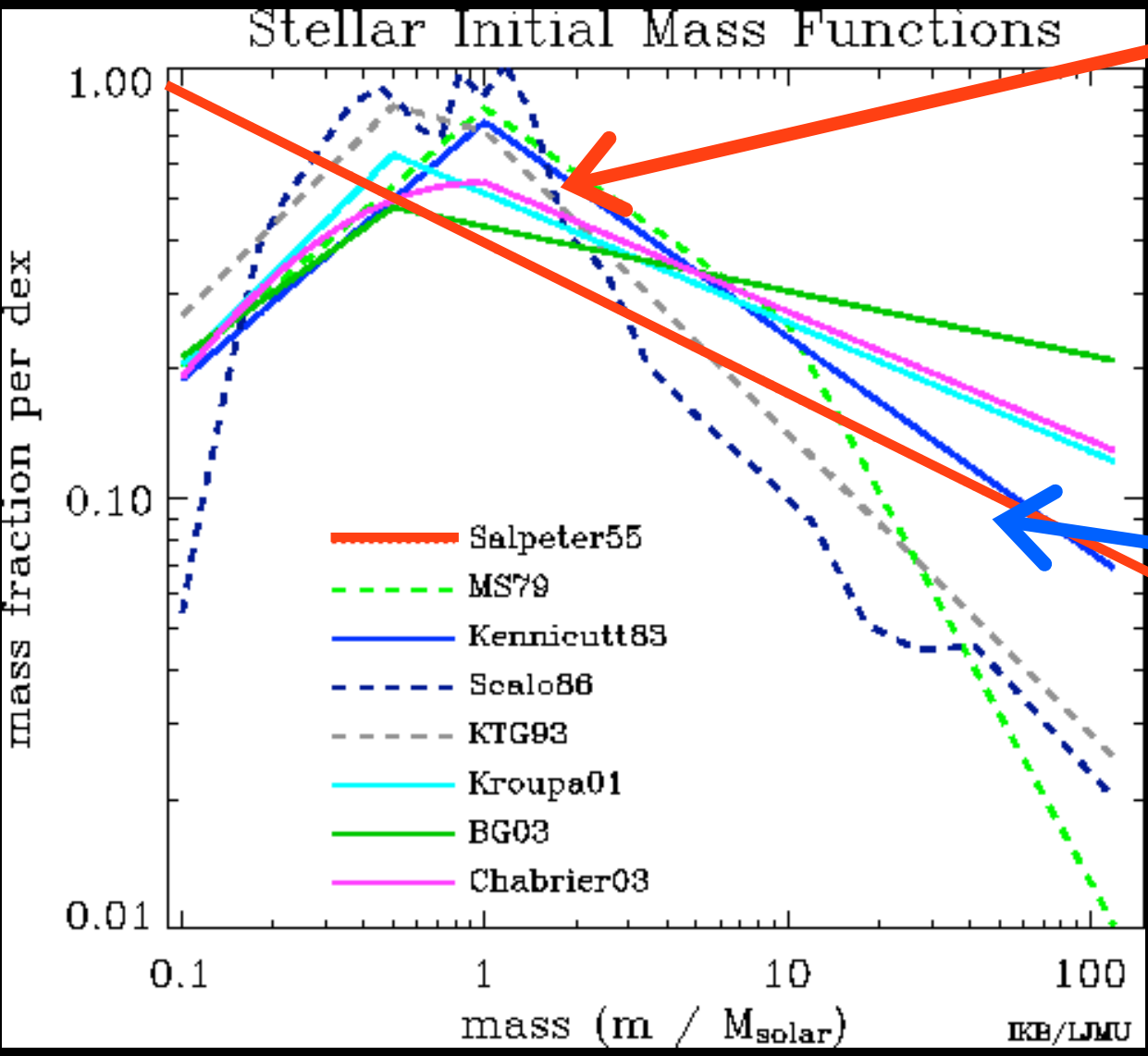
If  $x=1.35$ , you get the “Salpeter IMF”

\* Or as a series of “broken” power-laws over different mass ranges; See Maschberger for a proposed alternate form

# The Initial Mass Function (IMF):



# The Initial Mass Function (IMF):



Dominoes the stellar mass

$$M\xi(M) \propto M^{-1.35}$$

Dominoes the luminosity, UV, & ionizing output

$$L_M \propto M^{+3.5}$$

$$L\xi(M) \propto M^{+1.15}$$

# IMF variations for low mass stars

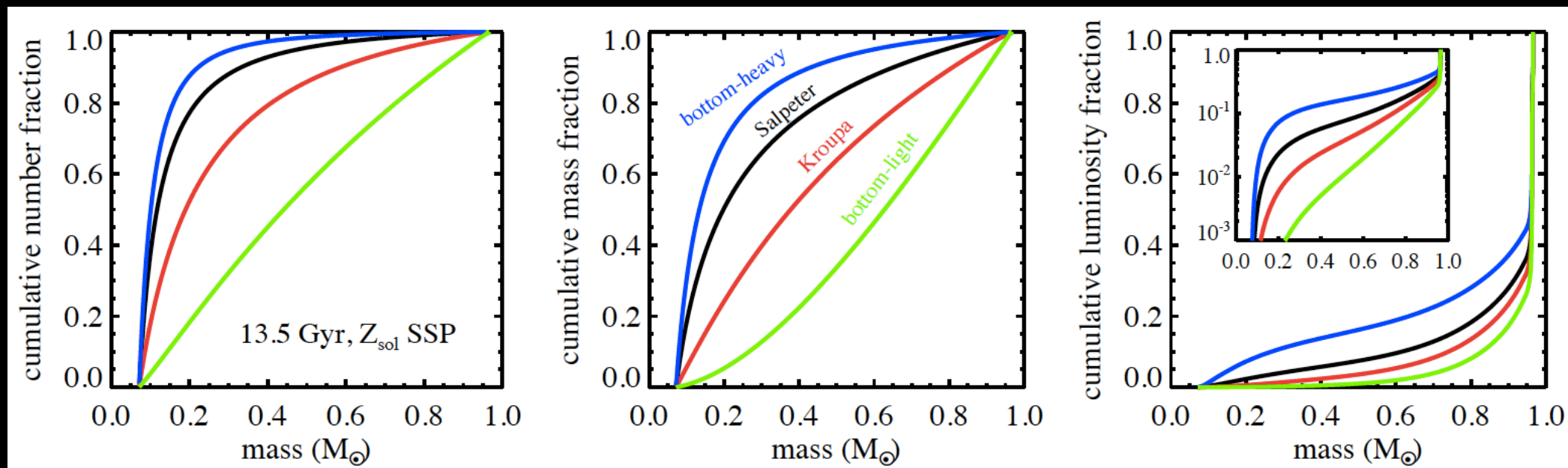
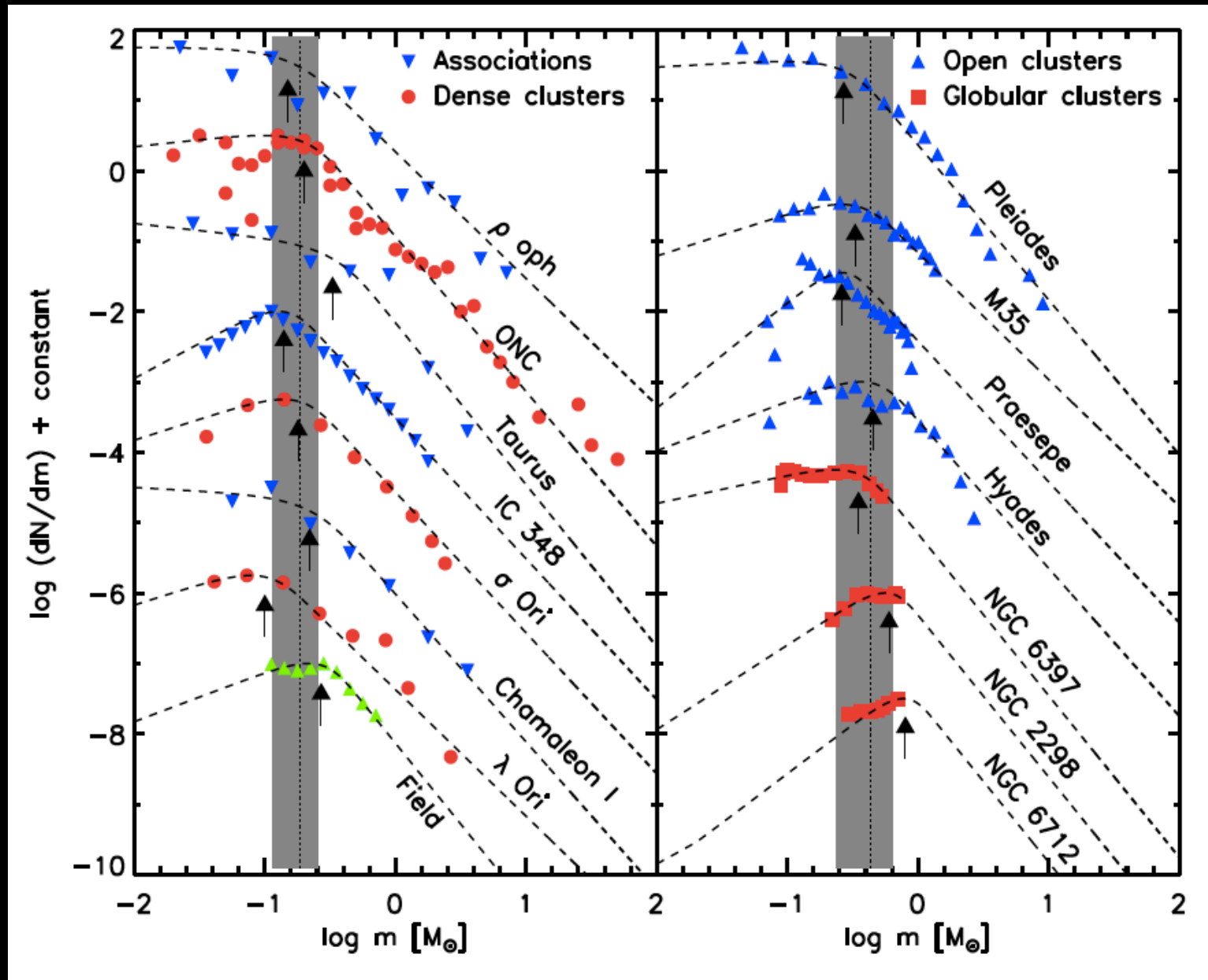


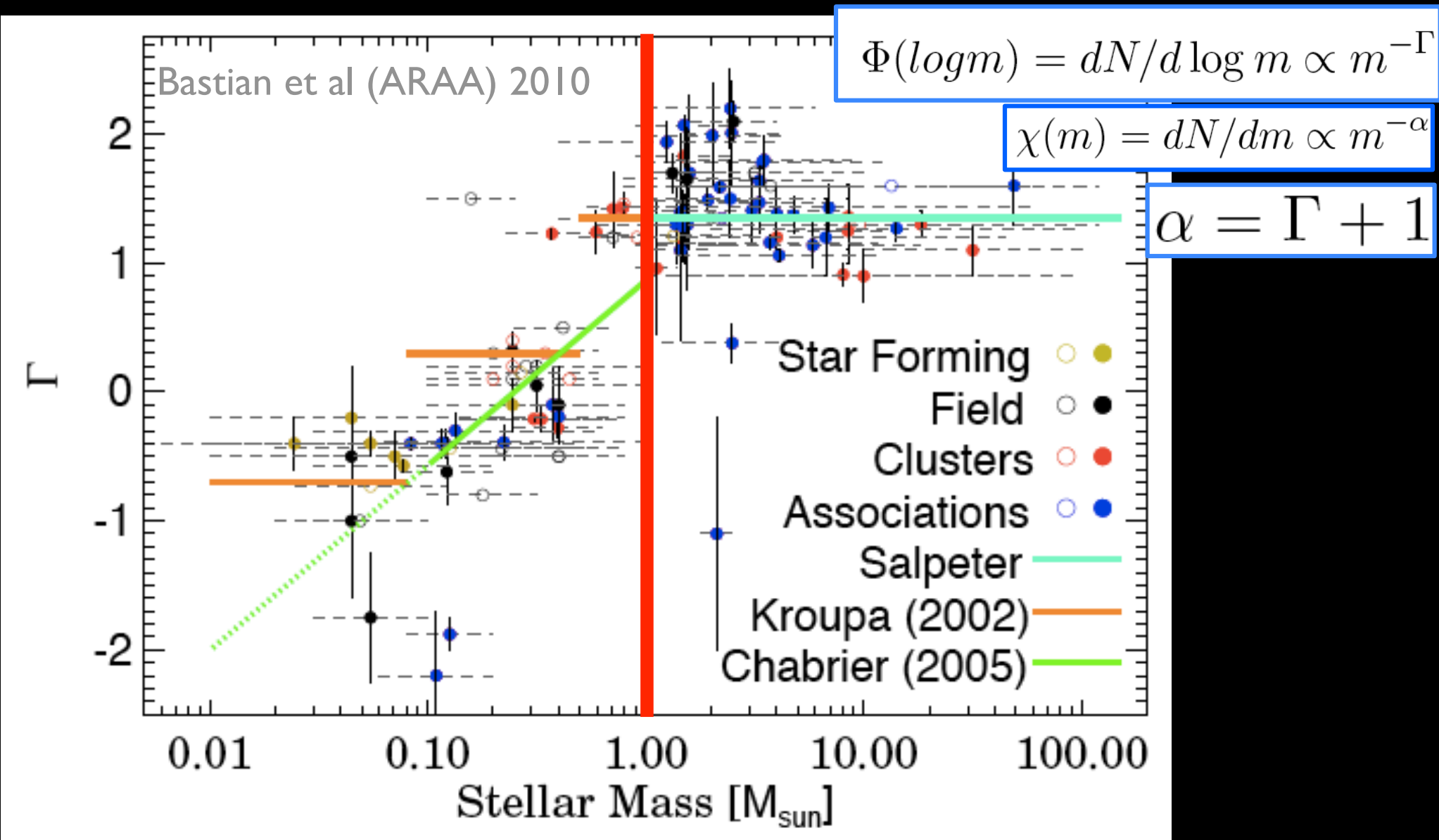
**Figure 4:**

Fractional contribution to the total number, mass, and bolometric luminosity as a function of stellar mass for a 13.5 Gyr solar metallicity model. Lines correspond to different IMFs: a bottom-heavy with logarithmic slope  $x = 3.0$  (blue line); Salpeter ( $x = 2.35$ ; black line); MW IMF (specifically a Kroupa IMF; red line); a bottom-light IMF (specifically of the form advocated by van Dokkum (2008); green line). The inset in the right panel shows the cumulative luminosity fraction in logarithmic units. Low mass stars dominate the total number and mass in stars, but contribute a tiny fraction of the luminosity of old stellar populations.

# Derived typically from stellar clusters

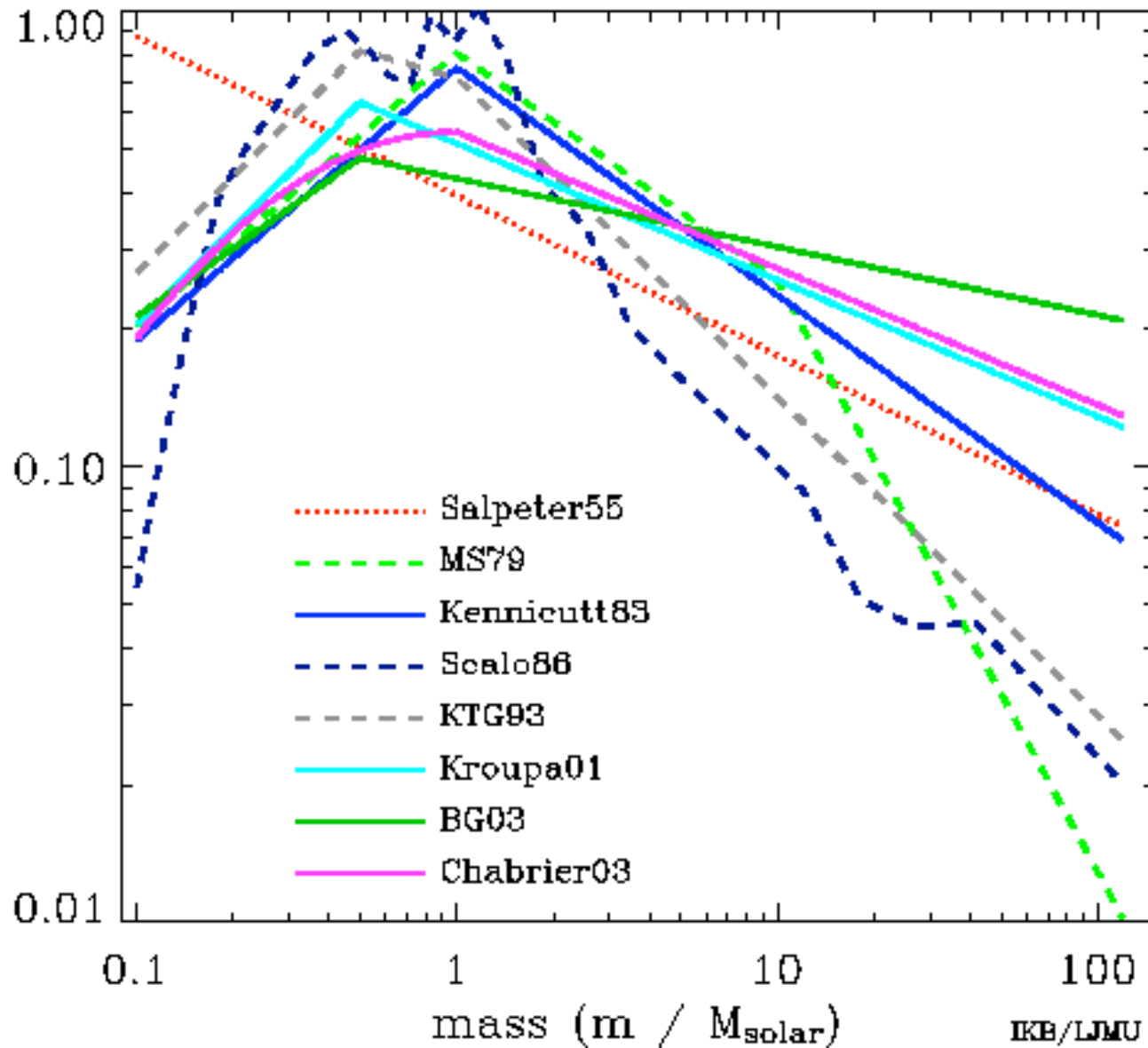


# Clear slope variations with mass



MW high-mass slope ( $> 1 M_{\odot}$ ) relatively constant

# Stellar Initial Mass Functions

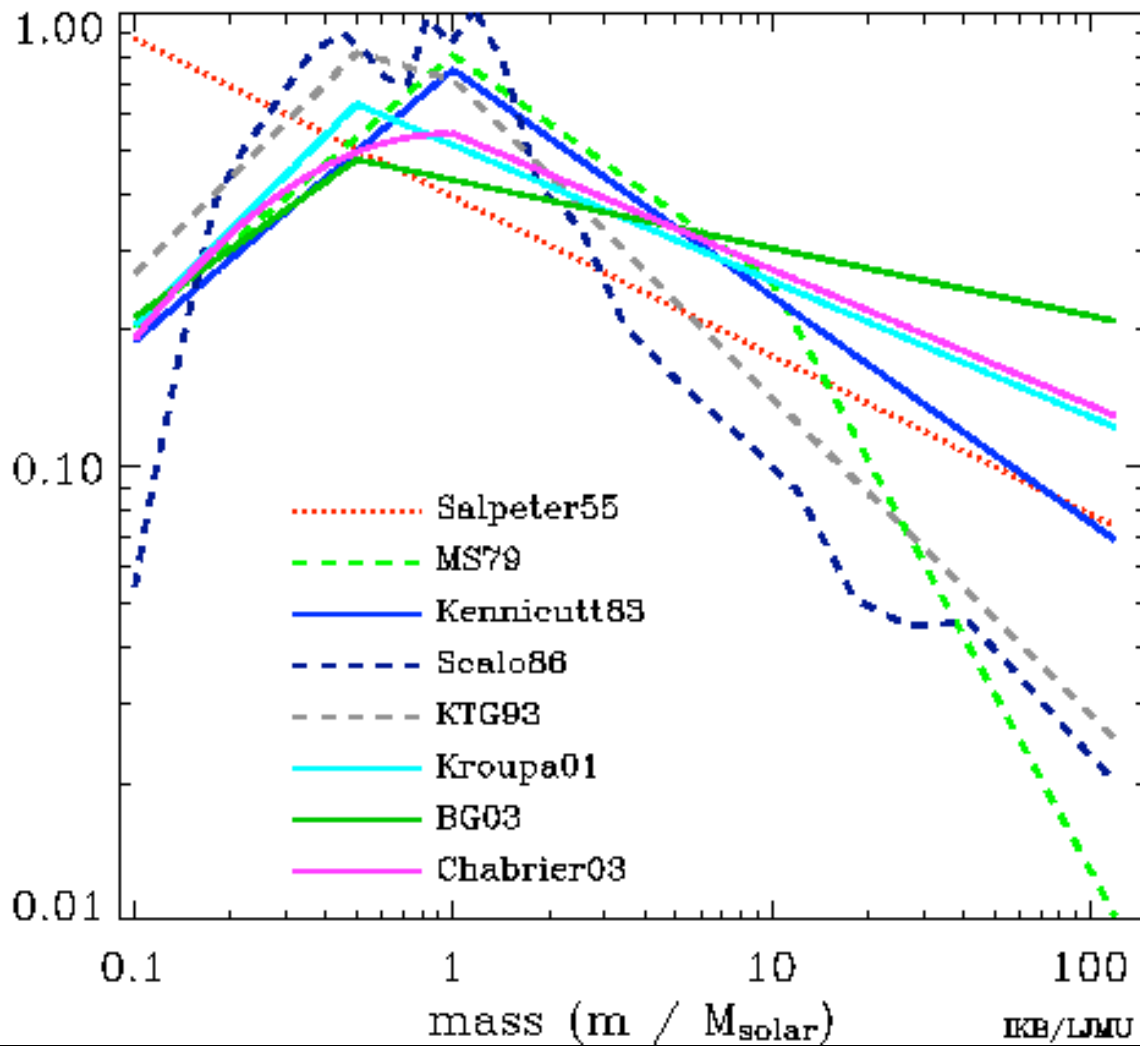


IMF propagates into nearly every aspect of extragalactic astronomy

- The Kennicutt, Kroupa01, BG03 and Chabrier IMFs are the best bet for reasonable mass-to-light ratios and galaxy colors (solid lines). The [BG03](#) analysis favoured a slope shallower than Salpeter at the high-mass end based on constraints from local luminosity densities and cosmic star-formation history; IMFs with high-mass slopes steeper than Kennicutt's were ruled out as a universal IMF.
- The Salpeter IMF has too many low mass stars (dotted line). It was never measured down to 0.1 solar masses by Salpeter.
- The MS79, Scalo and KTG93 IMFs have too few high mass stars (dashed lines). They were based on galactic disk measurements which cannot be used to accurately infer the high-mass end because of the complicated SFH of the galaxy. Measured IMFs within star clusters generally give a shallower IMF close to the Salpeter value. [Elmegreen '06](#) finds that galaxy-averaged IMFs are not in general steeper than this.

## Stellar Initial Mass Functions

Mass fraction per dex

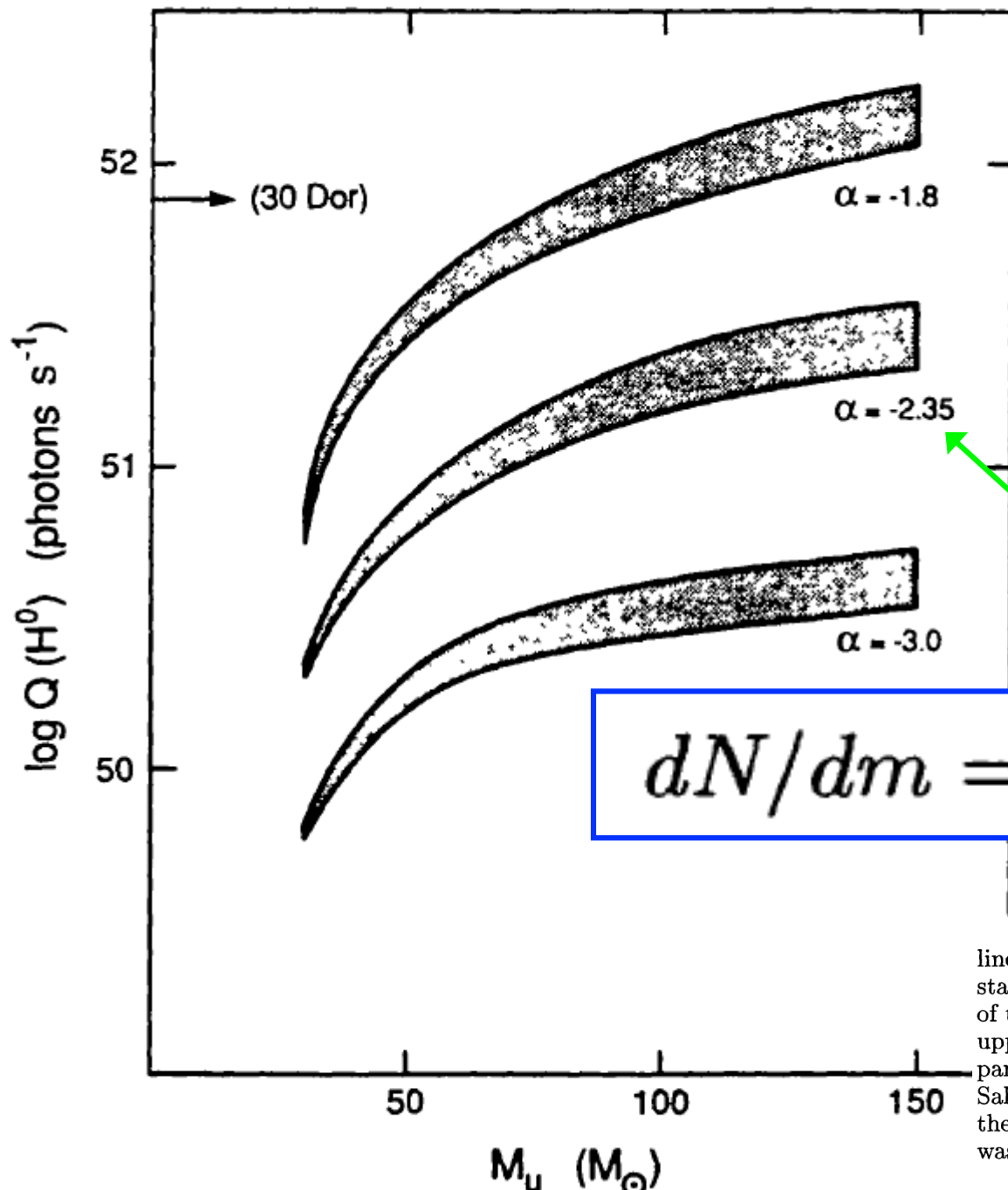


# The high-mass IMF slope has particularly large effects

- Metal production
- SN rates
- SN feedback
- Ionizing flux

- The Kennicutt, Kroupa01, BG03 and Chabrier IMFs are the best bet for reasonable mass-to-light ratios and galaxy colors (solid lines). The [BG03](#) analysis favoured a slope shallower than Salpeter at the high-mass end based on constraints from local luminosity densities and cosmic star-formation history; IMFs with high-mass slopes steeper than Kennicutt's were ruled out as a universal IMF.
- The Salpeter IMF has too many low mass stars (dotted line). It was never measured down to 0.1 solar masses by Salpeter.
- The MS79, Scalo and KTG93 IMFs have too few high mass stars (dashed lines). They were based on galactic disk measurements which cannot be used to accurately infer the high-mass end because of the complicated SFH of the galaxy. Measured IMFs within star clusters generally give a shallower IMF close to the Salpeter value. [Elmegreen '06](#) finds that galaxy-averaged IMFs are not in general steeper than this.

# Ionizing UV flux vs slope of high- mass IMF



$$dN/dm = a m^{-\gamma}$$

$$\gamma = 2.35$$

This sensitivity is most severe for SFRs based on nebular recombination lines such as H $\alpha$ , because the ionization of galaxies is dominated by very massive stars ( $>10 M_\odot$ ). This is illustrated in Figure 1, which shows the dependence of the ionizing flux for a fixed-mass star cluster on both IMF slope ( $\alpha$ ) and the upper mass limit ( $M_u$ ), from Kennicutt & Chu (1988). The IMF in this case is parametrized as a single power-law with slope  $\alpha = dN(m)/dm$  ( $\alpha = -2.35$  for a Salpeter function). The shading in each model indicates the effect of changing the age spread of the stars in the cluster. A fixed lower mass limit of  $0.1 M_\odot$  was assumed in the calculations.

Figure 1. Initial ionizing luminosity for a star cluster with fixed mass (luminosity  $M_V = -9$  at age 100 Myr), as functions of the IMF slope  $\alpha$  and upper mass limit  $M_u$ , from Kennicutt & Chu (1988).

Kennicutt IMF  
Review 1998

# IMF Questions

- What is the IMF?
- Is the IMF universal or does it depend on environment and conditions in the molecular cloud?
- What physics sets the IMF?
- Why is there a power-law slope at high masses?
- Why is there a roll-over at low masses?
- Do different types of galaxies have different characteristic IMFs?

How do we constrain the #'s of massive stars?

## “Direct” vs “Indirect”

Effectively “counts” massive stars through their flux or their #’s

Correlates with the presence of massive stars, but needs to be calibrated to get relation between observed flux and # of massive stars

Most direct method:  
Recombination lines

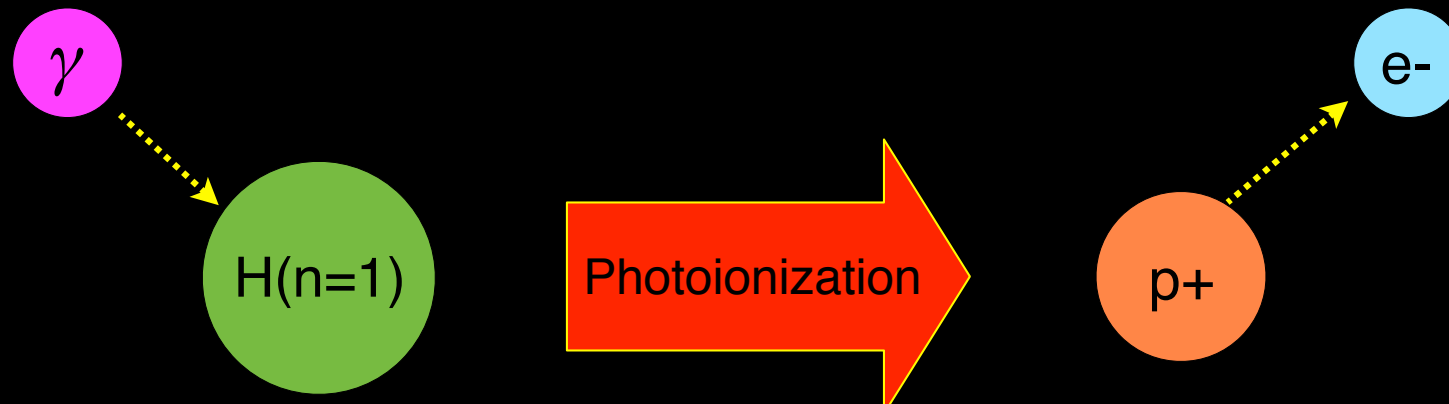
# Ionized gas implies massive young stars



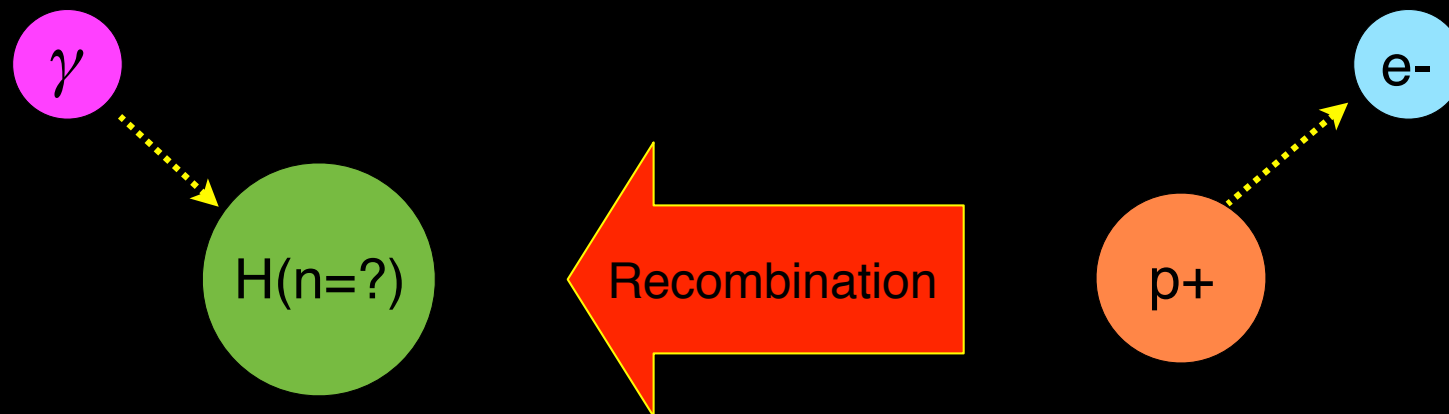
Orion Nebula

Ionized gas always produces strong, easily recognizable  
“recombination radiation”

# Massive stars' photons ionize hydrogen...

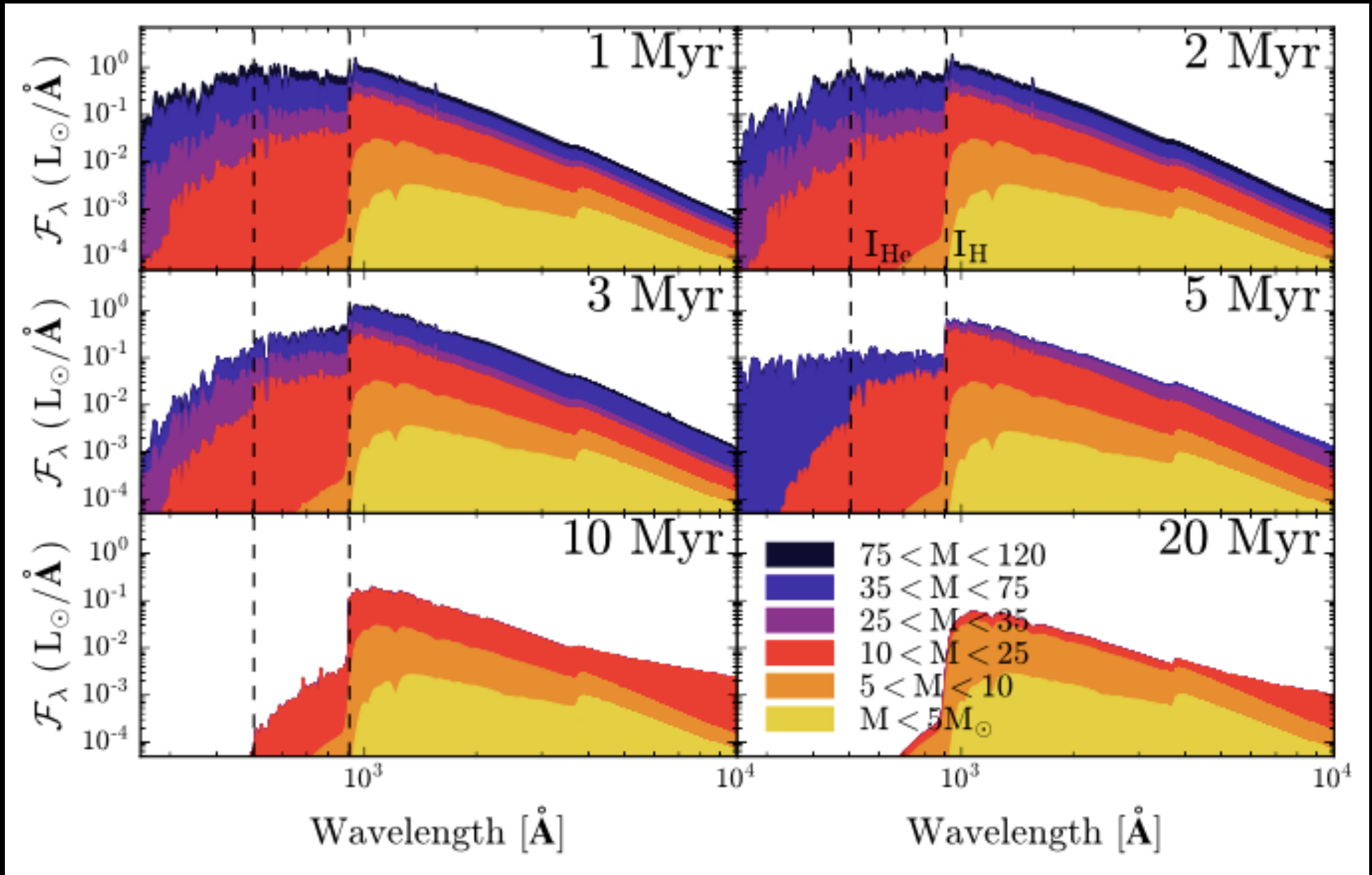


...which recombines temporarily, releasing photons

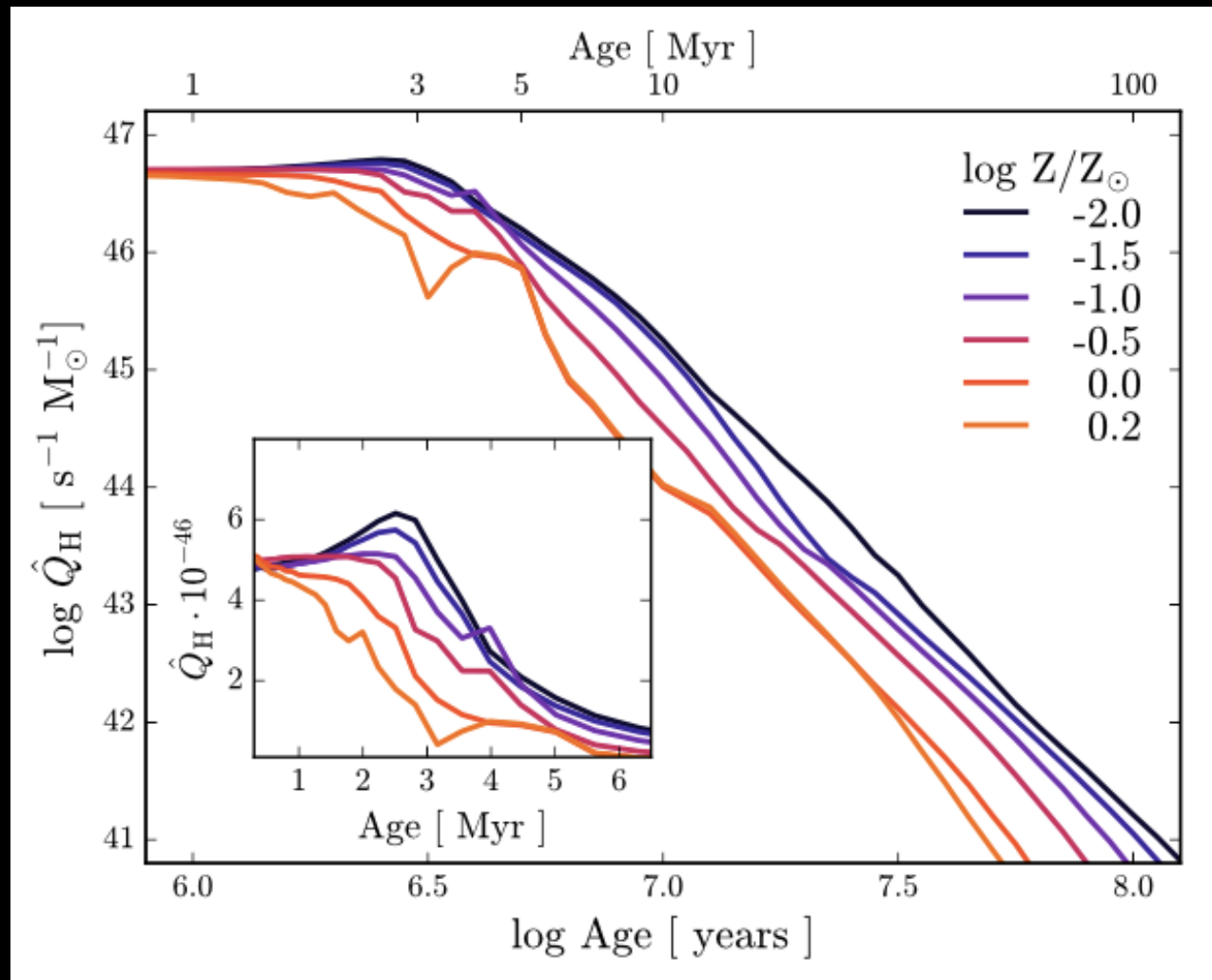


In steady state, the rates in both directions are equal, so measuring recombination rate gives the photoionization rate.

# Time scales & sources of ionizing flux



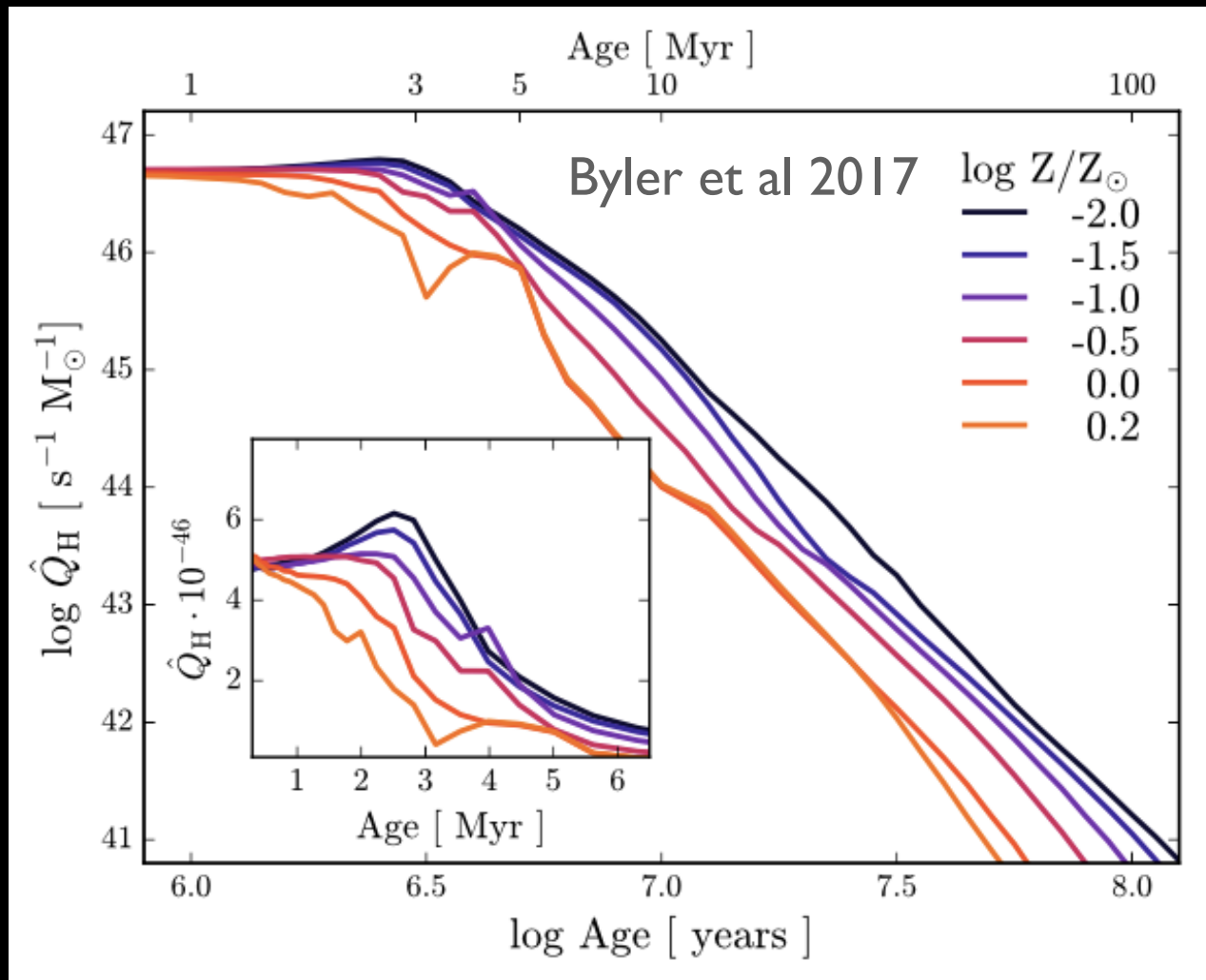
# Ionizing photon production down by $\times 10$ within $\sim 7$ Myr after a burst



Recombination lines: very recent SF

# Calibrating recombination lines as a SFR indicator

$Q_H$  is  
typical  
notation  
for  
ionizing  
photon  
rate



Use stellar population synthesis to calculate rate of  
ionizing photon production, assuming *constant* SFR

# Recombination Lines as SFR Tracers

## Advantages

- ✓ Directly traces the numbers of ionizing photons
- ✓ Effectively “counts” emission from O-stars in a physically motivated, calculable way
- ✓ Short, near “instantaneous” timescales

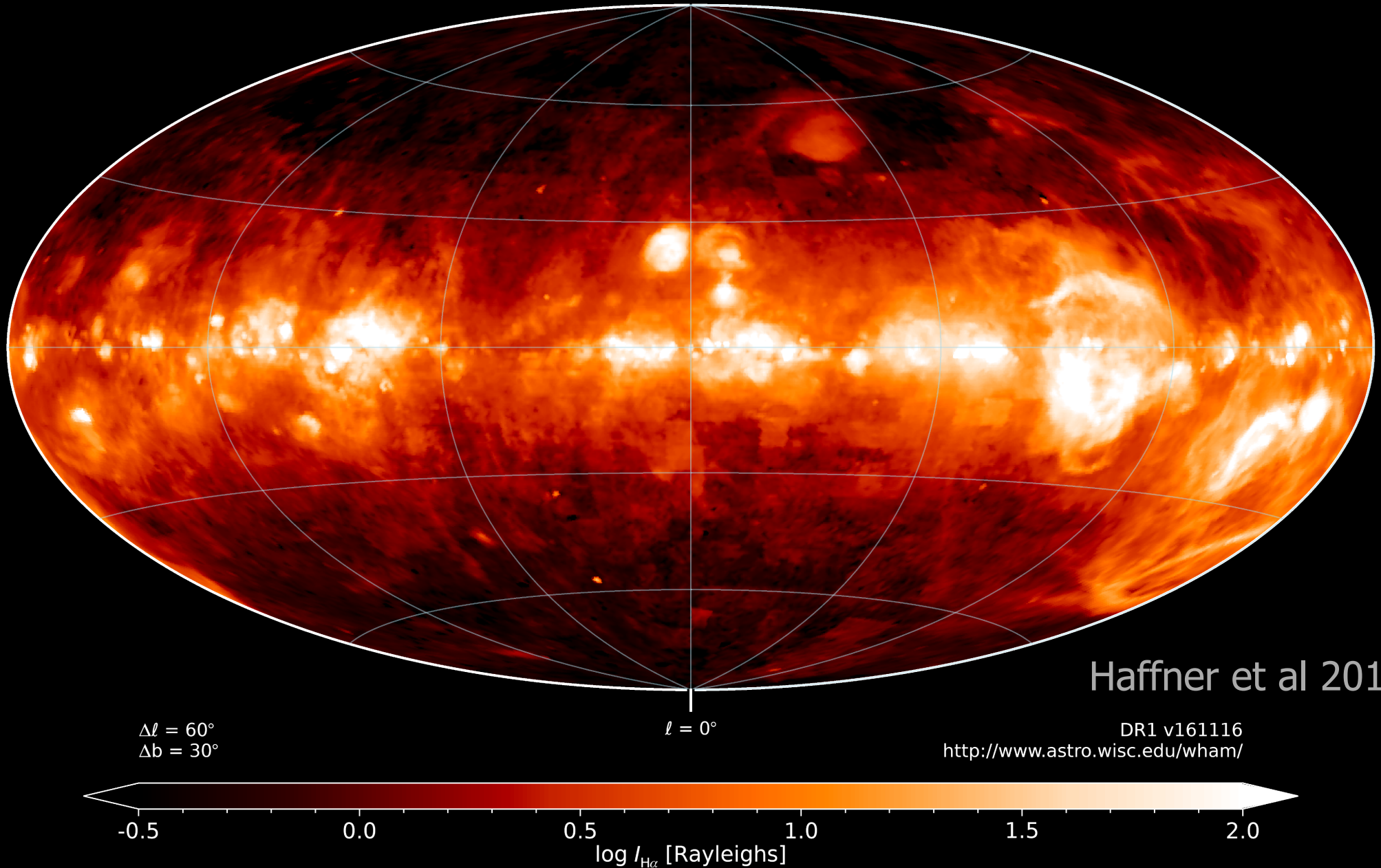
# Recombination Lines as SFR Tracers

## Possible Concerns

- Ly $\alpha$  may have issues with being resonance line...
- May not be photoionized by O-stars. Can have contributions from other sources of ionization (i.e., AGN, shocks)
- O stars are rare so low mass SF regions can be without (i.e., “stochasticity”)
- “Leakage” — not every ionizing photon may actually ionize gas *within* the galaxy

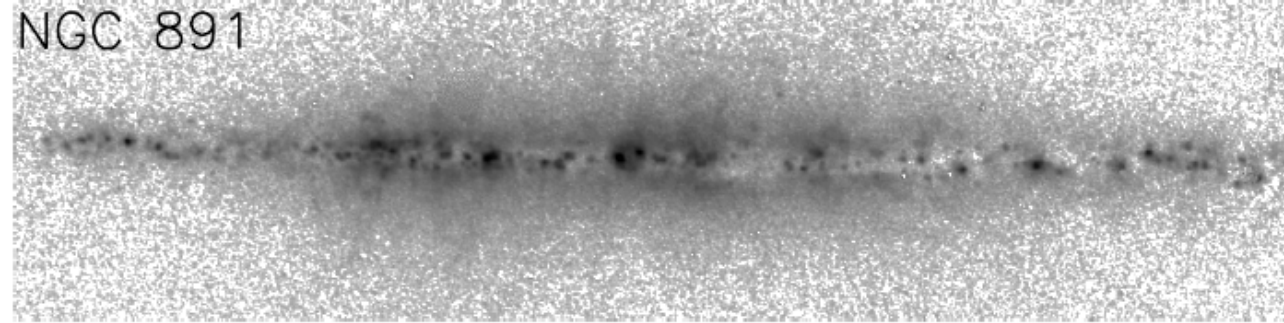
Wisconsin H-Alpha Mapper Sky Survey

Integrated Intensity ( $-80 \text{ km s}^{-1} < v_{\text{LSR}} < +80 \text{ km s}^{-1}$ )

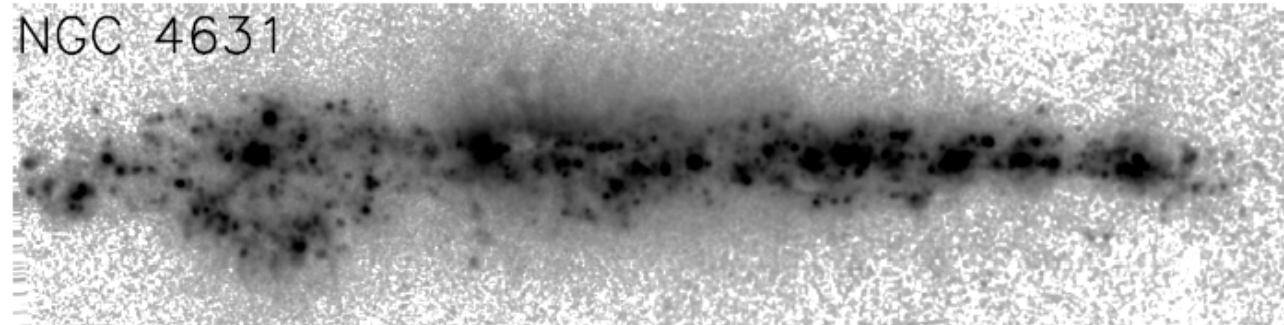


Not all H $\alpha$  is localized in HII regions

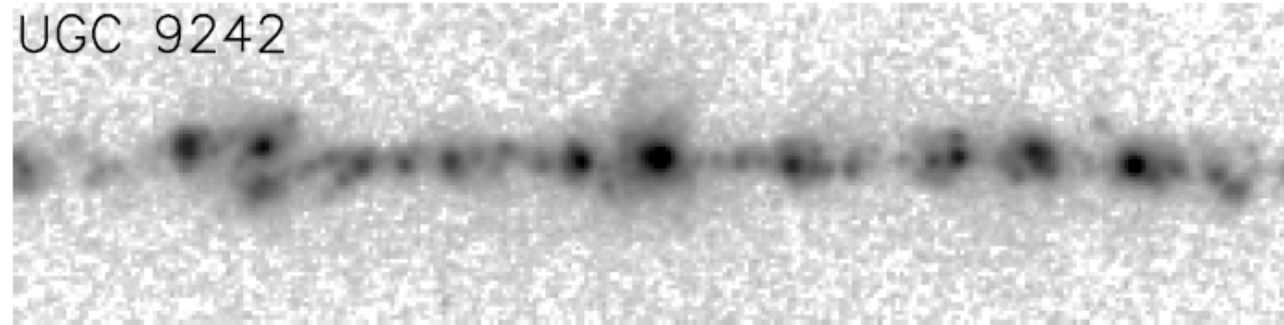
NGC 891



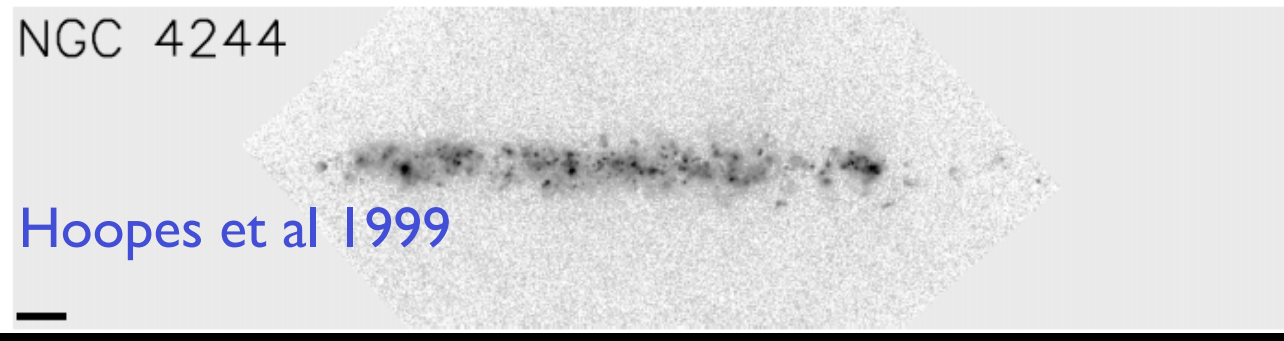
NGC 4631



UGC 9242



NGC 4244



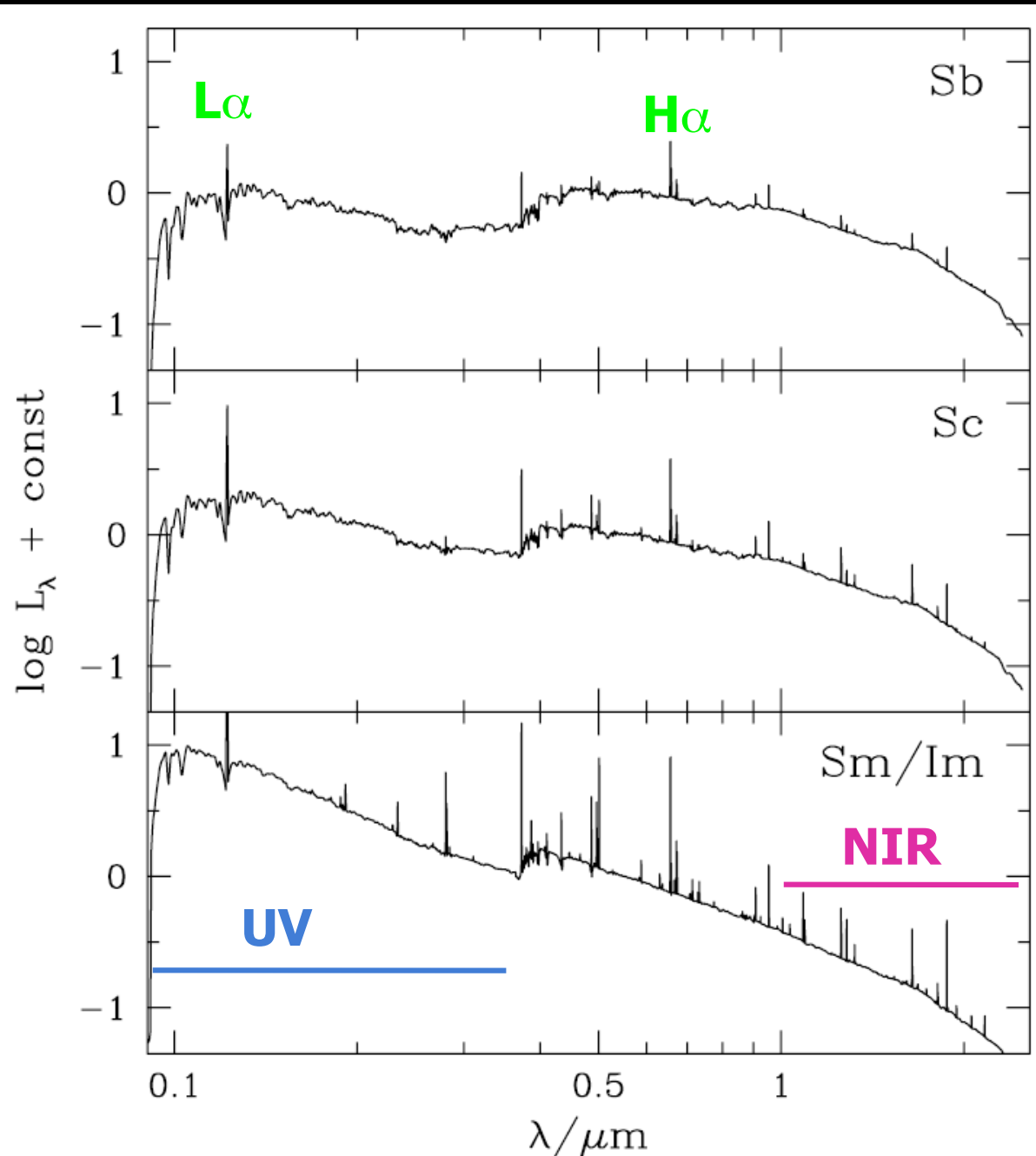
Hoopes et al 1999

The diffuse component is vertically extended (“eDIG”)

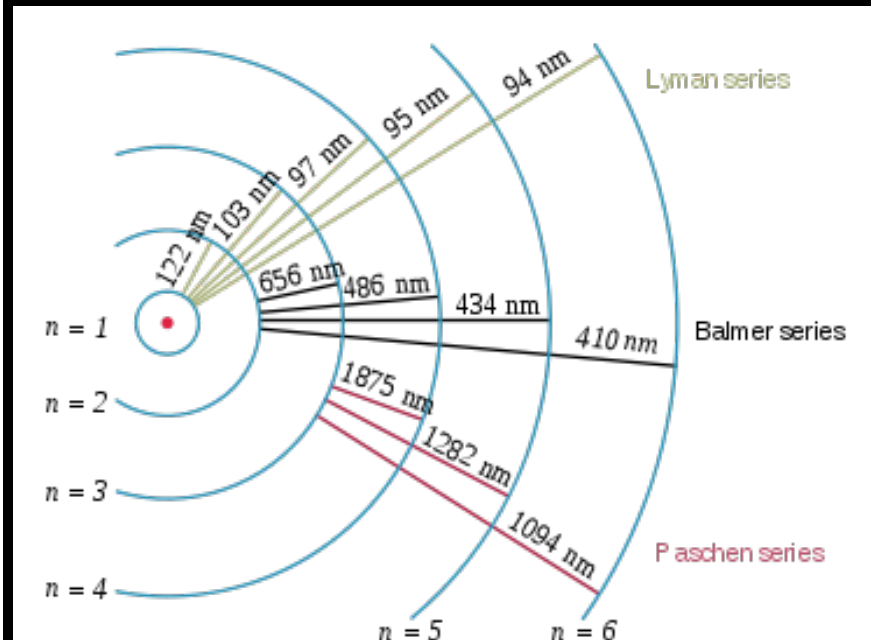
Large eDIG components are associated with galaxies with high star formation rates (“leakage” from HII regions?)

FIG. 6.—Comparison of the DIG layers in the galaxies in our sample. The images have been rotated so the disk is horizontal; see Figs. 1–5 for the correct orientation. The images all have the same spatial scale, shown by the 1 kpc bar in the bottom panel. They are all displayed with the same logarithmic stretch, from  $-2$  to  $1000 \text{ pc cm}^{-6}$ .

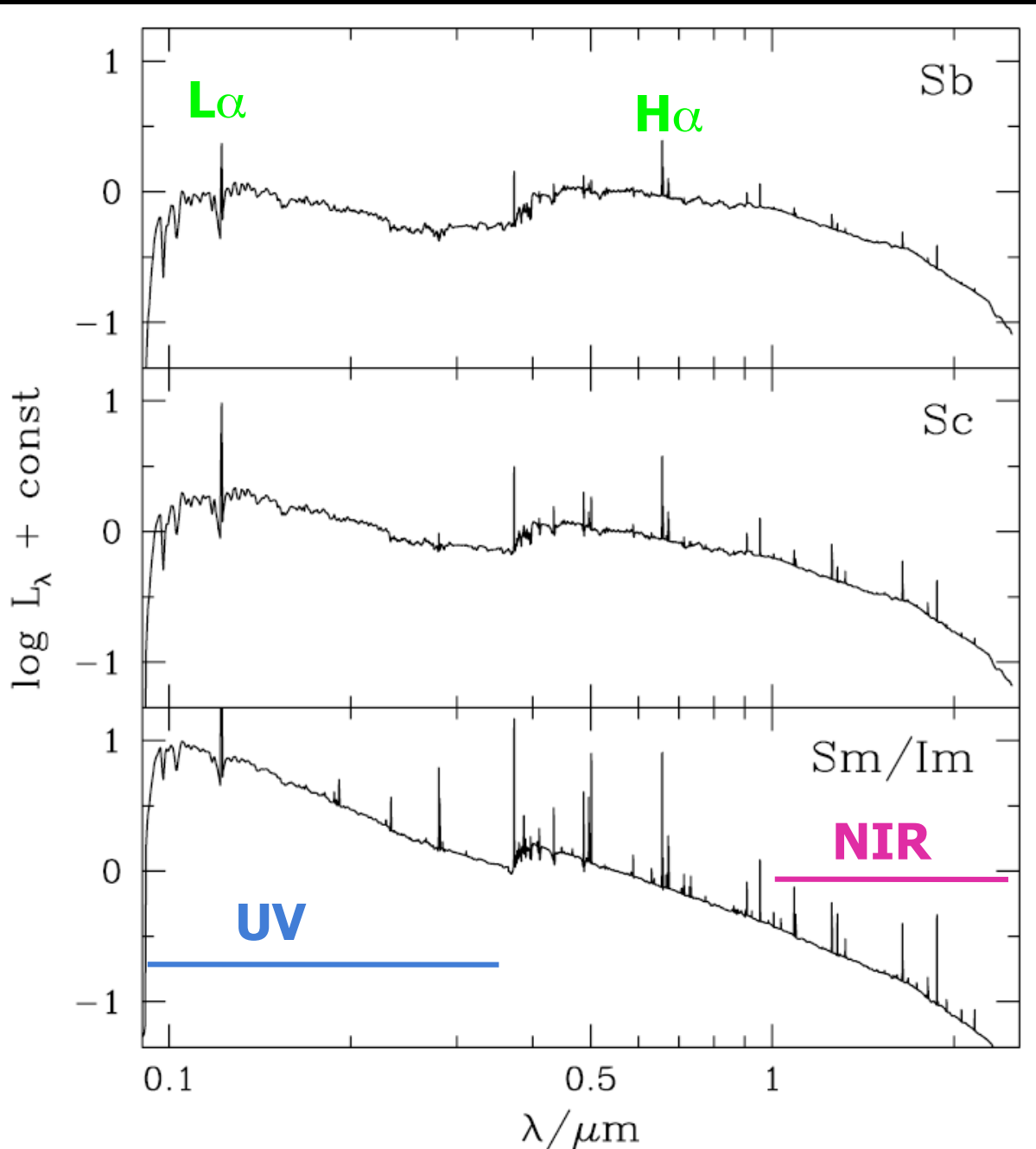
# Recombination lines appear in the UV, IR, and even radio



UV: Ly $\alpha$   
NIR: Paschen series



# Recombination lines appear in the UV, IR, and even radio



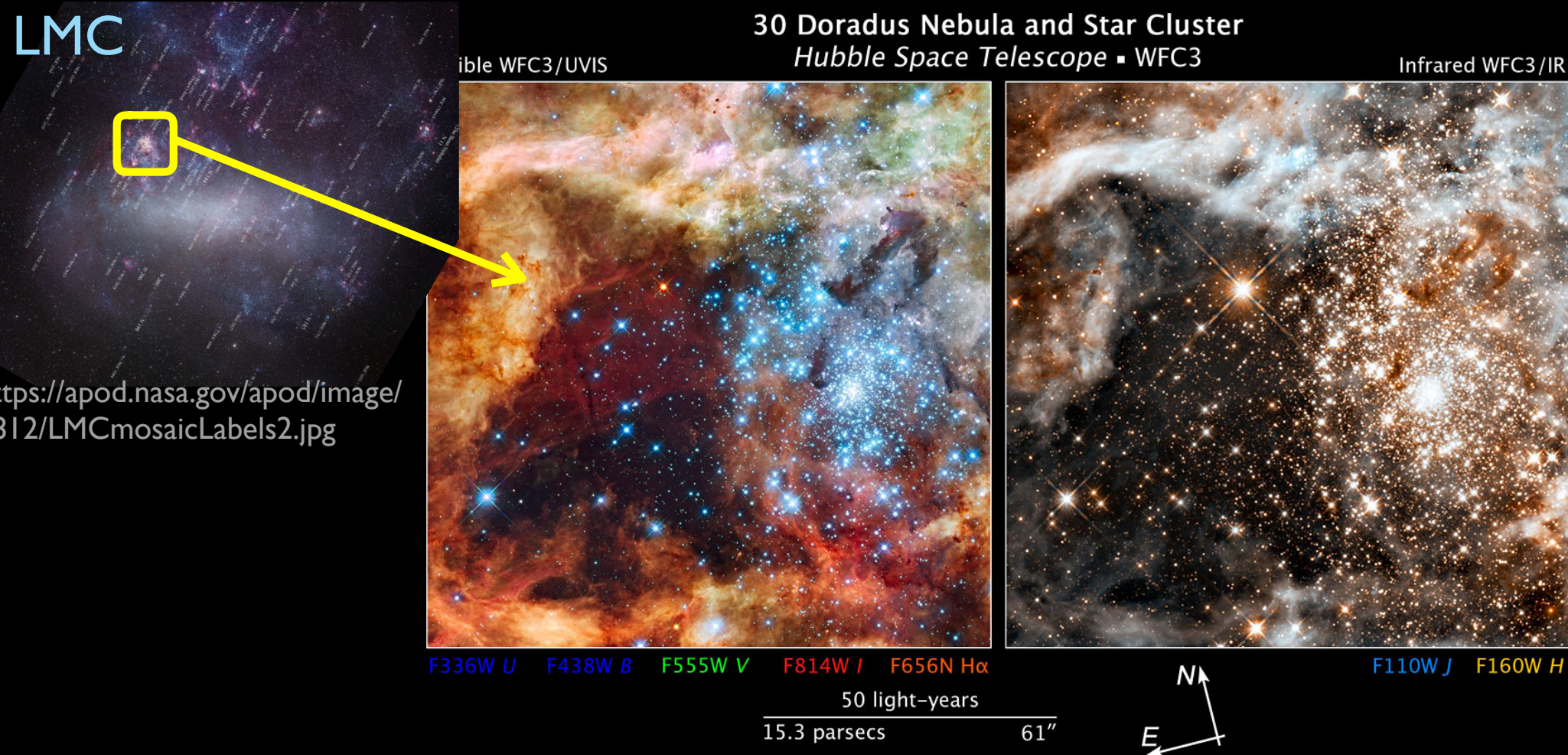
UV: Ly $\alpha$

NIR: Paschen series

- UV lines are good for higher redshift
- NIR lines are good for avoiding dust attenuation uncertainties, but are weaker

2nd most direct method:  
UV Flux

# Detect UV light from stars



Young, massive stars are the dominant source of UV light in most galaxies

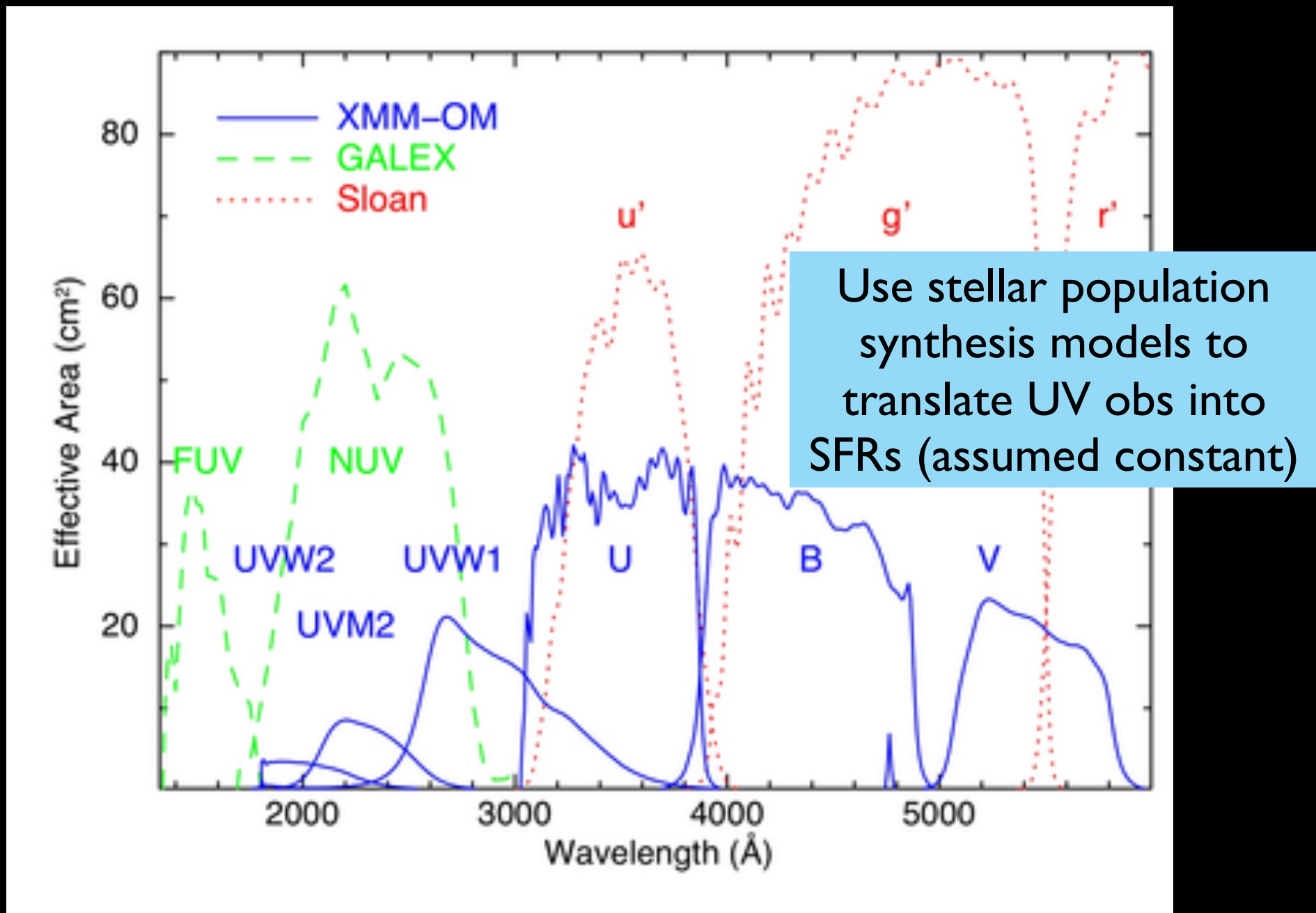
# UV maps clearly indicate where SF is occurring



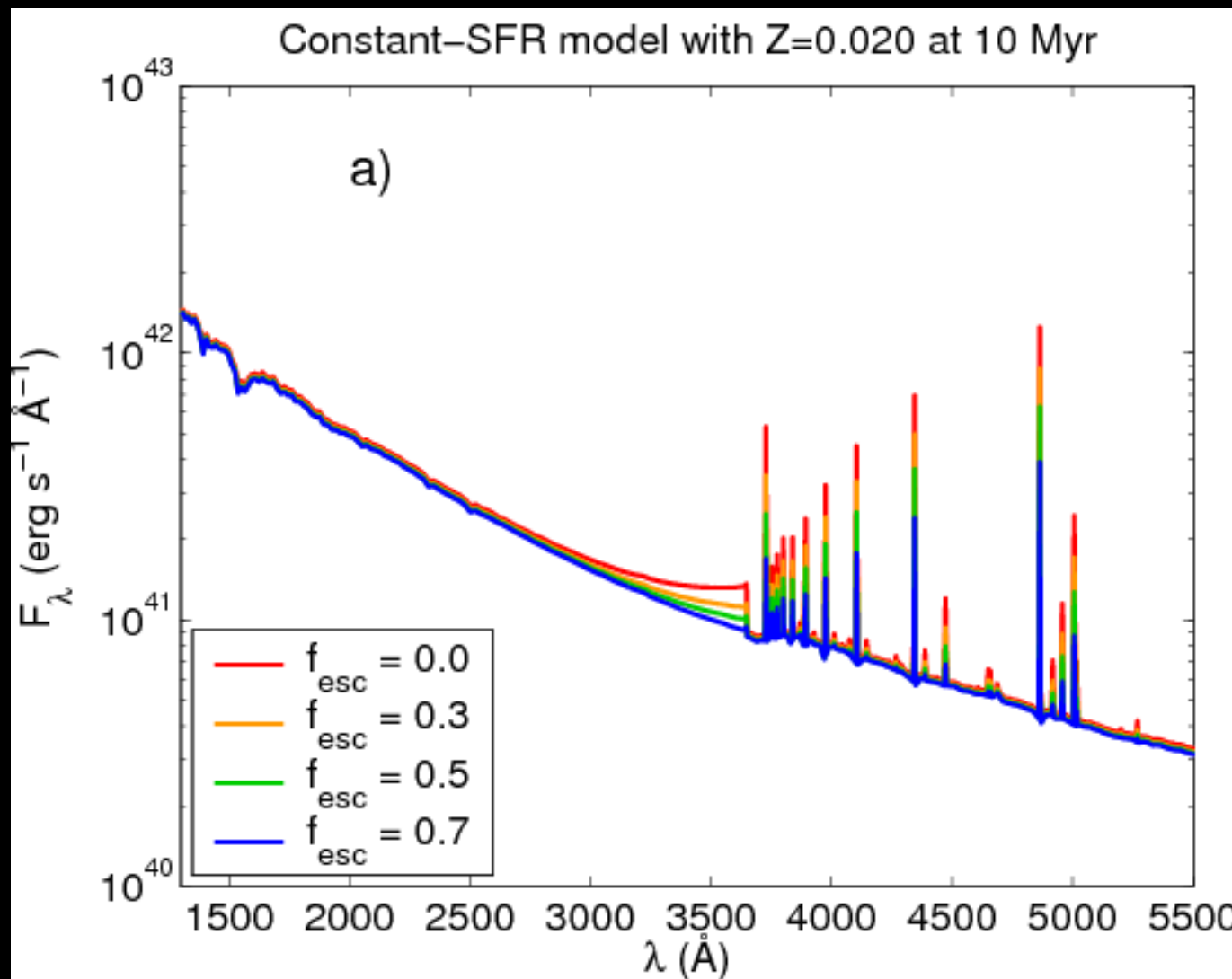
GALEX  
FUV: 1400-1700A  
NUV: 1800-2750A

Caveat: Other sources of UV light exist, including AGN and old, very hot horizontal branch stars

# Galex & Swift space satellites



# Calibrating UV SFR indicators



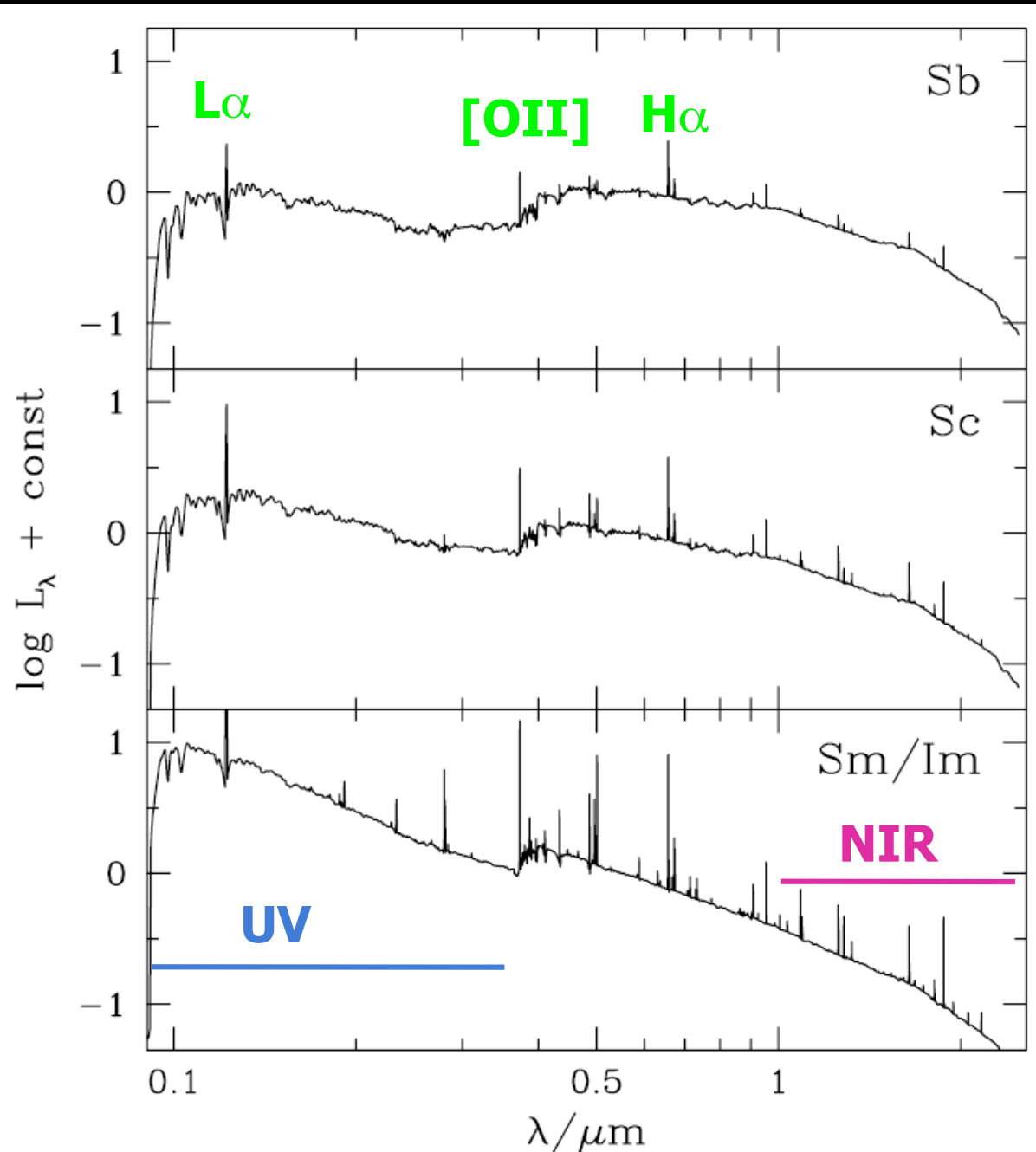
Again, use stellar population synthesis models of a constant SFR over >100Myr

# UV flux as indicator of SFR

- ✓ Measures the presence of O&B stars directly
- 100 Myr timescale not quite “instantaneous”
- Requires space to detect short wavelengths that are more sensitive to recent SF (higher mass stars).
- Strongly affected by dust

# Indirect Methods: Forbidden Lines

# Ionized gas also produces “forbidden lines”



- Less direct tracer of ionization
- Depends on metallicity, ionization parameter
- ✓ But, only lines accessible at some redshifts (e.g., [OII] doublet at 3727Å appears between  $\text{Ly}\alpha$  and  $\text{H}\alpha$ )

# Calibrating [OIII] forbidden line as SFR indicator

Compare observed OIII emission to more direct SFR indicators

Ciardullo et al 2013

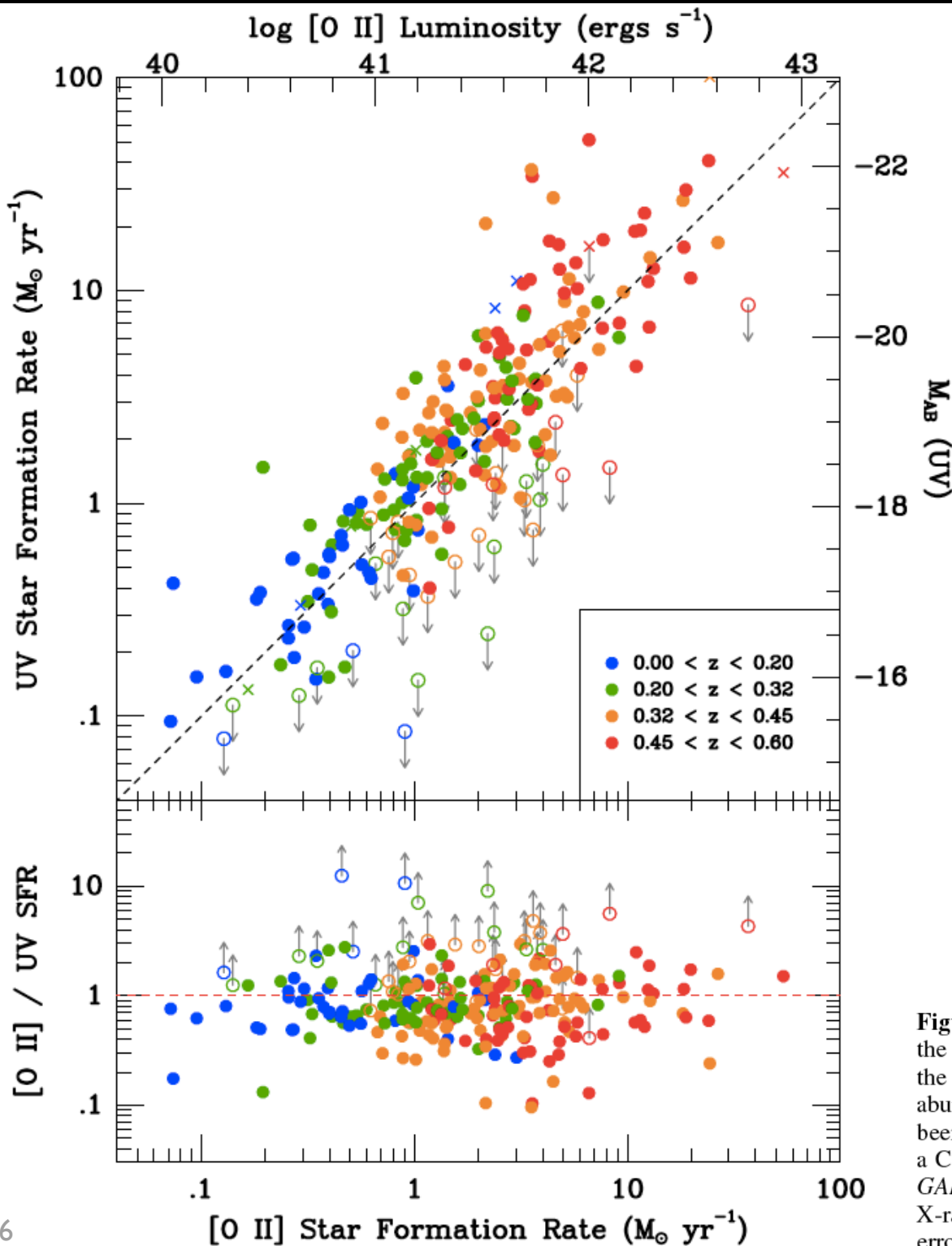


**Figure 4.** A comparison of star formation rates derived from measurements of the UV continuum (using the calibration of Kennicutt 1998) and  $[O\text{ II}]$  flux (via the calibration of Kewley et al. (2004) without the  $R_{23}$  correction for oxygen abundance). The UV fluxes have been  $k$ -corrected, and both quantities have been corrected for internal extinction via our SED-based reddening values and a Calzetti (2001) reddening law. Open circles mark objects that are not in the GALEX GR6 catalog, and denote approximate upper limits. The crosses show X-ray bright objects. The scatter in the diagram is substantial, but any systematic error between the two SFR indicators is small.

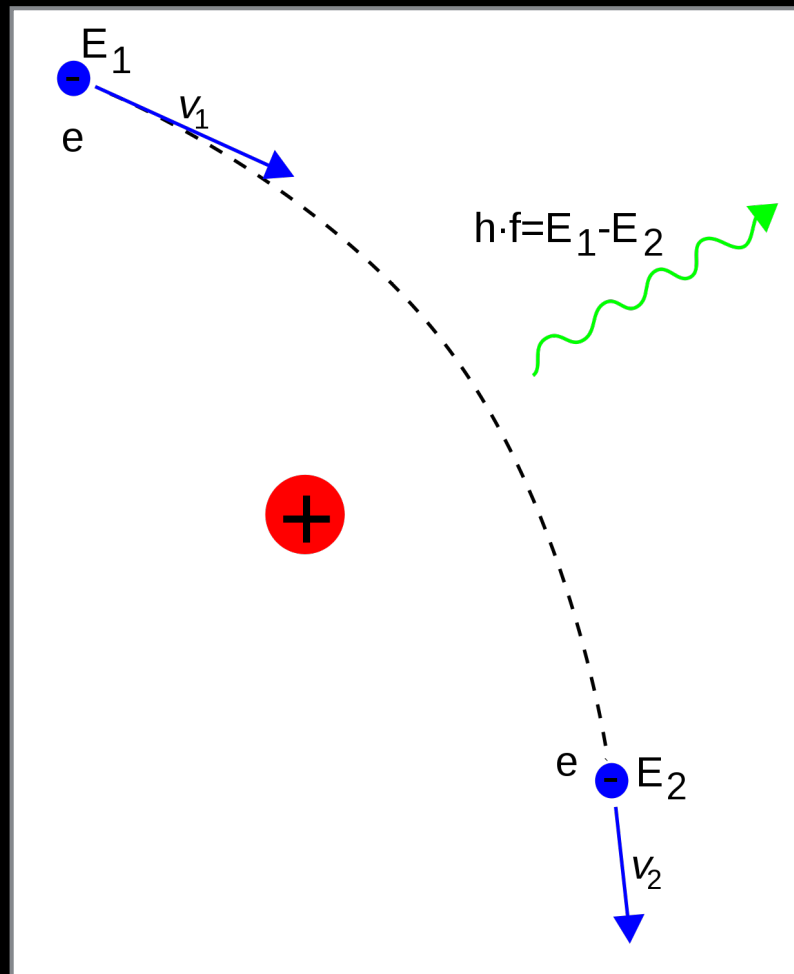
# For references: Wavelengths of emission lines

Table I. Computed lines: Hydrogen recombination lines (upper pannel),  
Elium and metal lines (lower pannel)

Ly $\alpha$ 1216	Ly $\beta$ 1025	Ly $\gamma$ 972	Ly $\delta$ 949	Ly 937	Ly 930
Ly 926	Ly 922	H $\alpha$ 6563	H $\beta$ 4861	H $\gamma$ 4340	H $\delta$ 4102
H 3970	H 3889	H 3835	H 3798	Pa $\alpha$ 18752	Pa $\beta$ 12819
Pa $\gamma$ 10939	Pa $\delta$ 10050	Pa 9546	Pa 9229	Pa 9015	Pa 8863
Br $\alpha$ 40515	Br $\beta$ 26254	Br $\gamma$ 21657	Br $\delta$ 19447	Br 18175	Br 17363
Br 16808	Br 16408	Pf $\alpha$ 74585	Pf $\beta$ 46529	Pf $\gamma$ 37398	Pf $\delta$ 32964
Pf 30386	Pf 28724	Pf 27577	Pf 26746	Hu $\alpha$ 123690	Hu $\beta$ 75011
Hu $\gamma$ 59071	Hu $\delta$ 51277	Hu 46716	Hu 43756	Hu 41700	Hu 40201
HeII 1640	HeII 1217	HeII 1085	HeII 4686	HeII 3203	HeII 2733
HeII 2511	HeI 4471	HeI 5876	HeI 6678	HeI 10830	HeI 3889
HeI 7065	[CI] 9850	[CI] 8727	[CI] 4621	[CI] 609 $\mu$ m	[CI] 369 $\mu$ m
[CII] 157.7 $\mu$ m	CII] 2326	CIII] 1908	[NI] 5199	[NI] 3466	[NI] 10400
[NII] 6584	[NII] 6548	[NII] 5755	[NII] 122 $\mu$ m	[NII] 205 $\mu$ m	NII] 2141
[NIII] 57 $\mu$ m	[OI] 6300	[OI] 6363	[OI] 5577	[OI] 63 $\mu$ m	[OI] 145 $\mu$ m
[OII] 3727	[OII] 7325	[OII] 2471	OIII] 1663	[OIII] 5007	[OIII] 4959
[OIII] 4363	[OIII] 2321	[OIII] 88 $\mu$ m	[OIII] 52 $\mu$ m	[OIV] 26 $\mu$ m	[NeII] 13 $\mu$ m
[NeIII] 15.5 $\mu$ m	[NeIII] 36 $\mu$ m	[NeIII] 3869	[NeIII] 3967	[NeIII] 3343	[NeIII] 1815
[NeIV] 2424	[NeIV] 4720	MgII 2800	[SiII] 35 $\mu$ m	[SII] 10330	[SII] 6731
[SII] 6717	[SII] 4070	[SII] 4078	[SIII] 19	[SIII] 33.5	[SIII] 9532
[SIII] 9069	[SIII] 6312	[SIII] 3722	[SIV] 10.4 $\mu$ m	[ArII] 69850	[ArIII] 7135
[ArIII] 7751	[ArIII] 5192	[ArIII] 3109	[ArIII] 3005	[ArIII] 22 $\mu$ m	[ArIII] 9 $\mu$ m

# Indirect Methods: Free-free emission

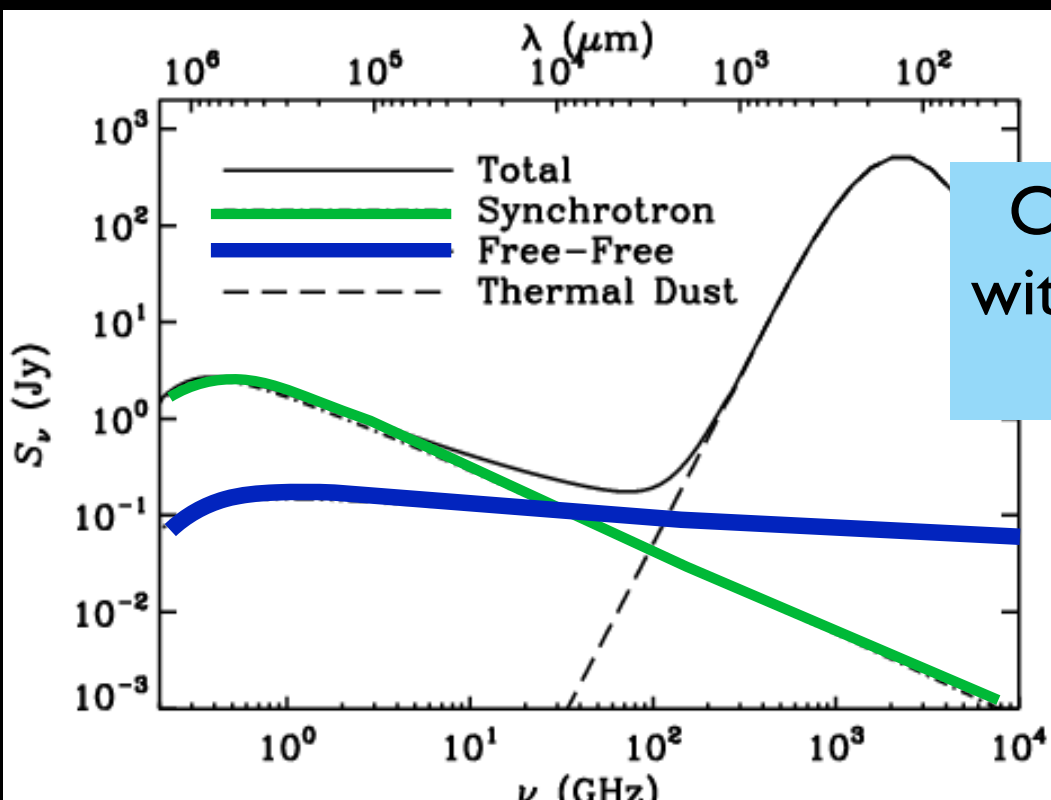
# Free-free (bremsstrahlung) emission\*



Constrains the density of free electrons, which requires ionization

\*Sometimes called “thermal emission”, along with synchrotron “non-thermal emission”

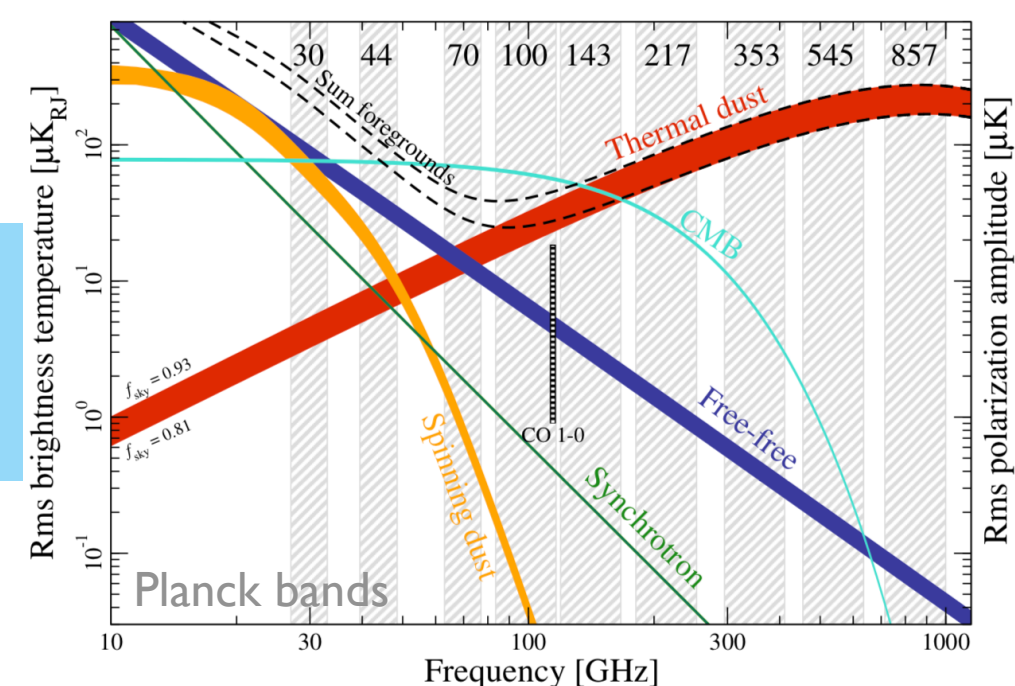
# Free-free emission is detected in radio



Murphy et al 2010

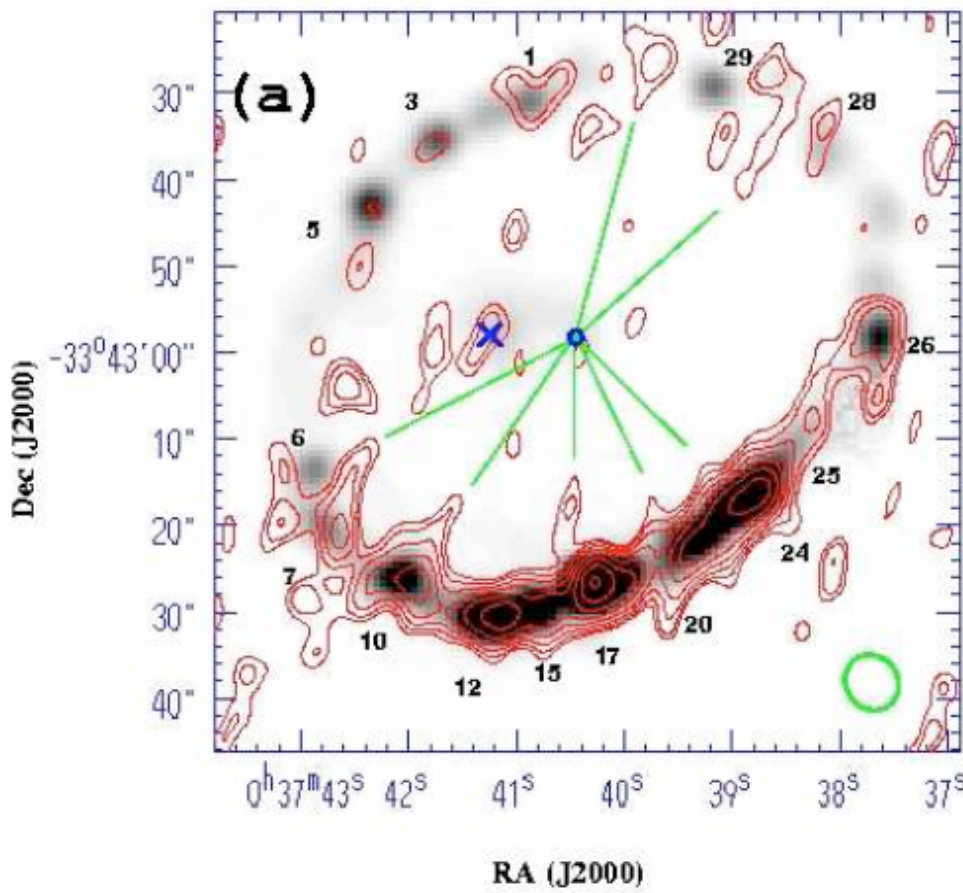
Old view: Contaminated with synchrotron (B-fields) & thermal emission

New view: Also contamination from “spinning dust”



# Example VLA map at 20cm

On H $\alpha$



On optical

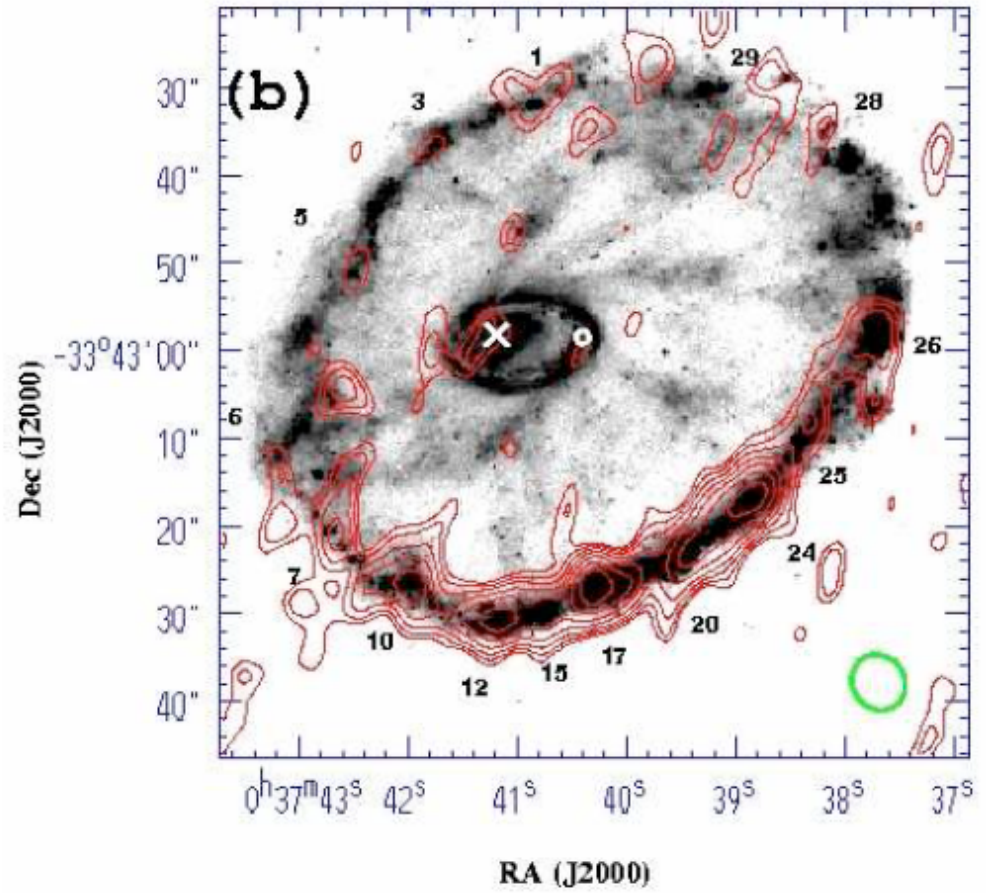


FIG. 1.— 20 cm RC intensity contours of the Cartwheel superimposed on (a) an H $\alpha$  image (gray scale), which has been smoothed to the resolution of the 20 cm RC image, and (b) the HST B-band image. The lowest contour level corresponds to  $60 \mu\text{Jy beam}^{-1}$  ( $\approx 2\sigma$ ), and the subsequent contour levels increase by a factor of  $\sqrt{2}$ . The ellipse at the bottom-right corner indicates the RC beam size. In (a) note the excellent positional correspondence between radio peaks and HII complexes, which have been labeled by their H95 numbers. Straight lines are drawn connecting the filamentary structures or *spokes* to the geometrical center of the ring. Unlike the optical spokes (features connecting the inner ring to the outer ring in (b)), the RC spokes are straight and short. The position of the nucleus is marked by a cross.

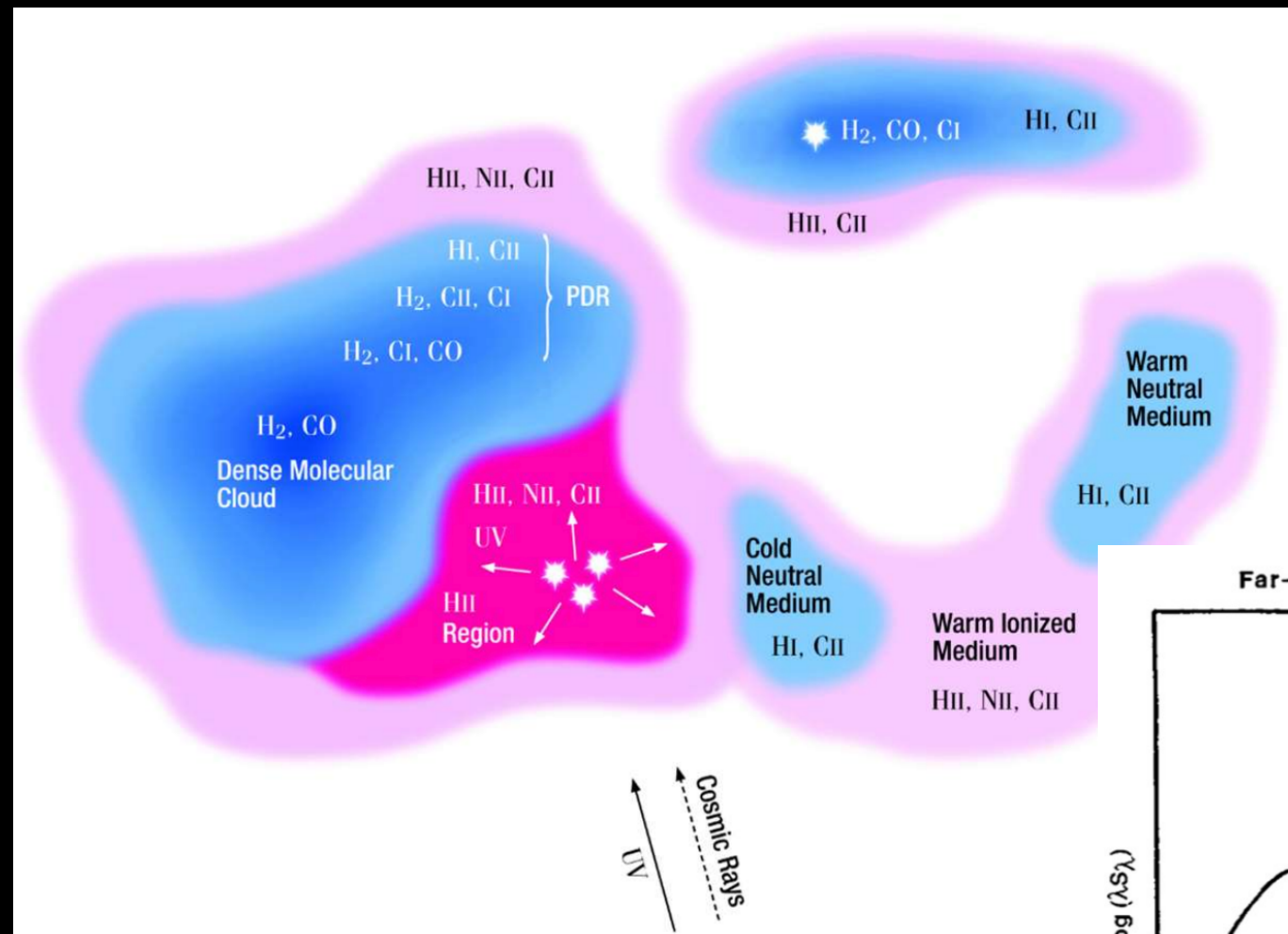
# Free-free emission as a SFR tracer

See Schober et al 2017

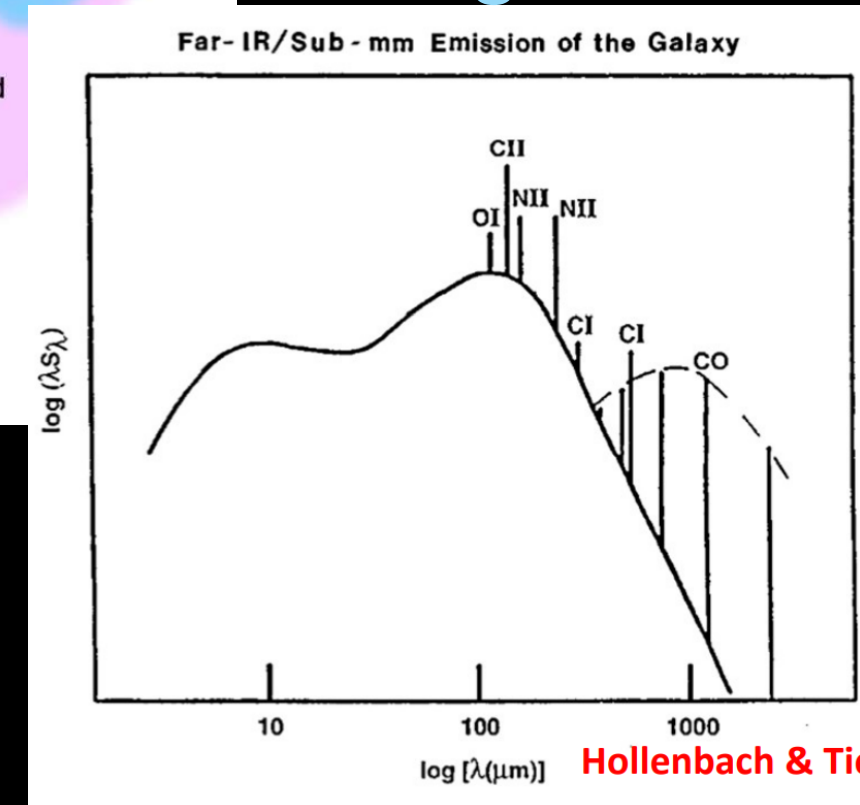
- ✓ Easy to measure from the ground in the radio  
(1.4 GHz, 4.3 GHz widely used)
- ✓ Unaffected by dust
- Needs calibration
- Can have contaminants from other sources

# Indirect Methods: [CII] Cooling Line

# [CII] 158 $\mu$ m FIR Line

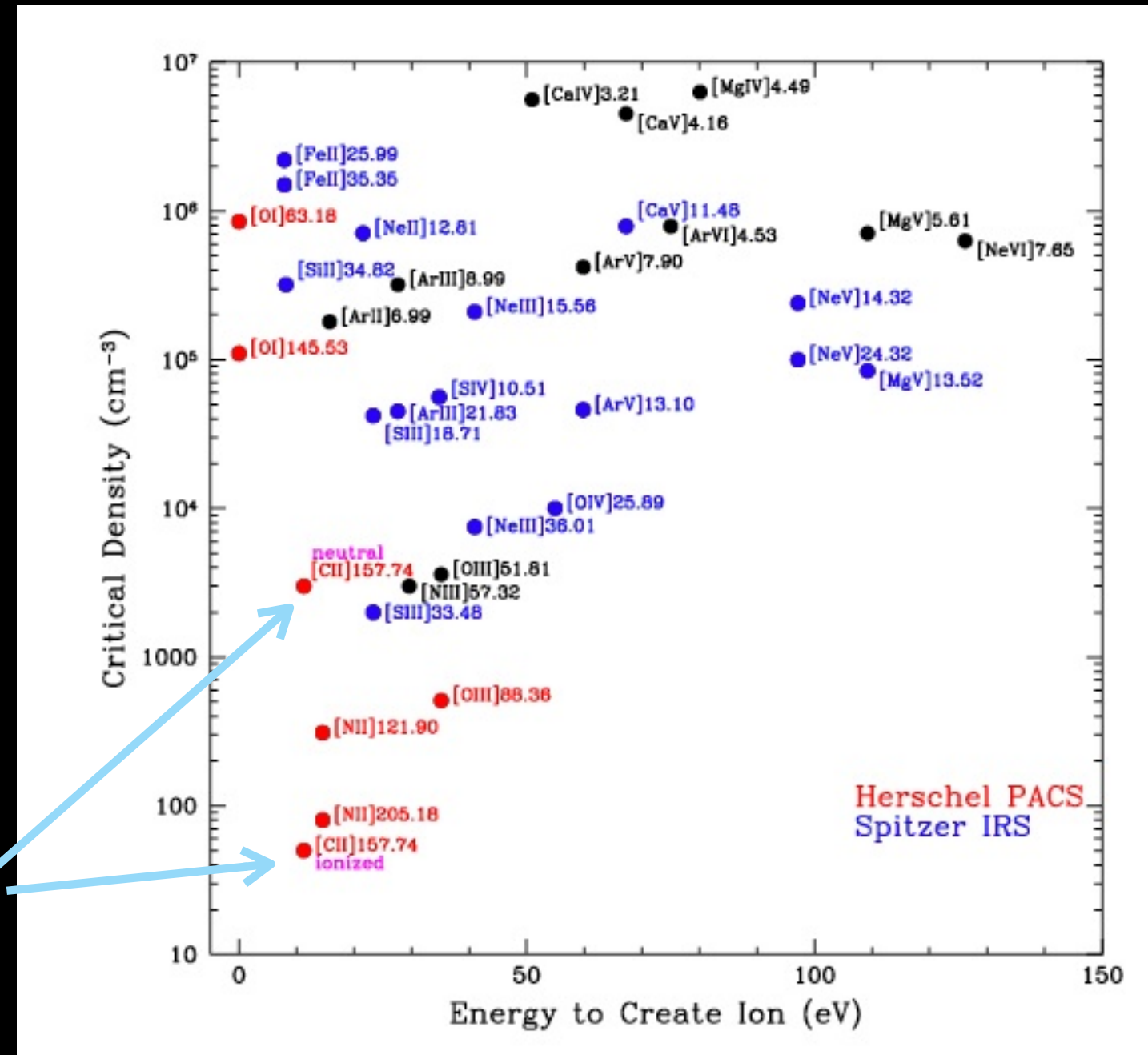


Strongest FIR line

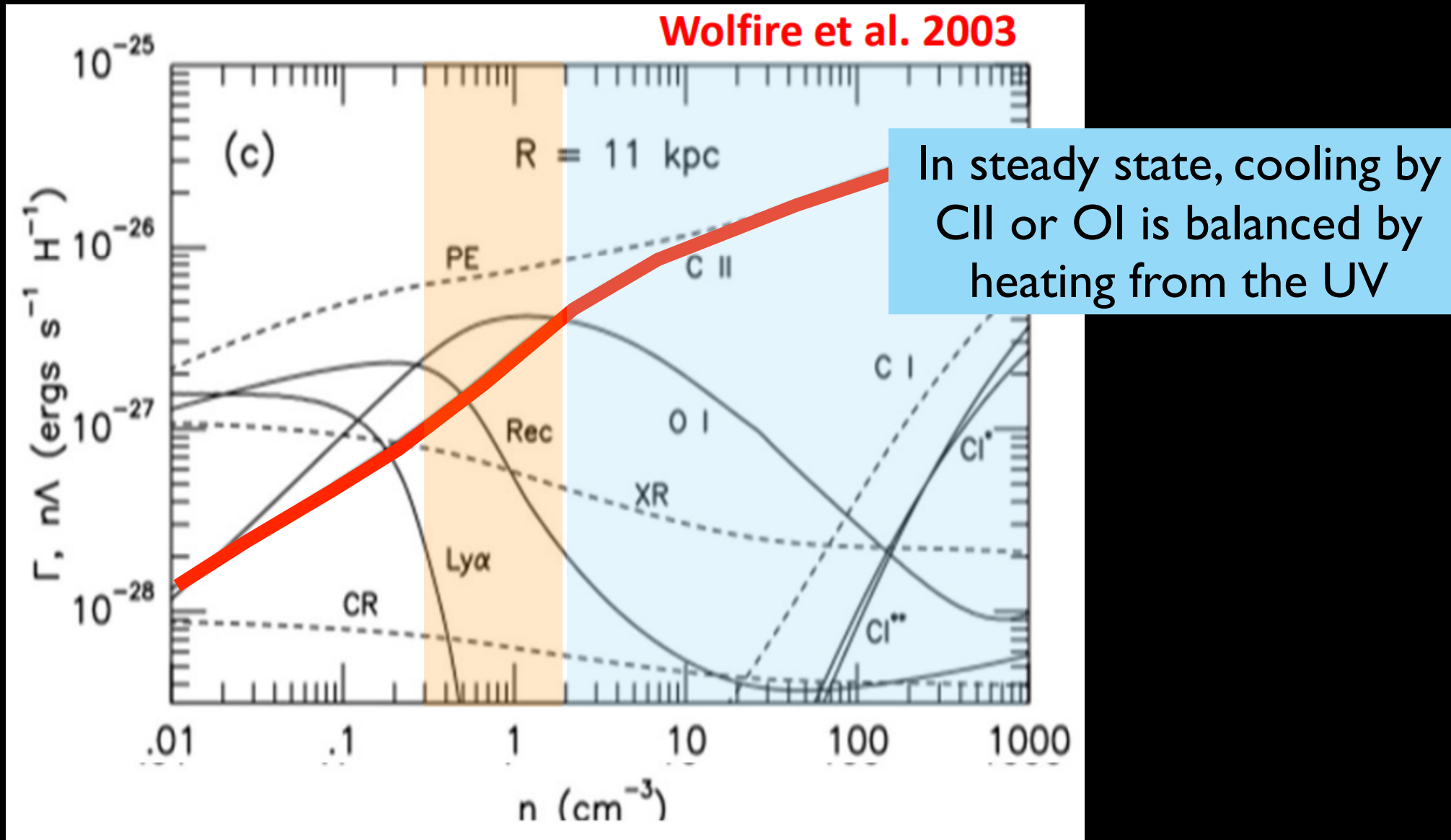


Hollenbach & Tielens

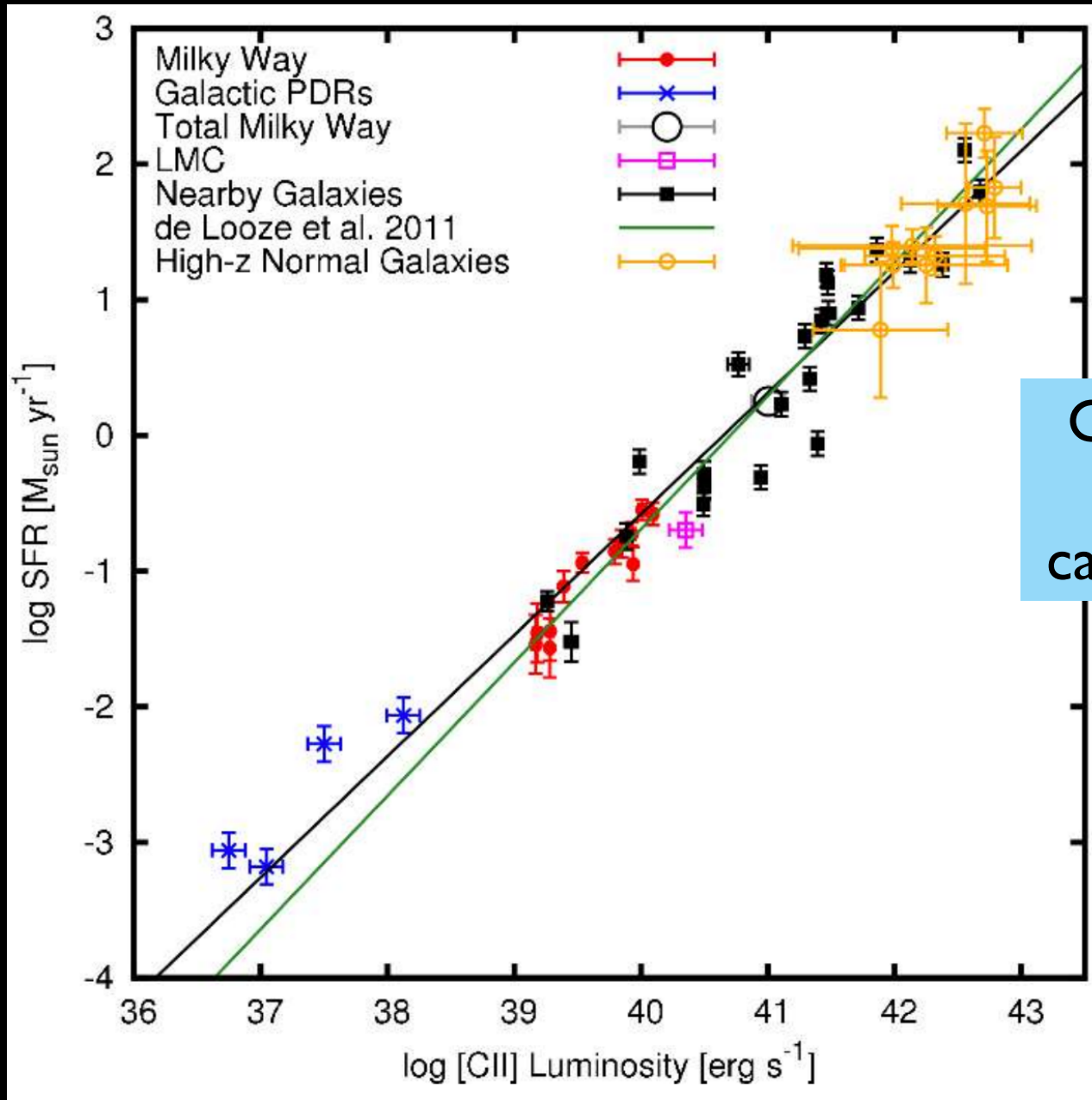
# FIR lines (for reference & context)



# CII is a dominant coolant in the ISM over a wide range of densities



# Calibrating [CII] 158μm as SFR indicator



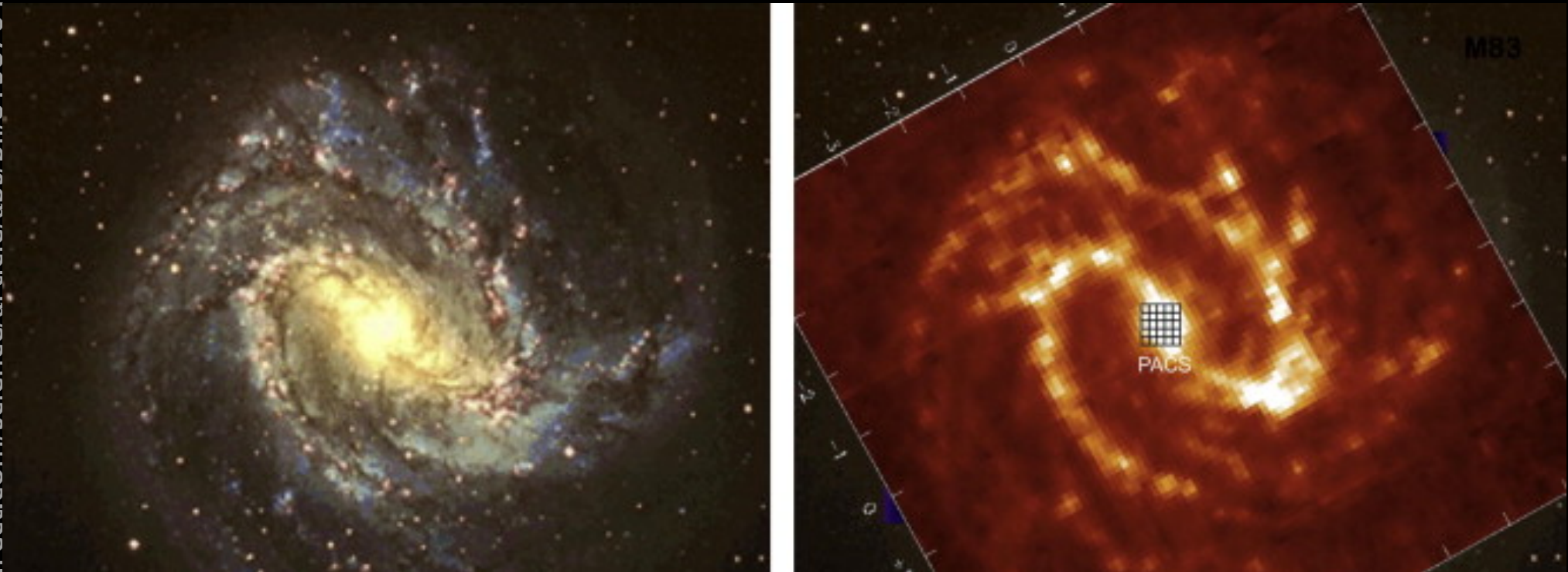
Compare observed CII emission to better calibrated SFR indicators

Pineda et al 2014

# Indirect Methods: Emission from warm dust

# Detect reprocessed UV light in far-IR

<https://www.sciencedirect.com/science/article/pii/S1387647309000451>



Optical

FIR

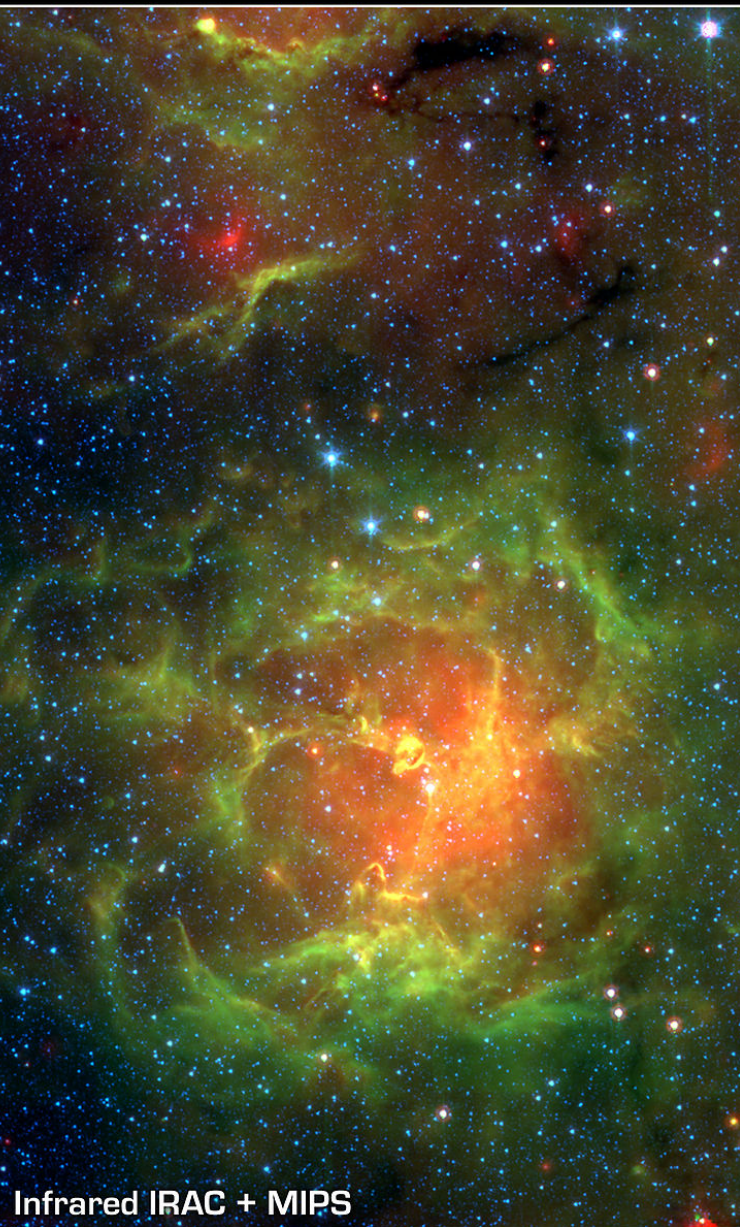
Presumes far-IR flux is due to dust heated by UV.

<sup>59</sup>Must be calibrated; no direct theoretical expectation for link to SFR

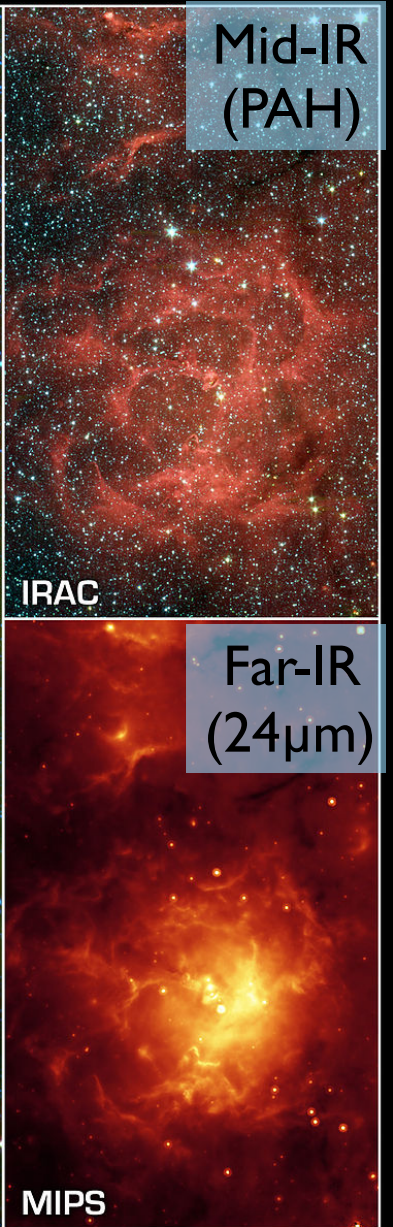
# Far-IR emission spatially correlated w/ SF



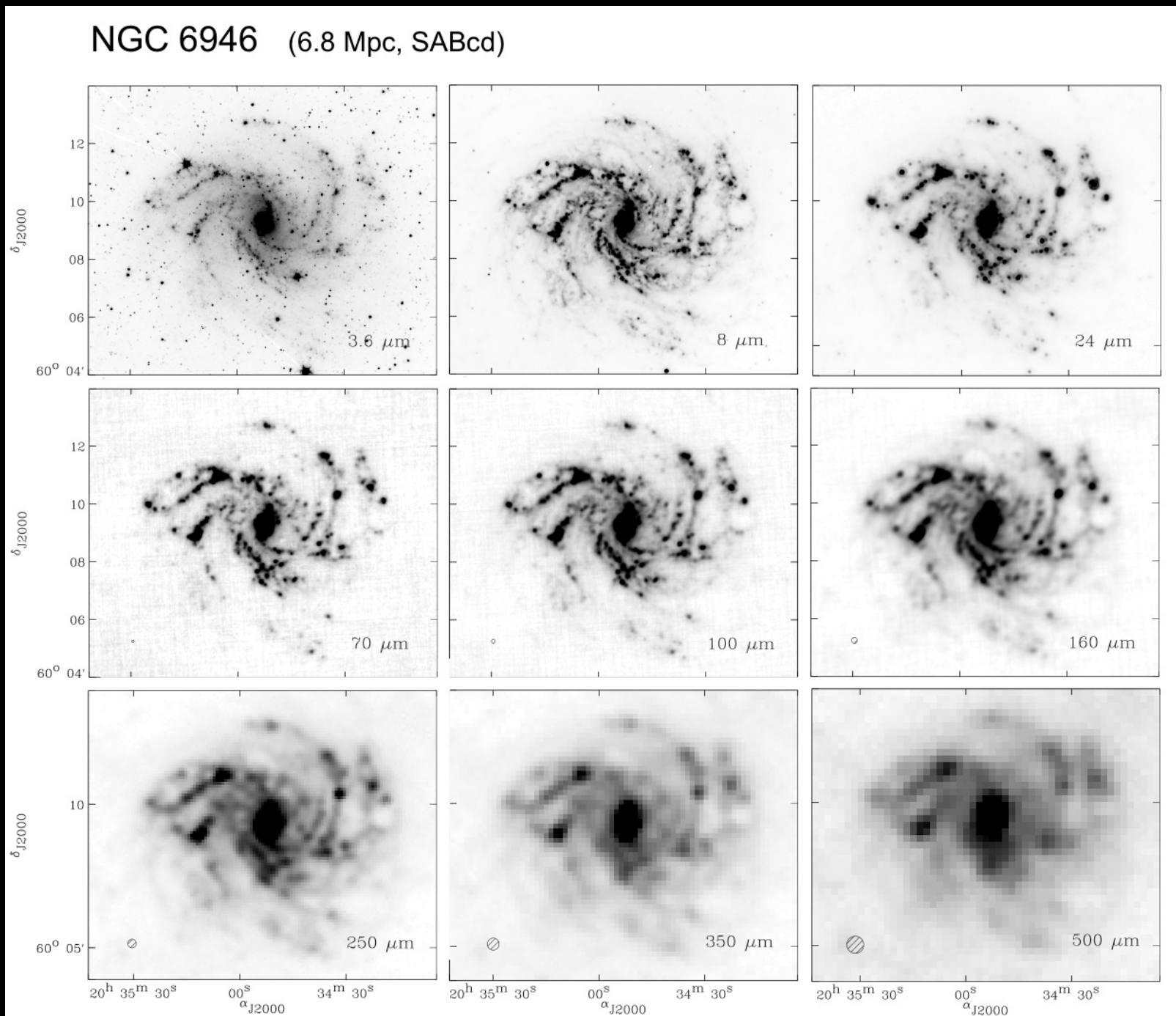
Trifid Nebula/Messier 20



Spitzer Space Telescope • IRAC + MIPS



# Far-IR emission spatially correlated w/ SF



# Mid- and Far-IR as tracer of SF

- ✓ Detects light missed in UV
- Depends on metallicity, dust optical depth
- Can be contaminated by cold dust heated by older stars
- Must be *calibrated* to map to SFR

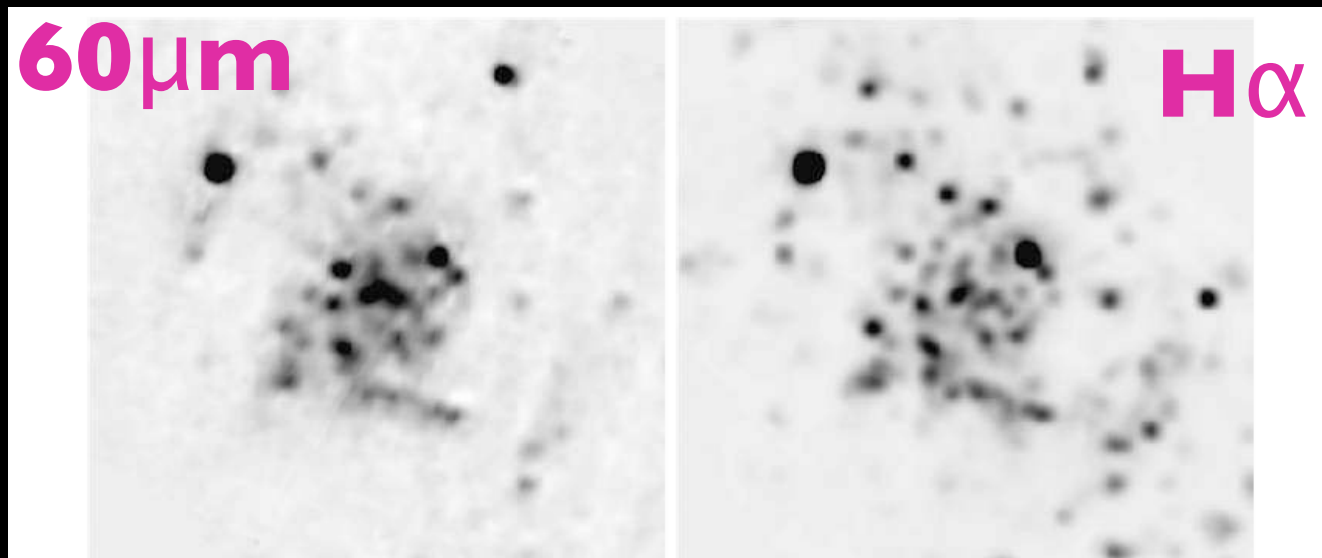
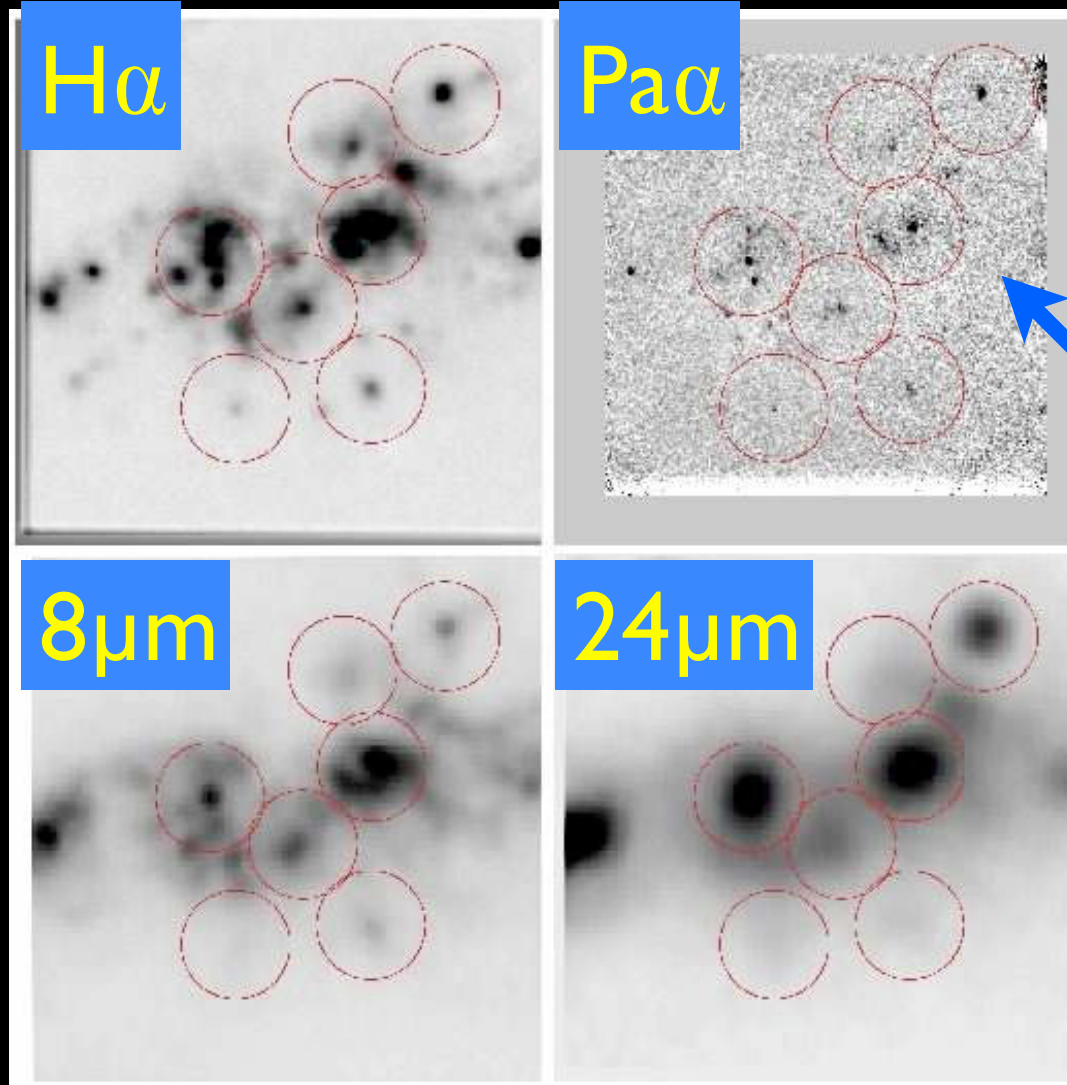


**FIGURE 3.** Left: Distribution of the localised warm dust component at  $60\ \mu\text{m}$ ,  $F_{60}^1$ , in M 33 (Hippelein et al. [42]). This is the scaled difference map  $2(F_{60} - 0.165 \times F_{160})$ , with the factor 0.165 given by the average flux density ratio  $F_{60}/F_{170}$  in the interarm regions. Right:  $\text{H}\alpha$  map of M 33 convolved to a resolution of  $60''$ .

Tuffs &  
Popescu  
2005

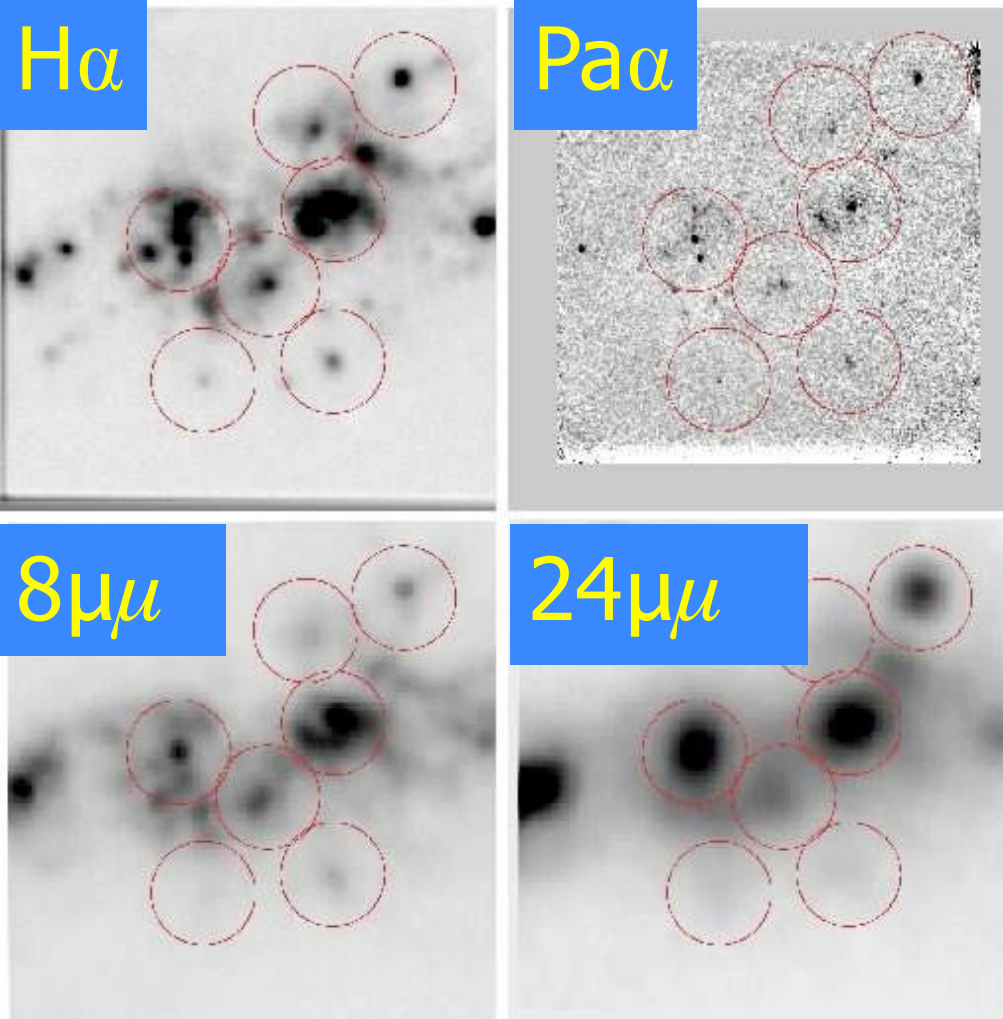
# Calibrating mid- and far-IR emission as a SFR indicator



Calibrate off of “direct” recombination radiation SFRs

Assume Pa $\alpha$  is  
“ground truth”  
(NIR, so little extinction)

# Verify a linear relation between SFR tracers



Note:  $8\mu\mu$  does not look nearly as linear.

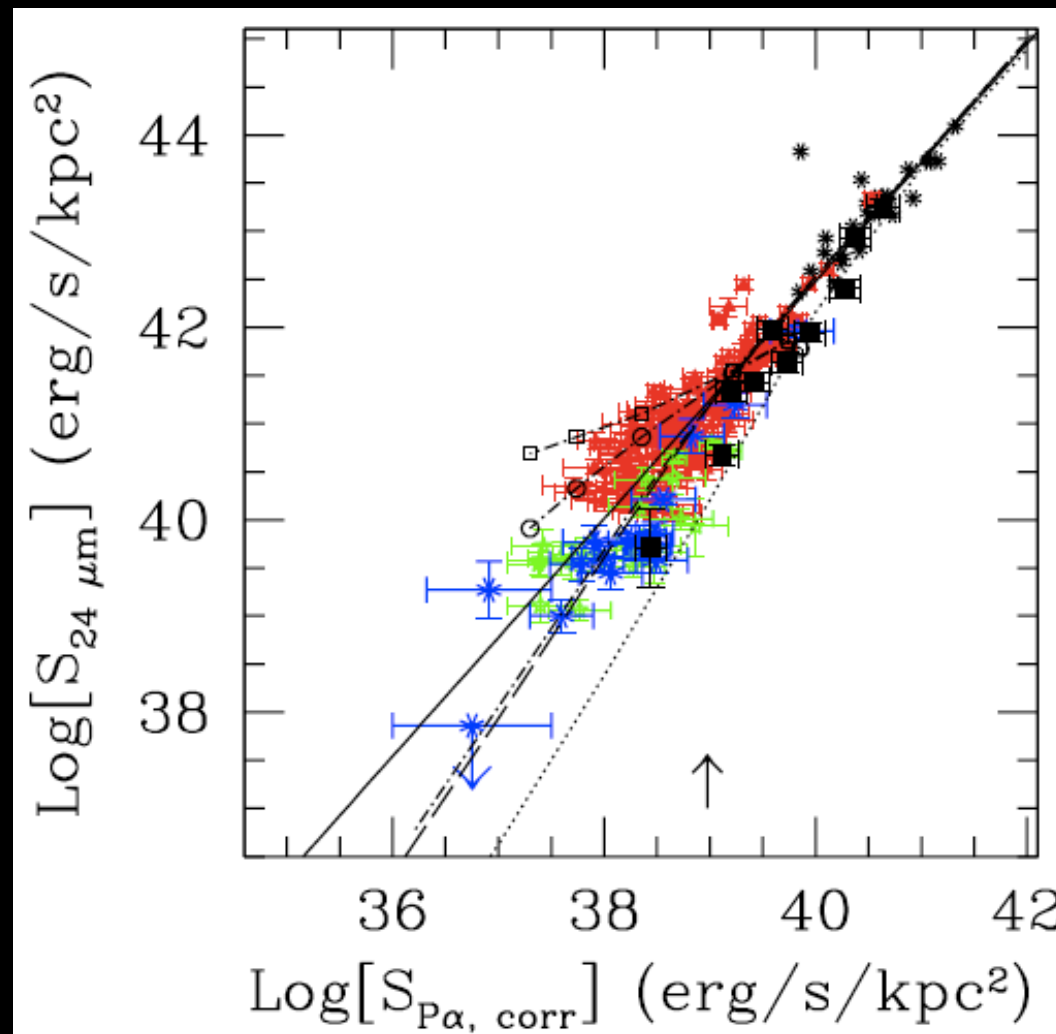


Fig. 9.—Luminosity surface density at  $24 \mu\text{m}$  as a function of the extinction-corrected  $\text{Pa}\alpha$  LSD for the same datapoints as Figure 4 (after removal of the Sy 2 nuclei, the foreground and background sources, and the NGC5033 HII knots data, leaving 164 independent datapoints in the high metallicity HII knot subsample). The continuous line shows the best linear fit through the high metallicity HII knots, from Figure 4. Models of infrared and ionized gas emission are superimposed on the data, for a variety of star formation histories, stellar population ages, and metallicity (see Appendix). Models with solar metallicity ( $Z = Z_\odot$ ) ISM and stellar populations include: 100 Myr-old constant star formation ( $\text{SFR}/\text{area} = 4 \times 10^{-5}$ – $4 M_\odot \text{ yr}^{-1} \text{ kpc}^{-2}$ , long-dash line); instantaneous burst with variable mass ( $10^3$ – $10^8 M_\odot \text{ kpc}^{-2}$ ) and color-excess, and constant age of 4 Myr (dot-dashed line); instantaneous bursts with constant mass ( $10^6 M_\odot \text{ kpc}^{-2}$ ) and variable age, and both variable color excess (dot-dashed line with empty circles) and constant color excess ( $E(B-V) = 2$  mag, dot-dashed line with empty squares). The circle and square symbols mark the population ages, right-to-left: 0.01, 2, 4, 6, 8, 10 Myr. The dotted line marks a  $1/10 Z_\odot$  model of constant star formation over the past 100 Myr. The upward-pointing arrow marks the approximate luminosity where the transition between single-photon heating and thermal equilibrium heating for the dust begins to occur.

Caveat: At fixed SFR, FIR emission varies with amount of dust, so  $24\mu\text{m}$  not perfect SFR indicator on its own

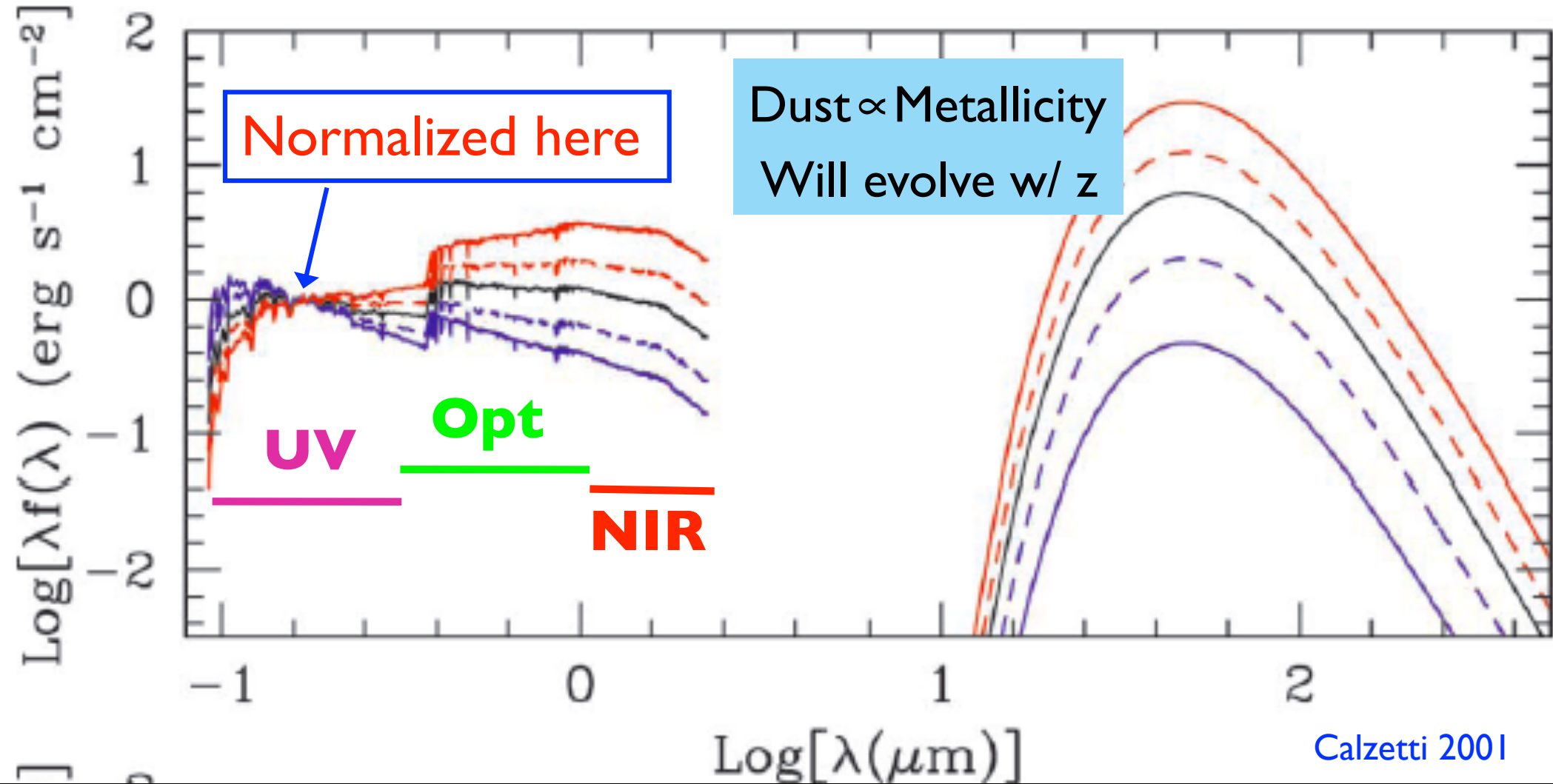


FIG. 11.—UV-to-IR SED of a 1 Gyr constant star formation population, attenuated by the starburst obscuration curve (eq. [8]), is shown for increasing amounts of dust:  $E(B-V)_{\text{gas}} = 0.05$  (blue solid line), 0.20 (blue dashed line), 0.40 (black line), 0.55 (red dashed line), and 0.75 (red solid line). All SEDs are arbitrarily normalized to the flux density at  $0.17\mu\text{m}$ . The infrared SED is schematically represented by a single-temperature dust component with (a)  $T = 50\text{ K}$  and  $\epsilon = 2$  and (b)  $T = 40\text{ K}$  and  $\epsilon = 1.5$  to highlight differences in the long-wavelength regime.

# The Summary

# SFR's ( $M_{\odot}/\text{yr}$ ) from measured luminosities:

Kennicutt & Evans 2012

$$\log \dot{M}_*(M_{\odot} \text{ year}^{-1}) = \log L_x - \log C_x$$

**Table 1** Star-formation-rate calibrations

Band	Age range (Myr) <sup>a</sup>	$L_x$ units	$\log C_x$ <sup>b</sup>	$\dot{M}_*/\dot{M}_*(\text{K98})$ <sup>c</sup>	Reference(s)
FUV	0-10-100	ergs s <sup>-1</sup> ( $\nu L_{\nu}$ )	43.35	0.63	Hao et al. (2011), Murphy et al. (2011)
NUV	0-10-200	ergs s <sup>-1</sup> ( $\nu L_{\nu}$ )	43.17	0.64	Hao et al. (2011), Murphy et al. (2011)
H $\alpha$	0-3-10	ergs s <sup>-1</sup>	41.27	0.68	Hao et al. (2011), Murphy et al. (2011)
TIR	0-5-100 <sup>d</sup>	ergs s <sup>-1</sup> (3–1100 $\mu\text{m}$ )	43.41	0.86	Hao et al. (2011), Murphy et al. (2011)
24 $\mu\text{m}$	0-5-100 <sup>d</sup>	ergs s <sup>-1</sup> ( $\nu L_{\nu}$ )	42.69		Rieke et al. (2009)
70 $\mu\text{m}$	0-5-100 <sup>d</sup>	ergs s <sup>-1</sup> ( $\nu L_{\nu}$ )	43.23		Calzetti et al. (2010b)
1.4 GHz	0-100	ergs s <sup>-1</sup> Hz <sup>-1</sup>	28.20		Murphy et al. (2011)
2-10 keV	0-100	ergs s <sup>-1</sup>	39.77	0.86	Ranalli et al. (2003)

<sup>a</sup>Second number gives mean age of stellar population contributing to emission; third number gives age below which 90% of emission is contributed.

<sup>b</sup>Conversion factor between SFR and the relevant luminosity, as defined by Equation 12 in Section 3.8.

<sup>c</sup>Ratio of star-formation rate (SFR) derived using the new calibration to that derived using the relations in Kennicutt (1998a). The lower SFRs now mainly result from the different initial mass function and from updated stellar population models.

<sup>d</sup>Numbers are sensitive to star-formation history; those given are for continuous star formation over 0–100 Myr. For more quiescent regions (e.g., disks of normal galaxies), the maximum age will be considerably longer.

Abbreviations: FUV, far ultraviolet; NUV, near ultraviolet; TIR, total infrared.

Typically calculated from models of stellar populations where the SFR is constant over the lifetime of O/B stars ( $\sim 10^8$  yrs). Sensitive to the assumed IMF and upper mass cutoff.

# Sensitivities of different methods (in SFR/M $\star$ )

- optical SED's:  $10^{-11} \text{ yr}^{-1}$
- UV fluxes:  $10^{-12} \text{ yr}^{-1}$
- Resolved UV stars & CMDs:  $10^{-14} \text{ yr}^{-1}$

# SFR Tracer Questions

- How well do these work?
- Do different methods give consistent answers?
- How well do they work when applied in uncalibrated regimes? (different redshifts, SFR intensities, metallicities, etc)
- Are they robust to presence of AGN?
- Are there additional correction that can make them more linear tracers of SFR in a broader range of physical conditions?

Correcting for “obscured” star  
formation  
(i.e., SF that is hidden by dust)

# Obscured vs Unobscured SF

UV emission



Recombination Lines

(Ly $\alpha$ , H $\alpha$ , P $\alpha$ )

Thermal emission  
from warm dust

# Obscured vs Unobscured SF

Total SF requires “counting” all photons from O-stars.

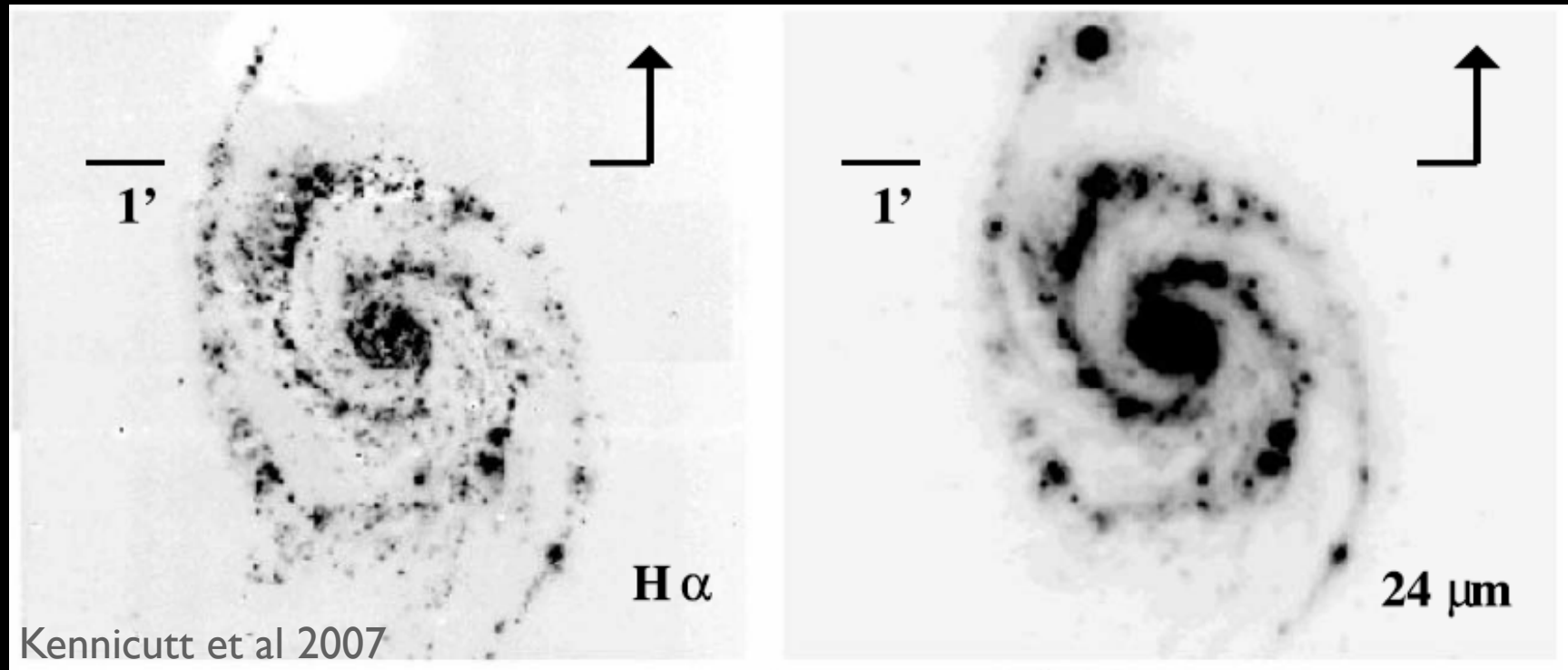


Need to “correct” the luminosity of SF tracers to include flux that would have been observed without dust

$$L_{\text{UV}}(\text{corr}) = L_{\text{UV}}(\text{observed}) + \eta L_{\text{IR}}$$

Note:  $\eta$  is a number that has to be calibrated, because it is not known from first principles.  
72

# Example prescription:



a first approximation, the amount of extinguished H $\alpha$  radiation should scale with the luminosity reradiated in the infrared,

$$L(\text{H}\alpha)_{\text{corr}} = L(\text{H}\alpha)_{\text{obs}} + aL(24) \quad (4)$$

# Summary of corrections:

**Table 2 Multiwavelength dust corrections for normal galaxies**

Composite tracer	Reference
$L(\text{FUV})_{\text{corr}} = L(\text{FUV})_{\text{obs}} + 0.46 L(\text{TIR})$	Hao et al. (2011)
$L(\text{FUV})_{\text{corr}} = L(\text{FUV})_{\text{obs}} + 3.89 L(25 \mu\text{m})$	Hao et al. (2011)
$L(\text{FUV})_{\text{corr}} = L(\text{FUV})_{\text{obs}} + 7.2 \times 10^{14} L(1.4 \text{ GHz})^{\text{a}}$	Hao et al. (2011)
$L(\text{NUV})_{\text{corr}} = L(\text{NUV})_{\text{obs}} + 0.27 L(\text{TIR})$	Hao et al. (2011)
$L(\text{NUV})_{\text{corr}} = L(\text{NUV})_{\text{obs}} + 2.26 L(25 \mu\text{m})$	Hao et al. (2011)
$L(\text{NUV})_{\text{corr}} = L(\text{NUV})_{\text{obs}} + 4.2 \times 10^{14} L(1.4 \text{ GHz})^{\text{a}}$	Hao et al. (2011)
$L(\text{H}\alpha)_{\text{corr}} = L(\text{H}\alpha)_{\text{obs}} + 0.0024 L(\text{TIR})$	Kennicutt et al. (2009)
$L(\text{H}\alpha)_{\text{corr}} = L(\text{H}\alpha)_{\text{obs}} + 0.020 L(25 \mu\text{m})$	Kennicutt et al. (2009)
$L(\text{H}\alpha)_{\text{corr}} = L(\text{H}\alpha)_{\text{obs}} + 0.011 L(8 \mu\text{m})$	Kennicutt et al. (2009)
$L(\text{H}\alpha)_{\text{corr}} = L(\text{H}\alpha)_{\text{obs}} + 0.39 \times 10^{13} L(1.4 \text{ GHz})^{\text{a}}$	Kennicutt et al. (2009)

<sup>a</sup>Radio luminosity in units of ergs s<sup>-1</sup> Hz<sup>-1</sup>.

Abbreviations: FUV, far ultraviolet; NUV, near ultraviolet; TIR, total infrared.

See updated relations in Boquien et al 2016

# Summary of corrections:

**Table 1.** SFR estimators.

Monochromatic				
Band	$\log C_{\text{band}}$	k	Method	Reference
FUV	-36.355	1.0000	Theoretical <sup>a</sup>	1
H $\alpha$	-34.270	1.0000	Theoretical <sup>a</sup>	1
24 $\mu\text{m}$	-29.134	0.8104	H $\alpha$ <sup>b</sup>	2
70 $\mu\text{m}$	-29.274	0.8117	H $\alpha$ <sup>b</sup>	3
100 $\mu\text{m}$	-37.370	1.0384	H $\alpha$ <sup>b</sup>	3
Hybrid				
Band	$\log C_{\text{band1}}$	$k_{\text{band1-band2}}$	Method	Reference
H $\alpha$ +24 $\mu\text{m}$	-34.270	0.031	H $\alpha$ <sup>b</sup>	2
FUV+24 $\mu\text{m}$	-36.355	6.175	H $\alpha$ +24 $\mu\text{m}$	4

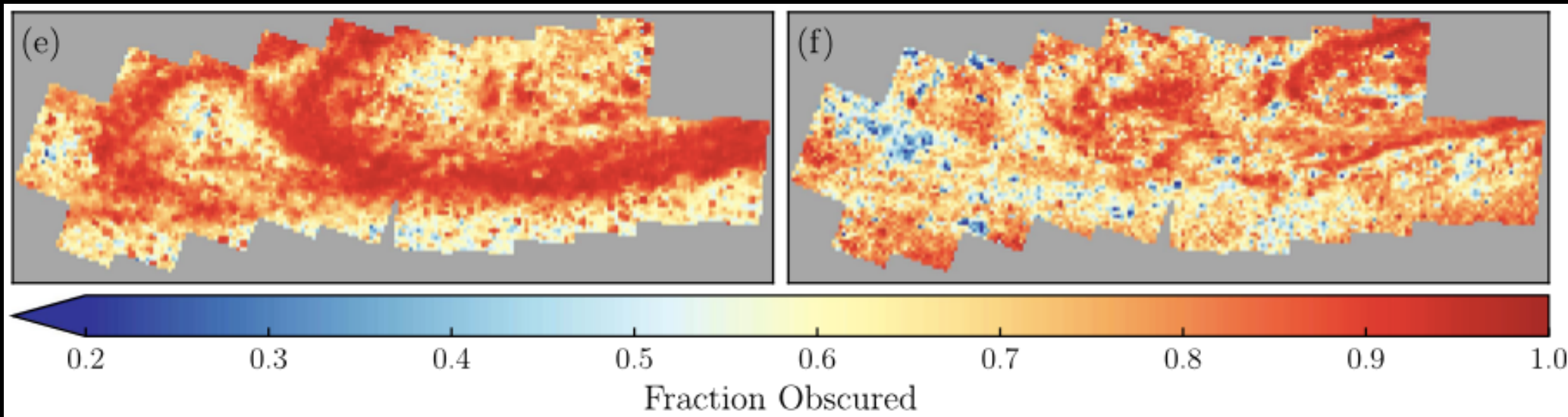
**References.** (1) Murphy et al. (2011), (2) Calzetti et al. (2007), (3) Li et al. (2013), (4) Leroy et al. (2008)

**Notes.** Monochromatic:  $\log \Sigma\text{SFR} = \log C_{\text{band}} + k \times \log S_{\text{band}}$ ; Hybrid:  $\log \Sigma\text{SFR} = \log C_{\text{band1}} + \log [S_{\text{band1}} + k_{\text{band1-band2}} \times S_{\text{band2}}]$ , with  $\Sigma\text{SFR}$  in  $M_{\odot} \text{ yr}^{-1} \text{ kpc}^{-2}$ , S defined as  $\nu S_{\nu}$  in  $\text{W kpc}^{-2}$ , and C in  $M_{\odot} \text{ yr}^{-1} \text{ W}^{-1}$ .

Empirical estimators have been calibrated on individual star-forming regions on typical scales of the order of  $\sim 200\text{--}500 \text{ pc}$ .

<sup>a</sup> Based on Starburst99 (Leitherer et al. 1999). <sup>b</sup> Extinction corrected, calibrated against near-infrared hydrogen recombinations lines (e.g., Pa $\alpha$  or Br $\gamma$ ).

# Corrections for obscured star formation are useful but break down in detail



True obscured fraction  
from CMD analysis

Obscured fraction  
from FUV+24 $\mu$

# What fraction of star formation is obscured?

Can characterize with

$$\text{IRX} = \log \left( \frac{L(\text{TIR})}{L(\text{FUV})_{\text{obs}}} \right)$$

$L(\text{TIR})$  = “Total” IR luminosity

(Defined assuming you have measurements of mid- and far-IR dust emission across several broad wavelengths)

High IRX = More obscured SF

e.g., Spitzer (SIRTF)

Def'n from Dale & Helou 2002;

alternative definitions appropriate for Herschel, ALMA, etc exist.

A simple combination of *SIRTF* Multiband Imaging Photometer fluxes recovers the total 3–1100  $\mu\text{m}$  flux (TIR) for the full range of normal galaxy infrared SED shapes,

$$L_{\text{TIR}} = \zeta_1 \nu L_\nu(24 \mu\text{m}) + \zeta_2 \nu L_\nu(70 \mu\text{m}) + \zeta_3 \nu L_\nu(160 \mu\text{m}) ,$$

where  $[\zeta_1, \zeta_2, \zeta_3] = [1.559, 0.7686, 1.347]$  for  $z = 0$ .

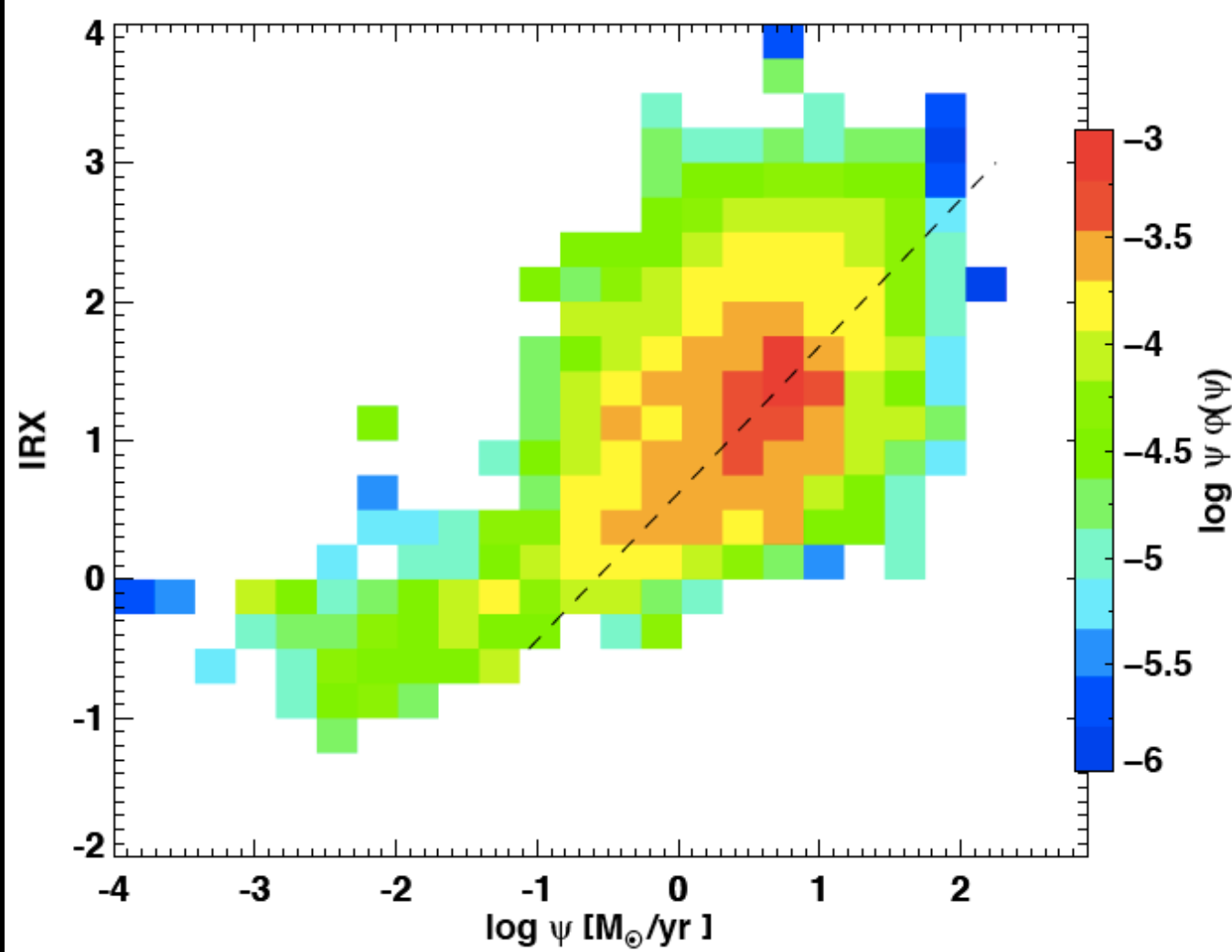


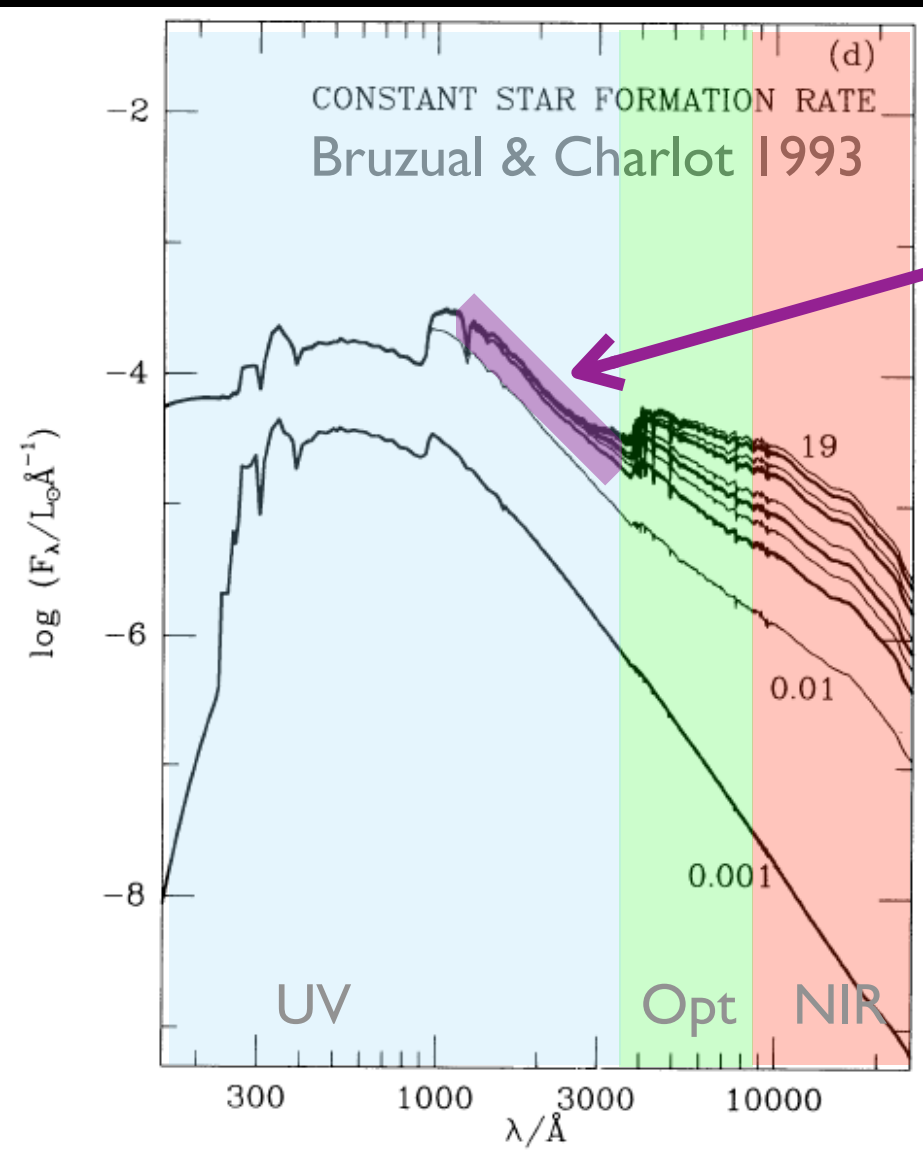
**Figure 10.** The star formation rate volume density function as a function of SFR (Fig. 5), further expanded in a second dimension (along the ordinate) to show the breakdown with IRX. The ‘z’ axis represents  $\psi \Phi(\psi)$ . The dotted line shows the IRX-SFR relationship derived from the LIR vs.  $E(B-V)$  relationship given by Hopkins et al. (2001).  $E(B-V)$  was converted into  $A_{FUV}$  using the Cardelli (1989) extinction law with  $R_V = 3.1$ , which gives  $A_{FUV} = 8.0 E(B-V)$ . IRX and  $\psi$  were obtained from  $A_{FUV}$  and LIR as above.

Bothwell et al 2011

IRX increases  
with SFR:  
More  
obscuration  
when SFR is high

- Highest SFRs occur in deeply embedded regions of molecular clouds?
- Highest SFRs occur in most massive galaxies w/ high metallicities and thus more dust?

# Test by comparing to UV slope



For a constant SFR, the slope of the spectrum in the UV is nearly constant as well (at fixed metallicity)

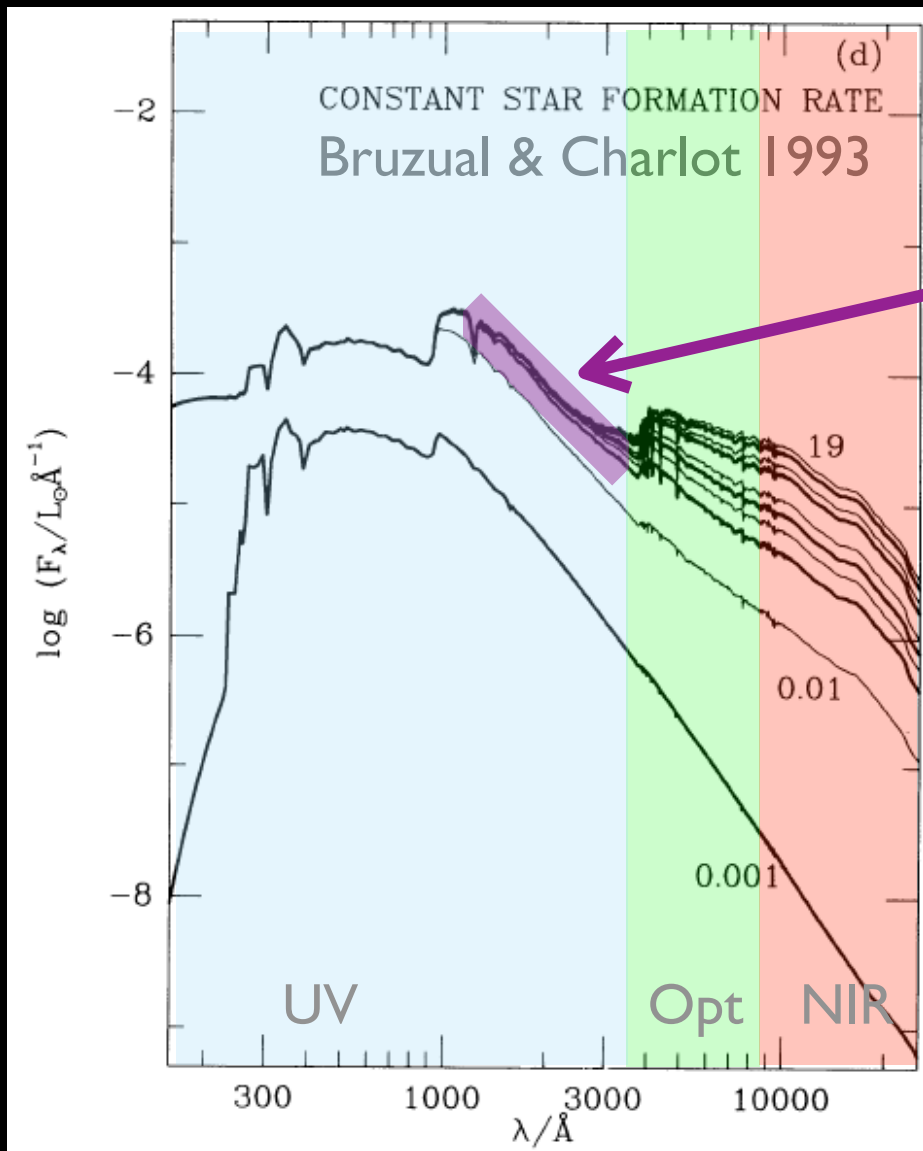
Dust reddening changes the apparent UV spectral slope

No reddening: flux *falls* towards red

Some reddening: flux flat with λ

High reddening: flux *rises* towards red

# Characterize UV slope with $\beta$

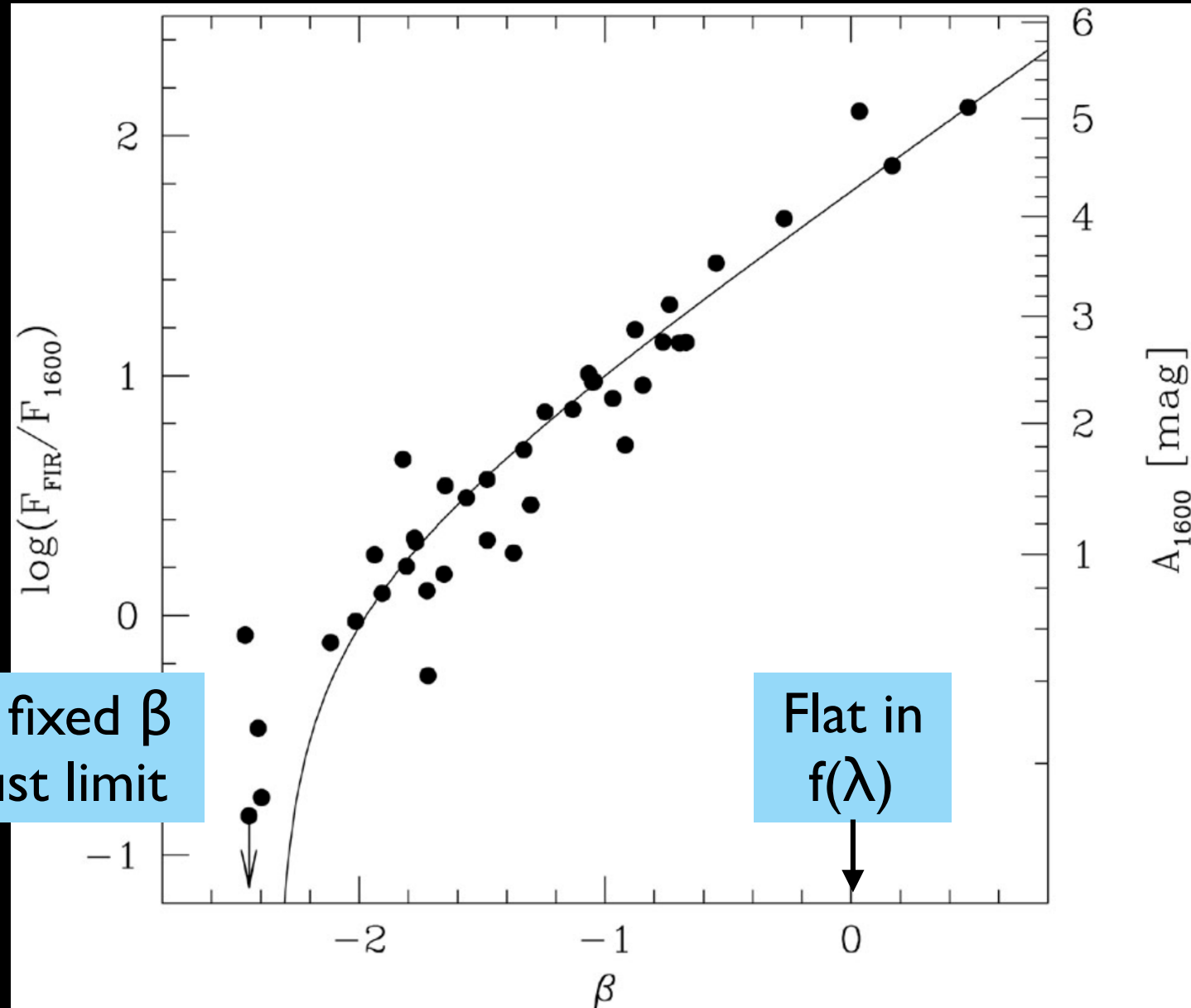


Define  $\beta$  such that  
flux  $\sim \lambda^\beta$   
(over some wavelength range)

No reddening:  $\beta < 0$   
Some reddening:  $\beta = 0$   
High reddening:  $\beta > 0$

Note: IRX is about *attenuation*, but UV slope is about *reddening*!  
Also: ratio of GALEX FUV/NUV is sometimes a proxy for  $\beta$

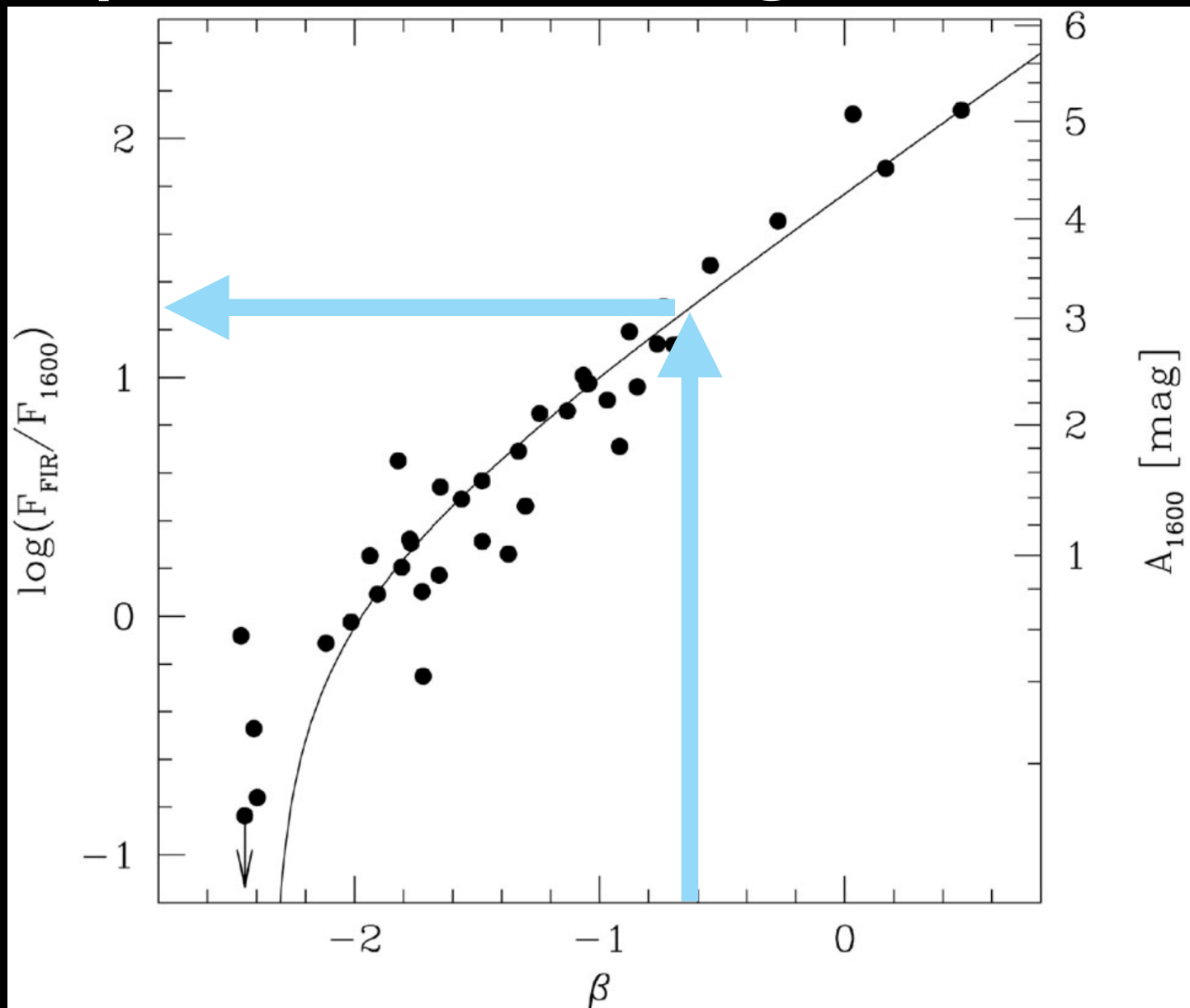
# In local starbursts, IRX increases w/ $\beta$



Sometimes IRX translated into “magnitudes of attenuation at a fiducial UV wavelength”; see Buat et al 2005

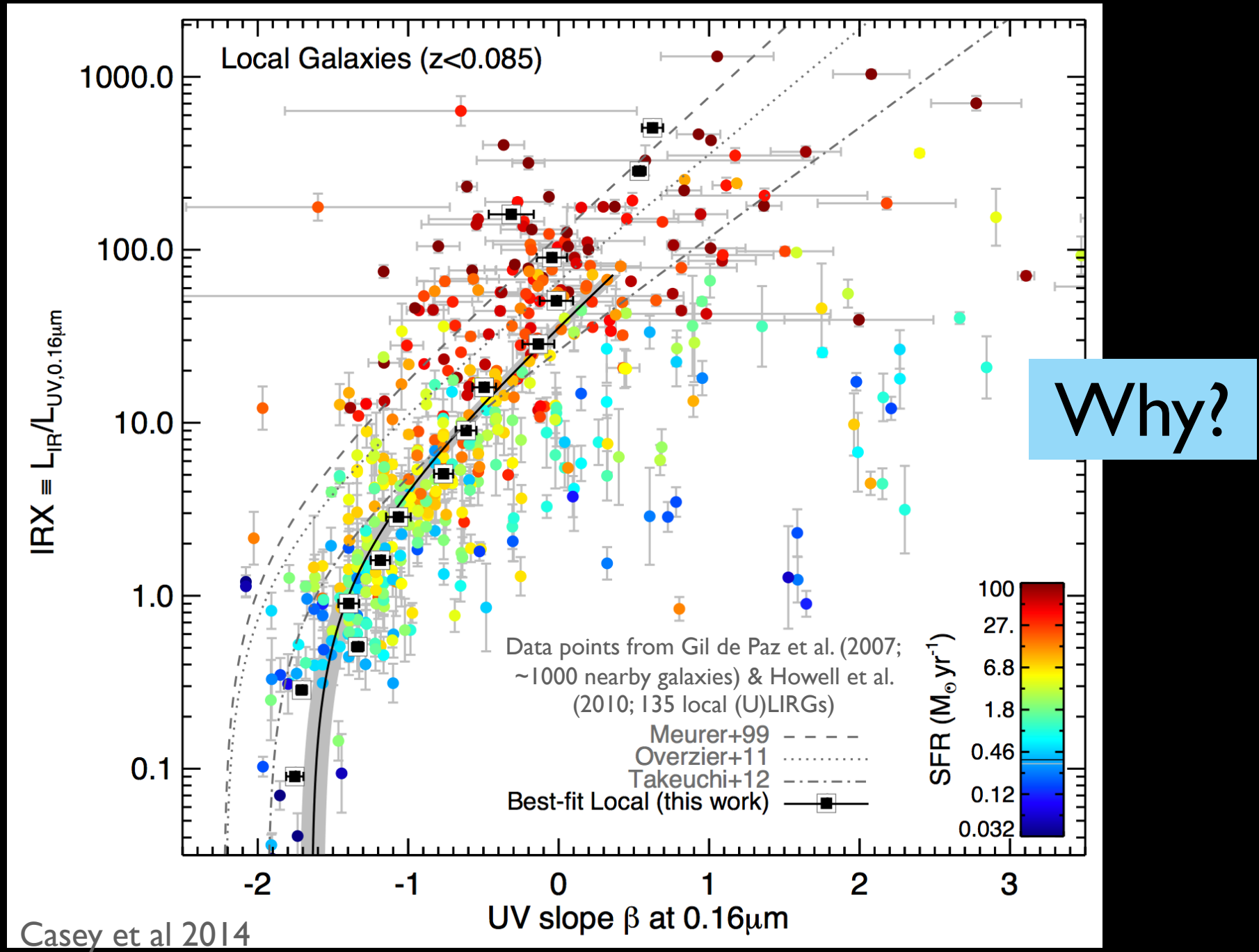
Original result from Meurer et al 1999,  
for UV bright SF galaxies with only modest dust

# Super useful at high redshift



At high  $z$ , the UV moves into the optical and NIR.  
Measure  $\beta$  to infer “correction” to measured UV flux

# But, broader samples = messier IRX- $\beta$ correlation



# Change to slope depends on the amount of dust & the extinction law

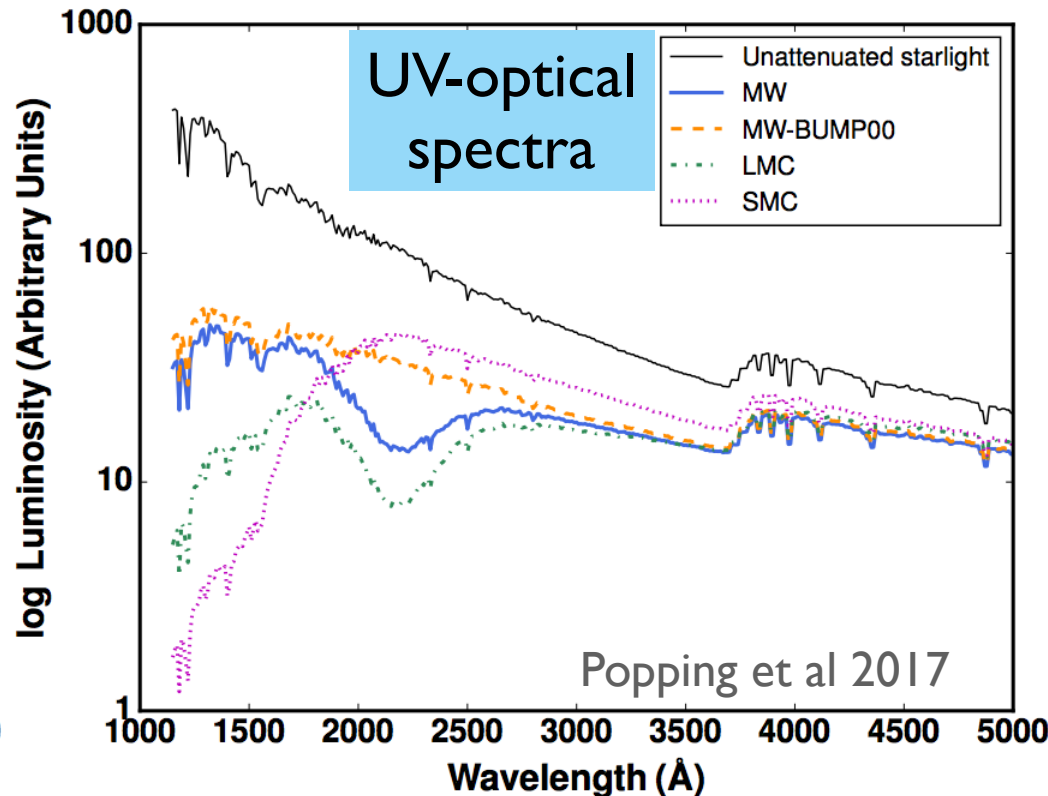
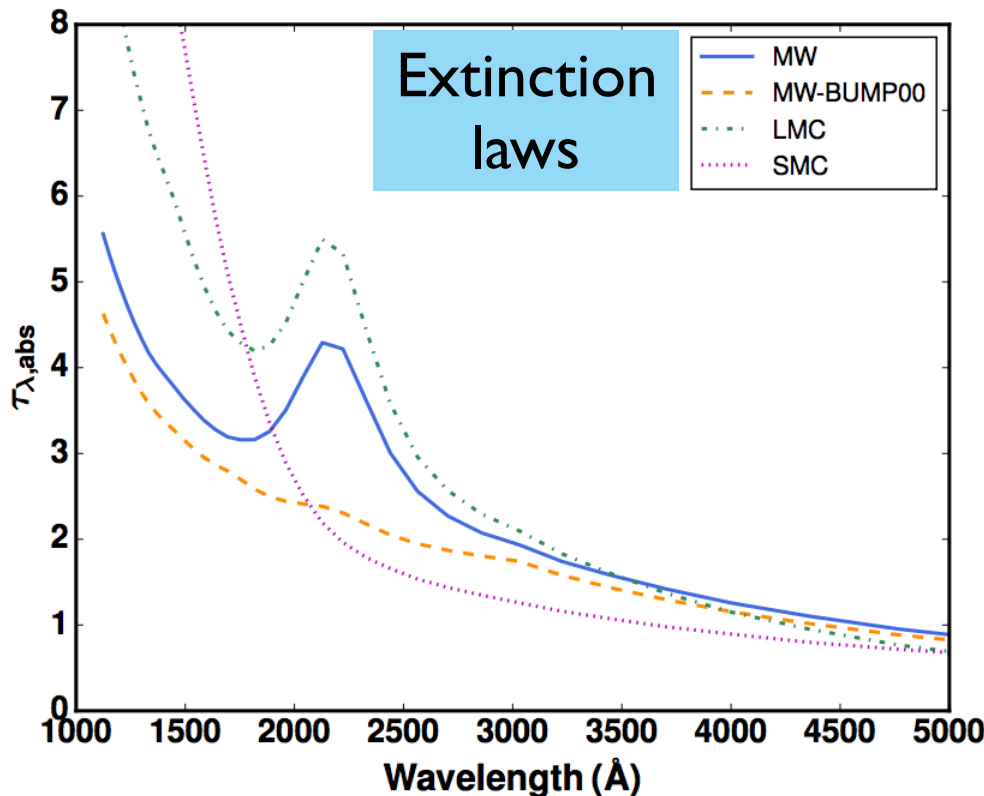


**Figure 1.** Left: The dust extinction curves applied in this work for a mean homogeneous optical depth in the V band of one ( $\langle \tau_V \rangle = 1$ ) and assuming a uniform medium ( $M = 0$ ) and  $R_s/R_d = 0$ . Right: The unobscured (black) and obscured (coloured) stellar emission spectra of a single burst population with an age of 10 Myr and solar metallicity. The obscured spectra are based on the attenuation curves shown in the left panel.

Effect of I optical depth of extinction in the V-band

# Different attenuation curves produce different $\text{IRX}-\beta$

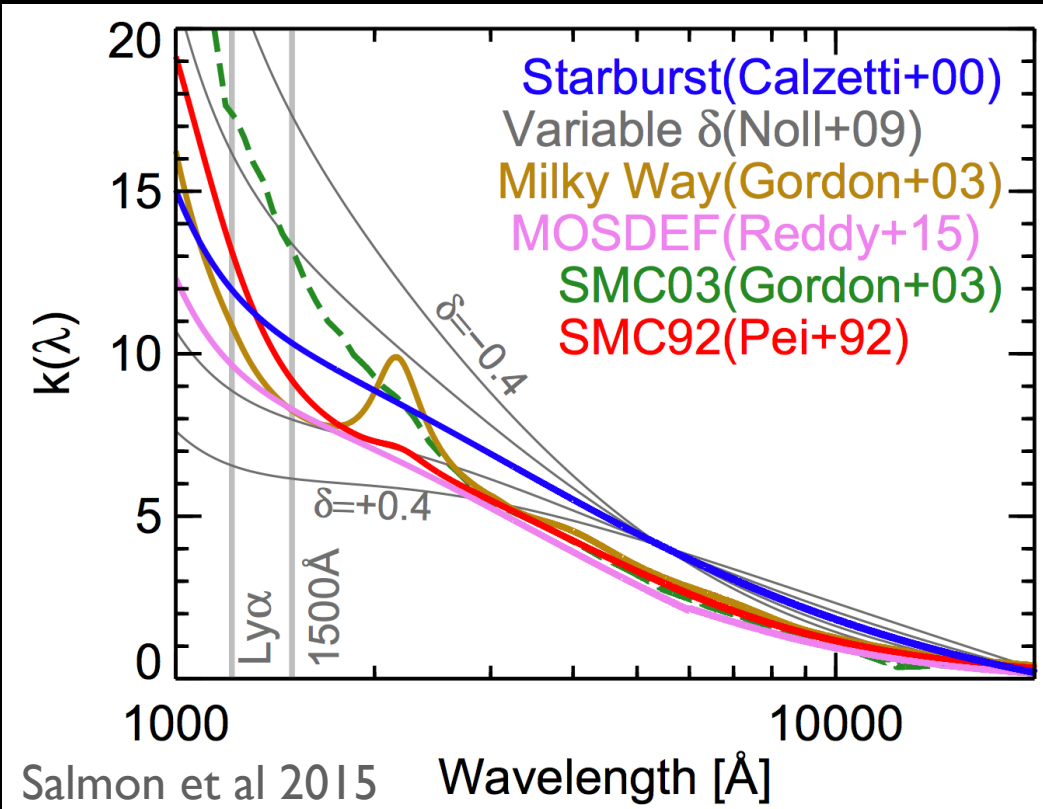


**Figure 2.** A variety of common dust laws shown by their total-to-selective extinction or attenuation as a function of wavelength. The Pei (1992) derivation of the SMC extinction (red, SMC92) will be used in this work to compare to the starburst prescription derived by Calzetti et al. (2000) (blue). Other dust laws are also shown including the MOSDEF (pink) attenuation curve derived from  $z \sim 2$  galaxies (Reddy et al. 2015), and the Milky Way (green) and SMC (SM03, black dashed) extinction curves derived by Gordon et al. (2003). In addition, we consider a power-law deviation to the starburst curve by Equation 7 to be more ( $+\delta$ ) or less ( $-\delta$ ) grey. The wavelengths of 1500 Å and the Lyman  $\alpha$  emission line are shown for reference.

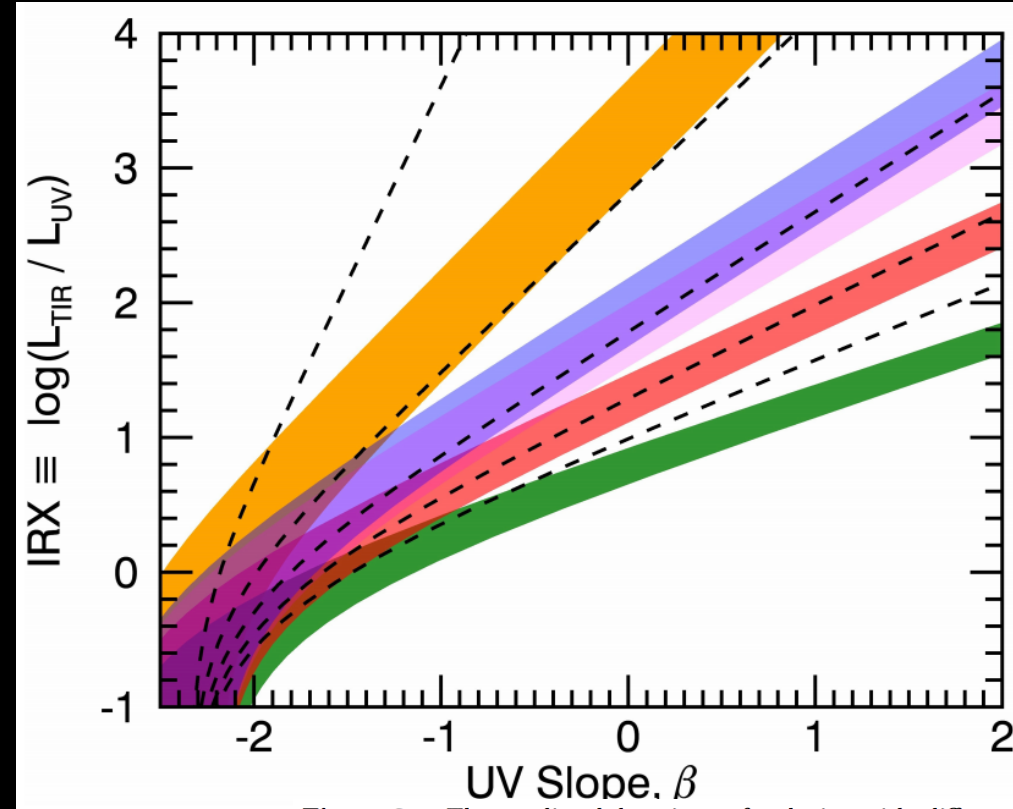
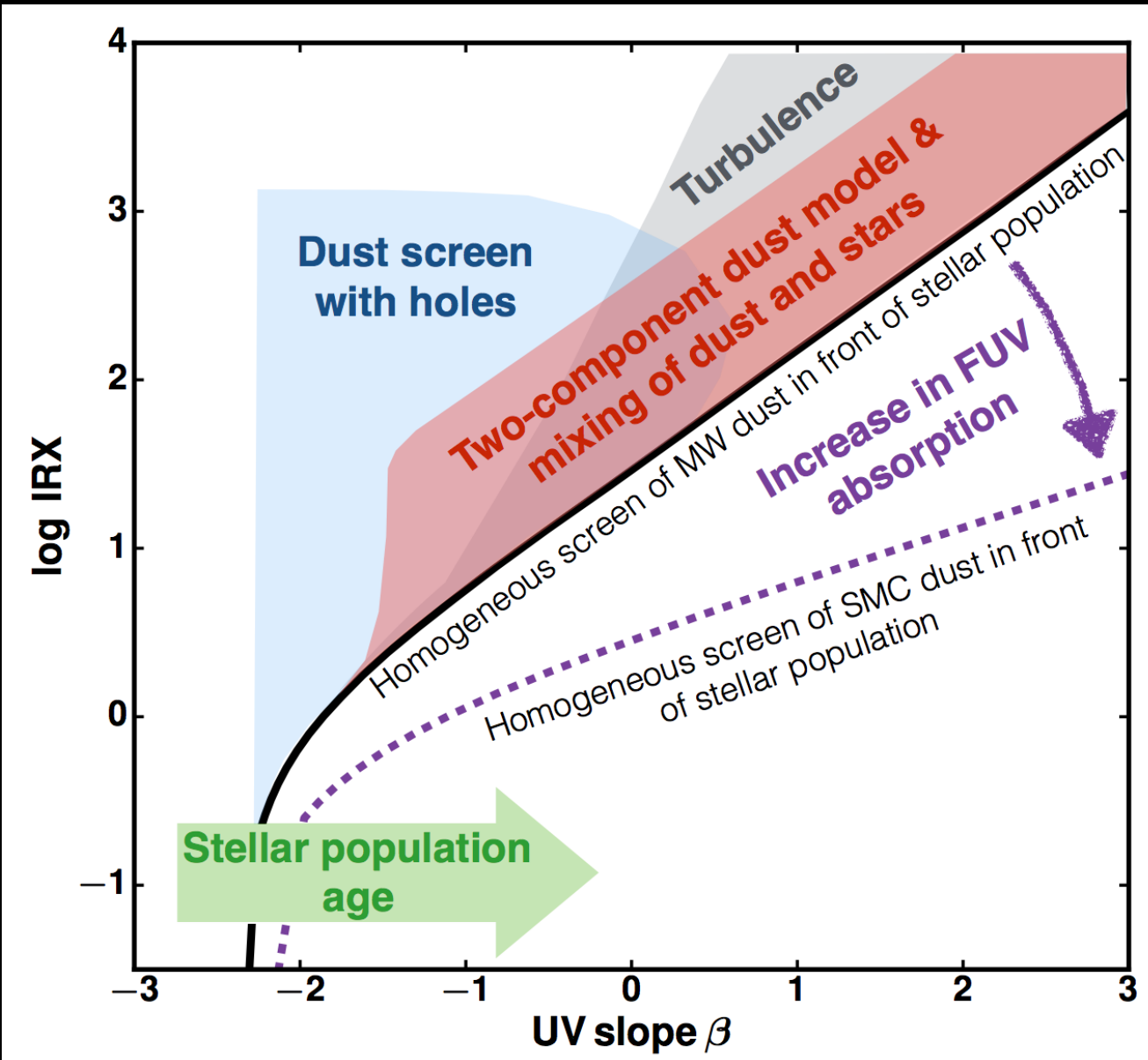


**Figure 3.** The predicted locations of galaxies with different dust laws on the plane of the UV slope  $\beta$  and infrared excess ( $L_{\text{TIR}}/L_{\text{UV}}$ ). The colored swaths correspond to the same dust laws as in Figure 2, clockwise from top left: Milky Way, starburst, MOSDEF, SMC92, and SMC03. The width of each  $\text{IRX} - \beta$  relation accounts for the scatter in the intrinsic  $\beta$  from the effects of stellar population age (50 Myr to 1 Gyr), SFH ( $SFR \sim e^{-t/\tau}$ , with  $1 \text{ Gyr} < \tau < 100 \text{ Gyr}$ ), and metallicity ( $0.02 Z_{\odot} < Z < 2.5 Z_{\odot}$ ). The dashed lines show the relations according to the parameterized dust law (see §5) with (clockwise from left)  $\delta = +0.4, +0.2, 0.0, -0.2$ , and  $-0.4$ .

# Dust geometry, stellar population also matters



# Obscured SF Questions

- How do we best correct for obscured SF, at any redshift?
- What physics produces scatter in  $\text{IRX}-\beta$  relation?
- What drives correlation between  $\text{IRX}$  and  $\text{SFR}$ ?
- What is the appropriate dust attenuation law for integrated galaxy fluxes, for different galaxy types & redshifts?
- What does the above tell us about the sites of SF?

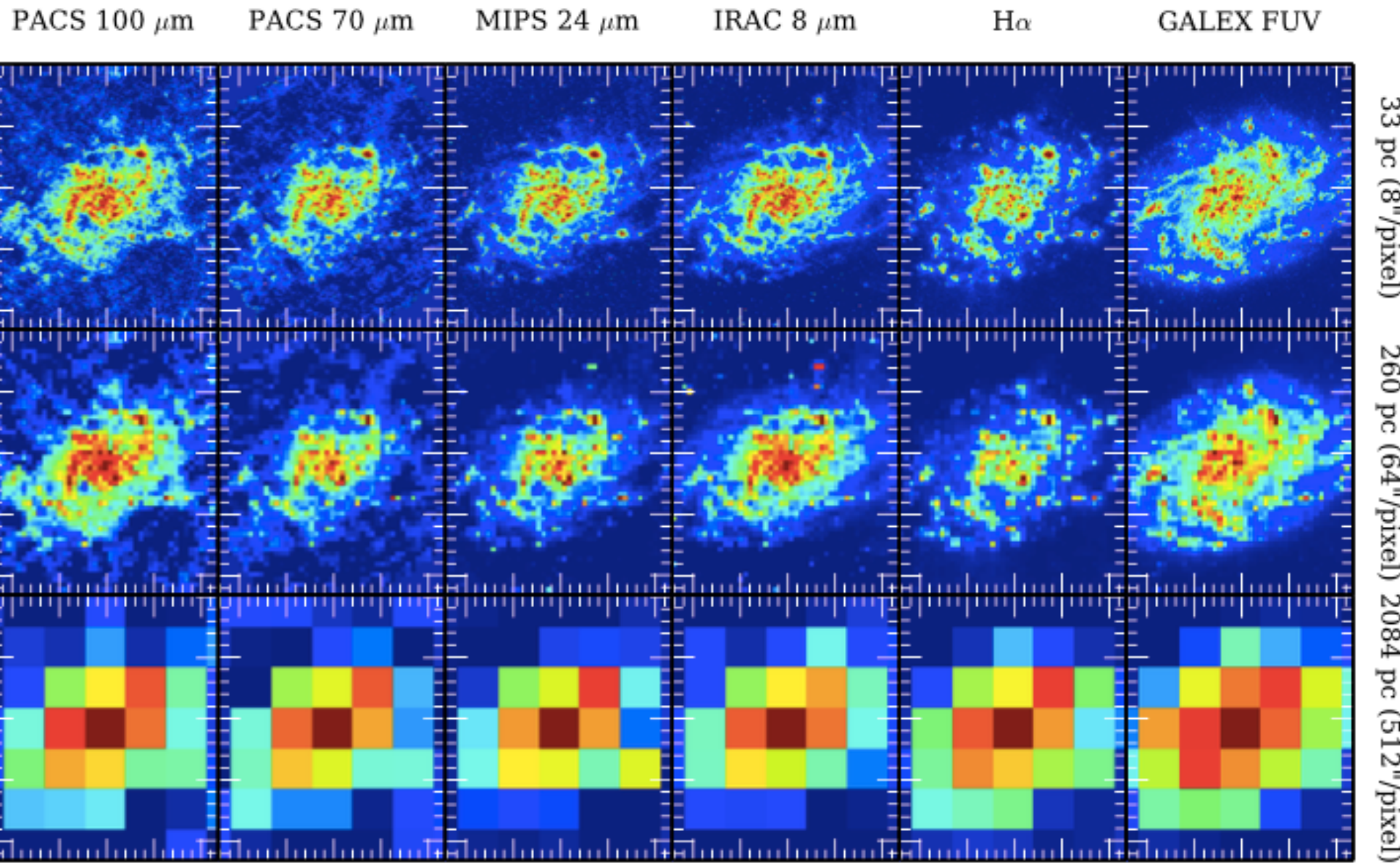
Over what physical scales are SFR  
tracers valid?

# Major issue

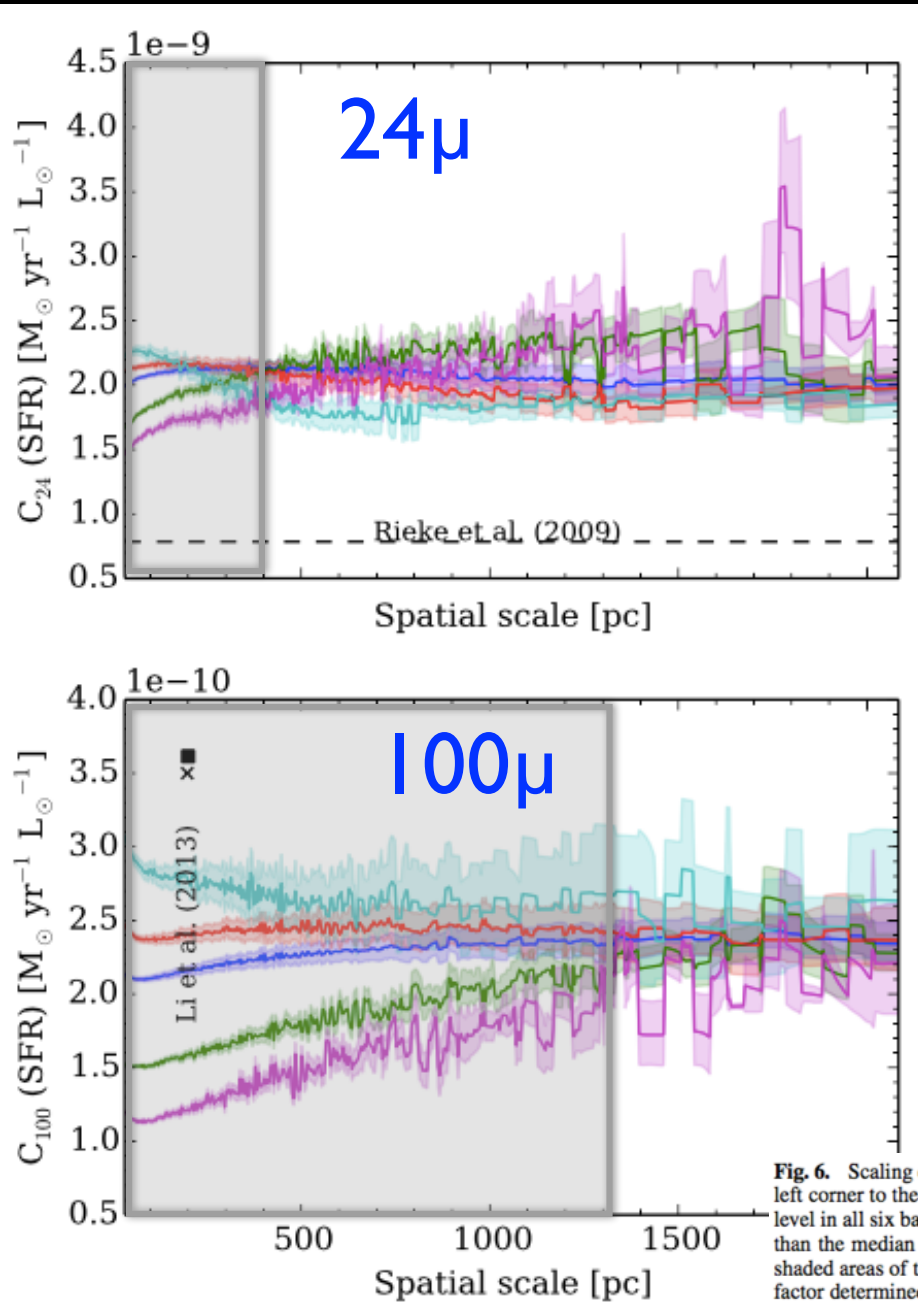


The closer you get to the scale of individual SF regions, the more scaling laws will break down.

# Example of SFRs vs scale (in M33)



# Example of SFRs vs scale (in M33)

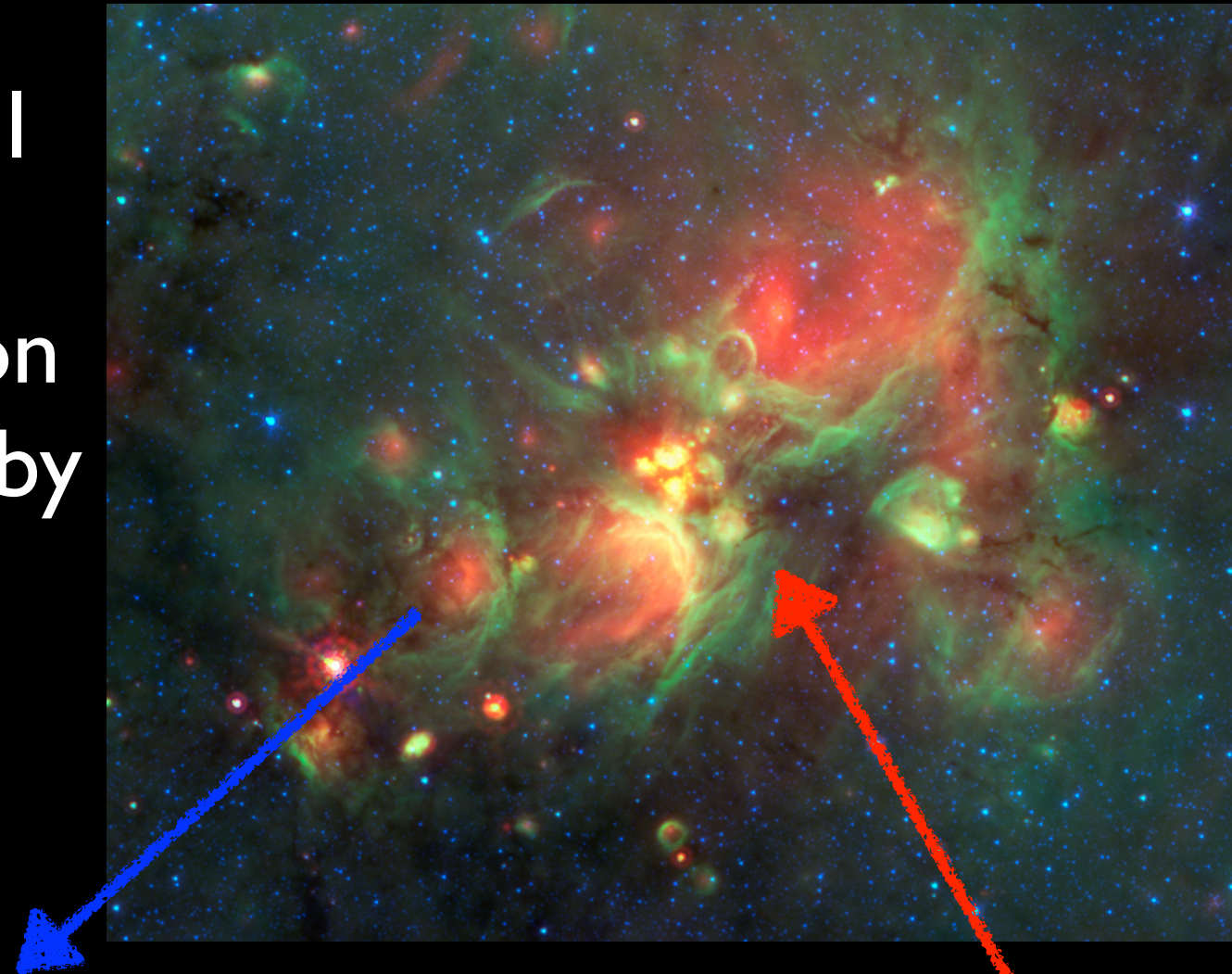


- Inferred SFR does not converge until 0.1-1.5 kpc scales are reached
- Different behavior w/ different SFR tracers

**Fig. 6.** Scaling coefficients from the luminosity in infrared bands to  $\Sigma\text{SFR}$  versus the pixel size, at  $8\mu\text{m}$ ,  $24\mu\text{m}$ ,  $70\mu\text{m}$ , and  $100\mu\text{m}$ , from the top left corner to the bottom right corner. The blue line indicates the value of the scaling factor when taking into account all pixels detected at a  $3-\sigma$  level in all six bands. The red (respectively green) line indicates the scaling factor when considering only pixels with a  $\Sigma\text{SFR}$  higher (resp. lower) than the median  $\Sigma\text{SFR}$  at a given resolution. The cyan and magenta lines represent regions in the top and bottom 15% in terms of  $\Sigma\text{SFR}$ . The shaded areas of the corresponding colours indicate the  $1-\sigma$  uncertainties. The horizontal dashed line at  $24\mu\text{m}$  (resp.  $70\mu\text{m}$ ) indicates the scaling factor determined by Rieke et al. (2009) (resp. Calzetti et al. 2010) for entire galaxies. The crosses for the  $70\mu\text{m}$  and  $100\mu\text{m}$  bands indicate the scaling factor determined for individual galaxies at a scale of 200 pc (Li et al. 2013) and 700 pc (Li et al. 2010). The squares indicate mean values over several galaxies. The empty squares denote that no background subtraction was performed.

# Why do things break down?

Not all  
dust  
emission  
heated by  
SF



UV emission  
escapes

SFR not  
constant

Not all SF is in form  
of massive stars

# Global Measures of Star Formation & Basic Trends in Galaxy Population

# Different measures of star formation

- Star formation rates (SFR)
- Specific star formation rates (sSFR)
- Star Formation intensity ( $\Sigma_{\text{SFR}}$ )
- Star Formation efficiency

## Different meanings & utilities

# I. Total Star Formation Rates

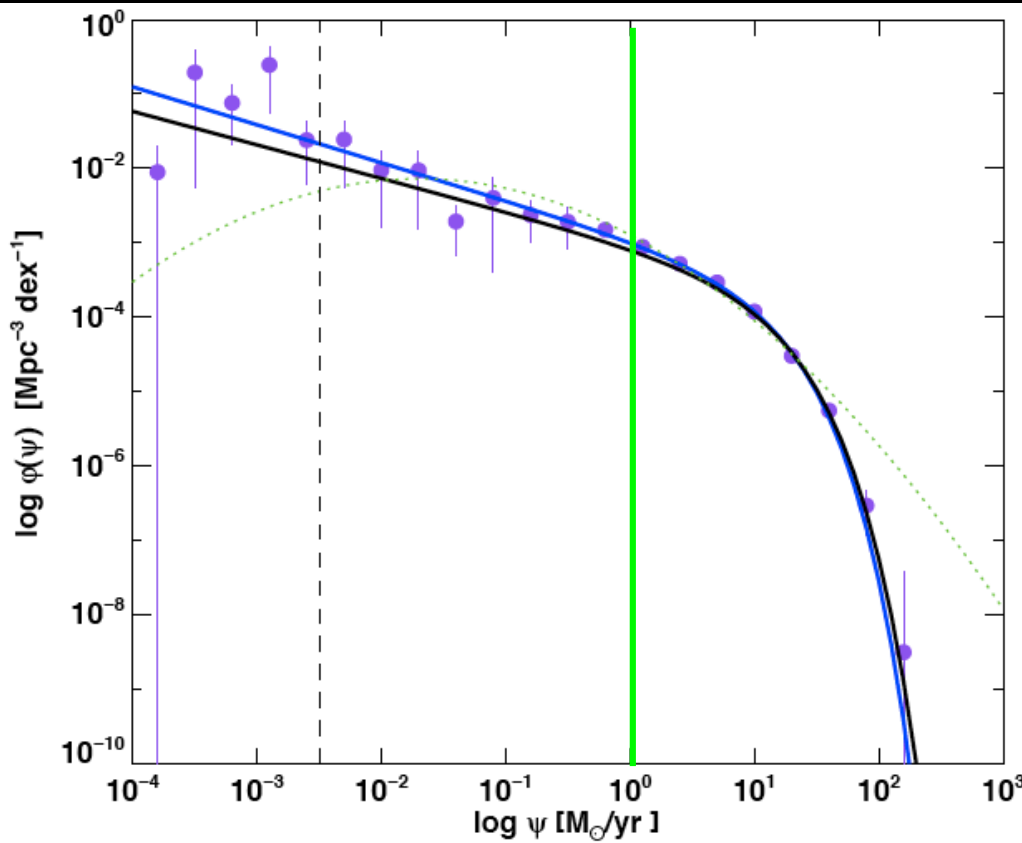


**Figure 4.** The star formation rate distribution function for the resultant combined sample, as described in §3.3. The black line is a least squares Schechter function fit to these points, the blue line is the maximum likelihood Schechter function fit. The vertical dashed line is drawn at  $\log \text{SFR} = -2.5 \text{ M}_\odot \text{ yr}^{-1}$ , the level at which incompleteness becomes significant. The green log-normal function indicates the SFR function given by Martin et al. (2005). Errors ( $1\sigma$ ) were calculated using Monte Carlo bootstrapping.

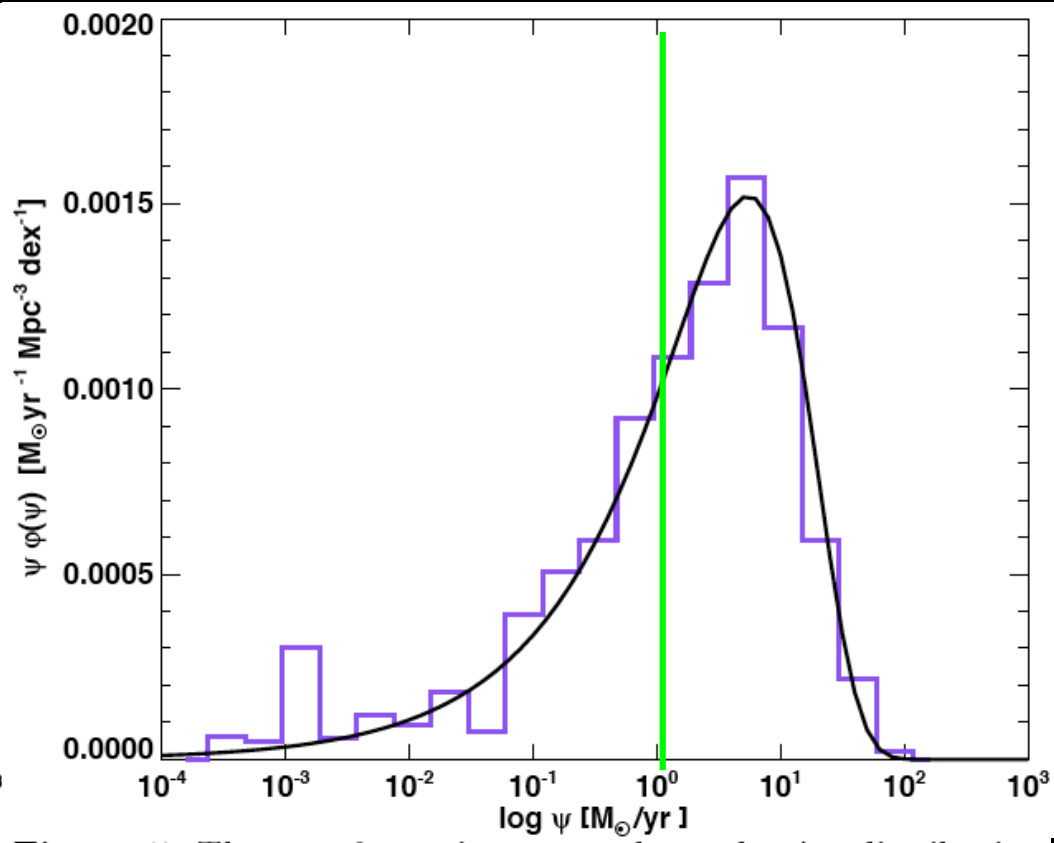


**Figure 5.** The star formation rate volume density distribution function, for the resultant combined sample as in Fig. 4. The purple histogram shows the  $V_{\max}$ -derived data as above, and the black fit to the data is the convolved Schechter function  $\psi \Phi(\psi)$ , with the maximum-likelihood fit parameters as above.

Bothwell et al 2011

Most galaxies have low SFRs (<1  $M_\odot/\text{yr}$ ), but integrated SFR dominated by galaxies with  $\sim 10 M_\odot/\text{yr}$  of SF.

# I. SFR: Increases with Stellar Mass

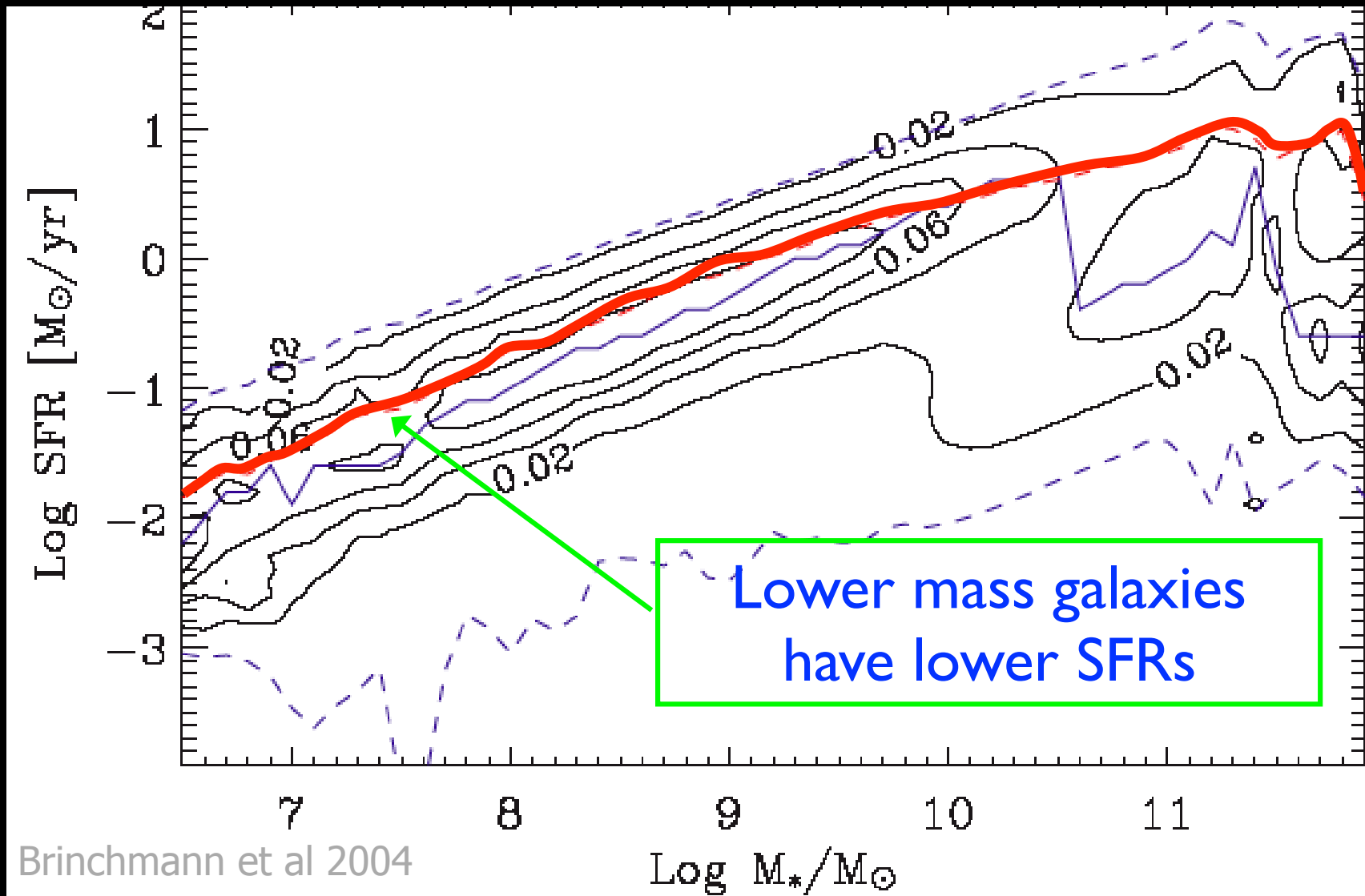
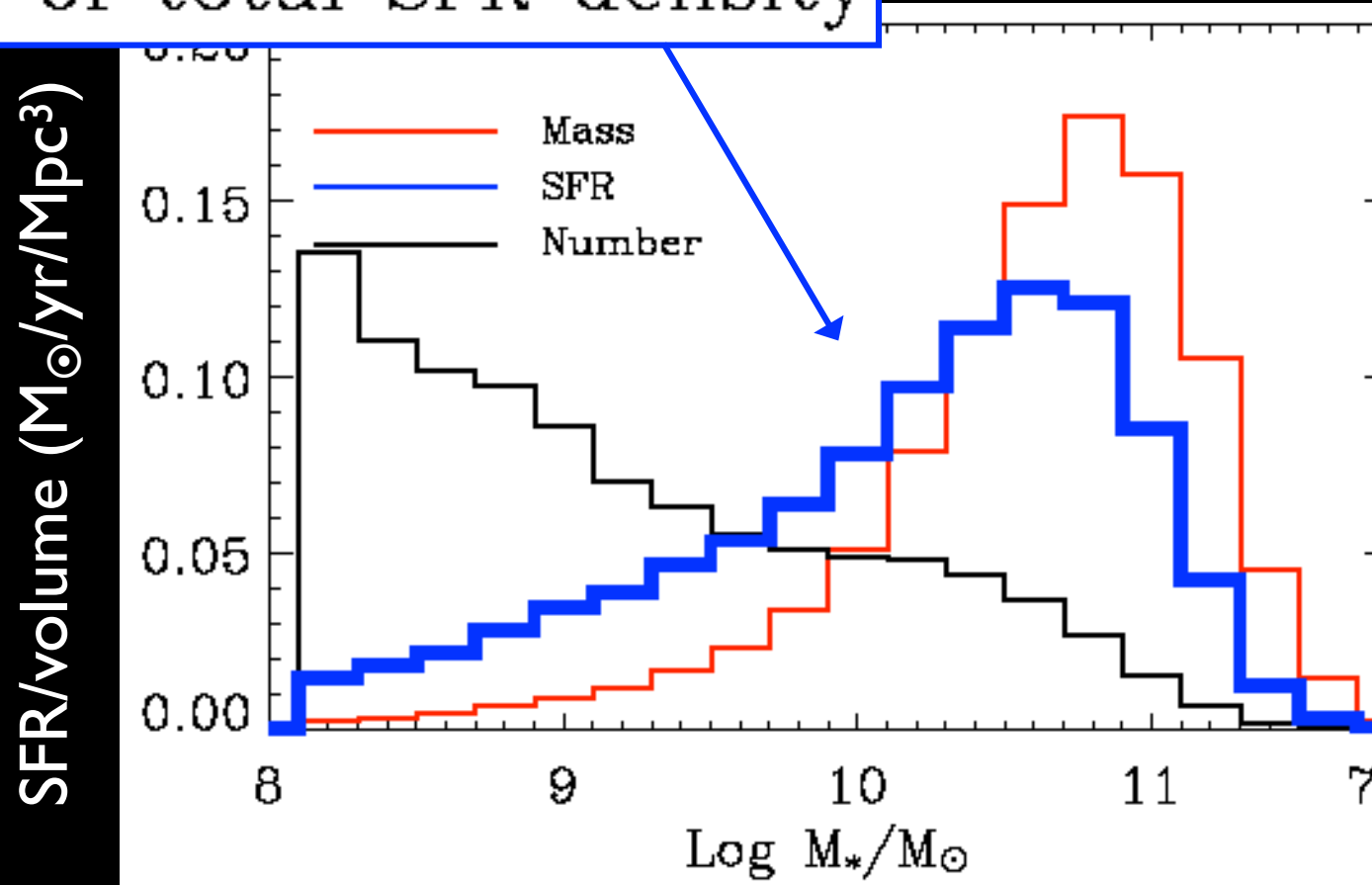


Figure 17. The relationship between the stellar mass and the SFR (both inside the fibre) for all galaxies with no AGN contribution. The figure has been volume weighted and normalized in bins of stellar mass. The contours are therefore showing the conditional likelihood of SFR given a stellar mass. The bin size is  $0.1 \times 0.1$  in the units given in the plot. The red line shows the average at a given stellar mass, whereas the blue line shows the mode of the distribution. The dashed lines show the limits containing 95 per cent of the galaxies at a given stellar mass.

But, bigger things are bigger,  
so not profound...

(calculated within SDSS fibers)

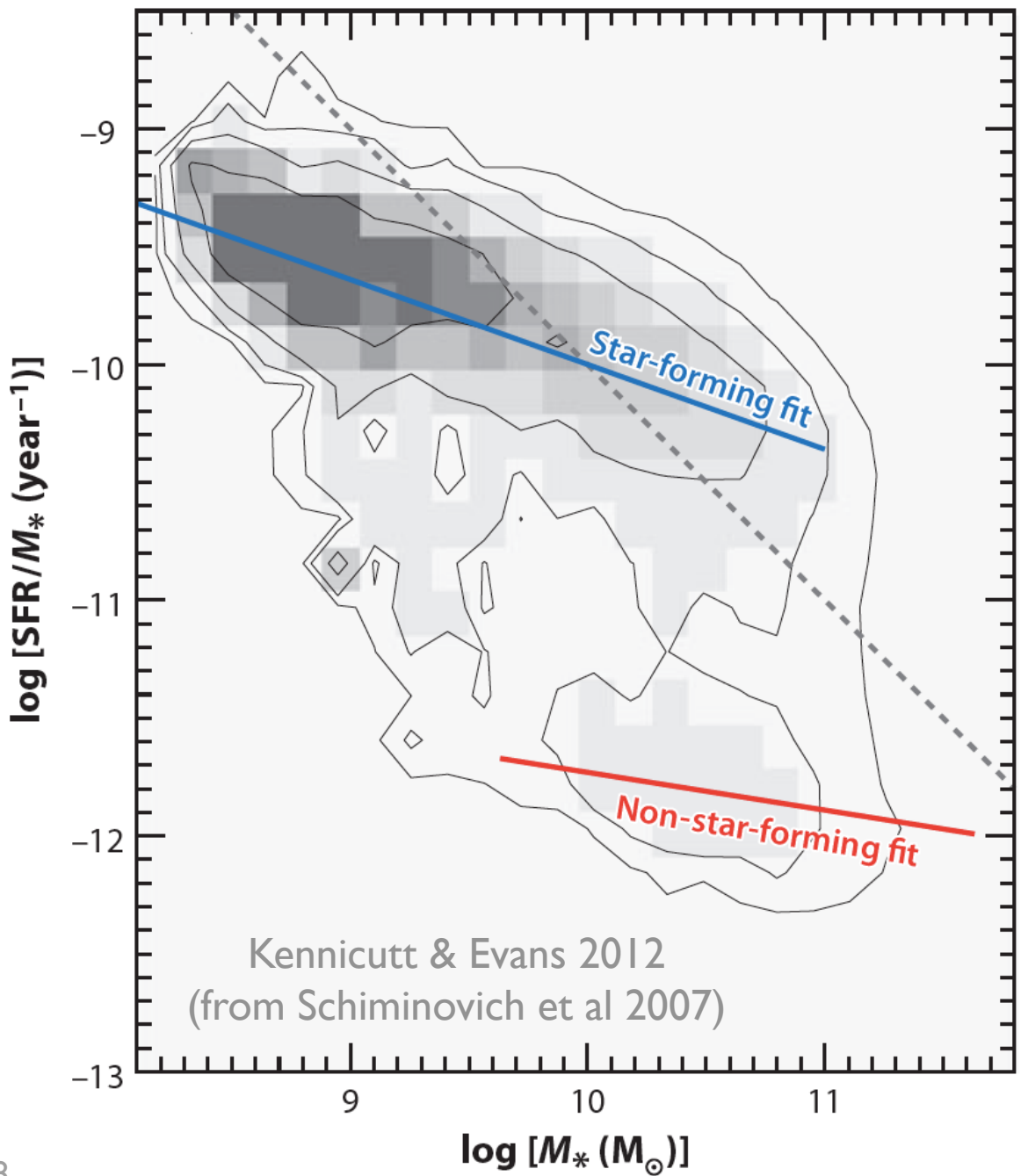
# Fraction of total SFR density



**Figure 20.** The contribution to the total number, mass and star formation density as a function of various galaxy parameters. The SF density is shown in blue, the mass density in red and the number density in black. *Top left:* The contribution to the different densities as a function of the concentration of the galaxies. *Top right:* The same, but as a function of the half-light radii of the galaxies. *Lower left:* The density contributions as a function of log stellar mass and *Lower right:* The contributions as a function of log of the stellar surface density in  $M_\odot/\text{kpc}^2$

Massive galaxies dominate the current production of stars, since they own most of the baryons

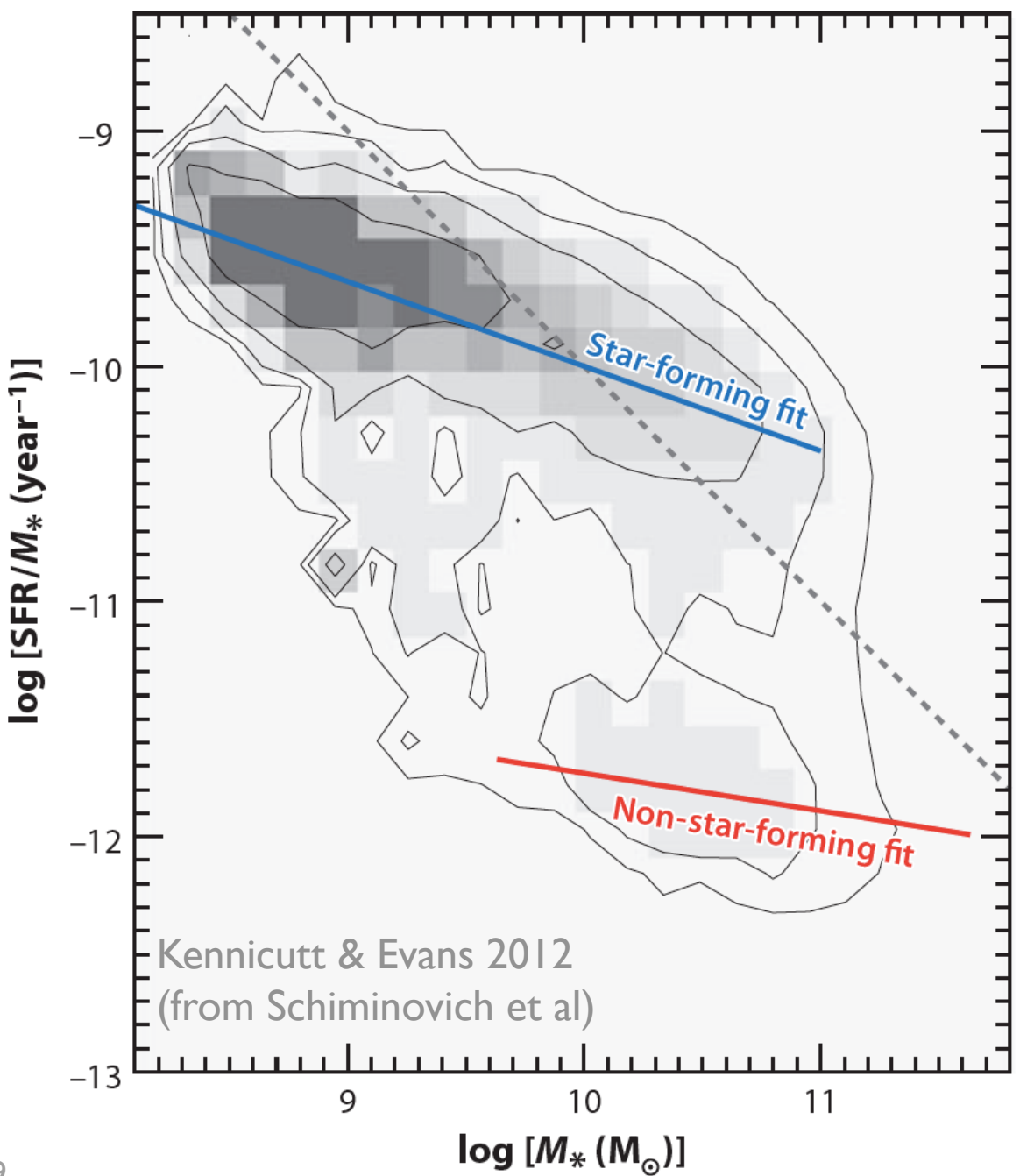
## 2. Specific SFR = SFR / stellar mass



Relative importance of current to past SF

Units of inverse time (i.e., How long would it take to make the current stellar mass, at the current SFR)

## 2. sSFR shows two sequences



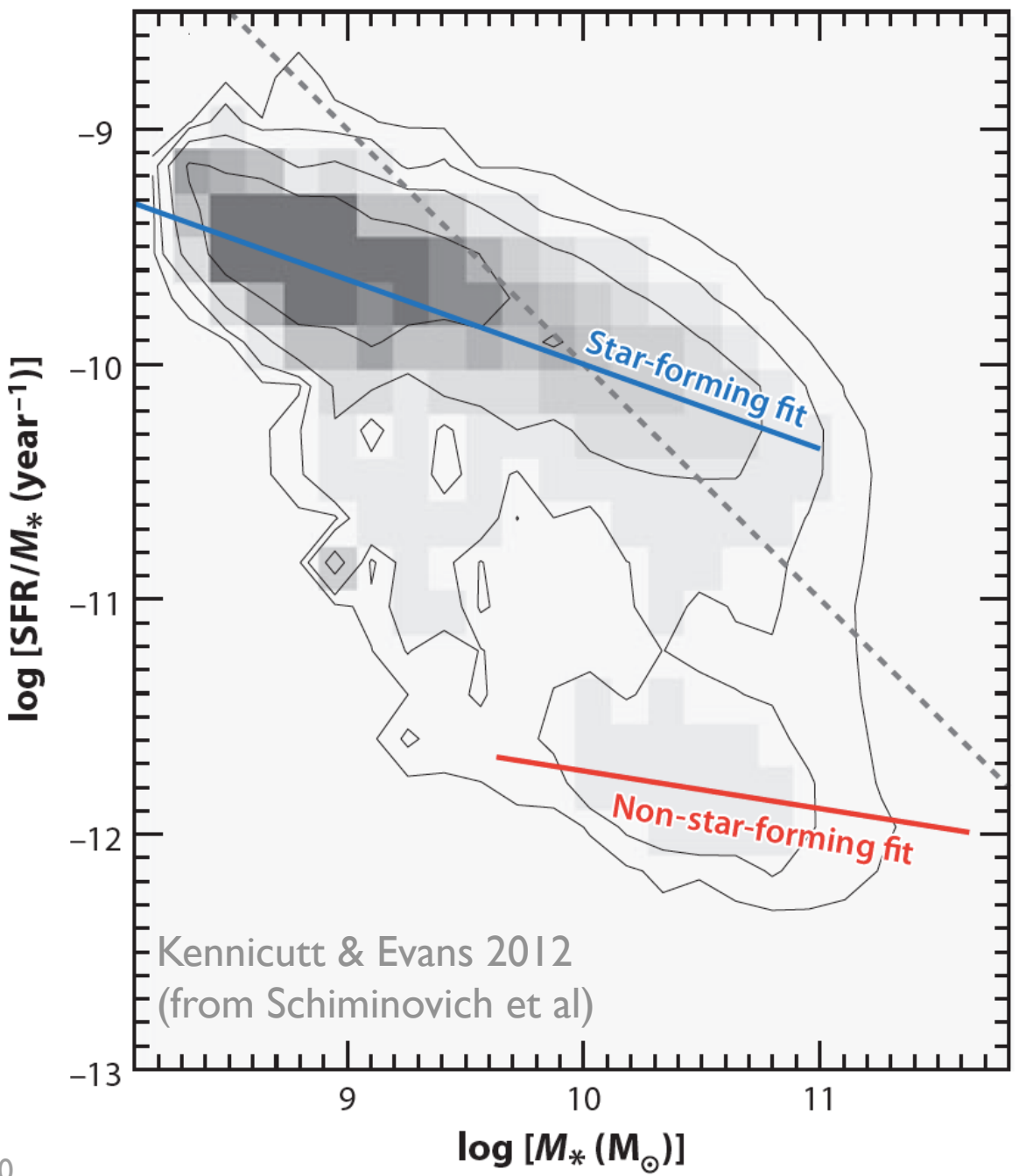
“Red” and “Blue”

Blue SF sequence

“Green Valley”

Red sequence

## 2. sSFR shows two sequences



“Star Forming”  
“Star Forming Main Sequence” 😱

“Quiescent”  
“Passive”  
“Passively evolving”  
“Quenched”

## 2. Related def'n of sSFR

Scalo Birthrate Parameter:  
Ratio of Current to Past SFR

$$b = \text{SFR}_{\text{now}} / \langle \text{SFR} \rangle$$

$b < 1$ : SFR greater in the past

$b = 1$ : SFR  $\sim$  constant

$b > 1$ : SFR higher today than in past

$b > 2-3$ : Classified as Starburst

Note:  $b$  alone does not distinguish between a steady increase in SF to the present day, or an episodic burst

# Measuring the Birthrate Parameter

$$b = \text{SFR}_{\text{now}} / \langle \text{SFR} \rangle$$

Use any SF indicator

Proportional to the total mass in stars  
 $(\sim M_{\text{star}}/t_{\text{universe}})$

Will correlate with lots of measures, like:

- $L_{\text{FIR}}/L_{\text{NIR}}$
- $\text{SFR}/M_{\text{star}}$
- H $\alpha$  Equivalent Width

## 2. Specific SFR: Lower mass galaxies have systematically higher sSFR's

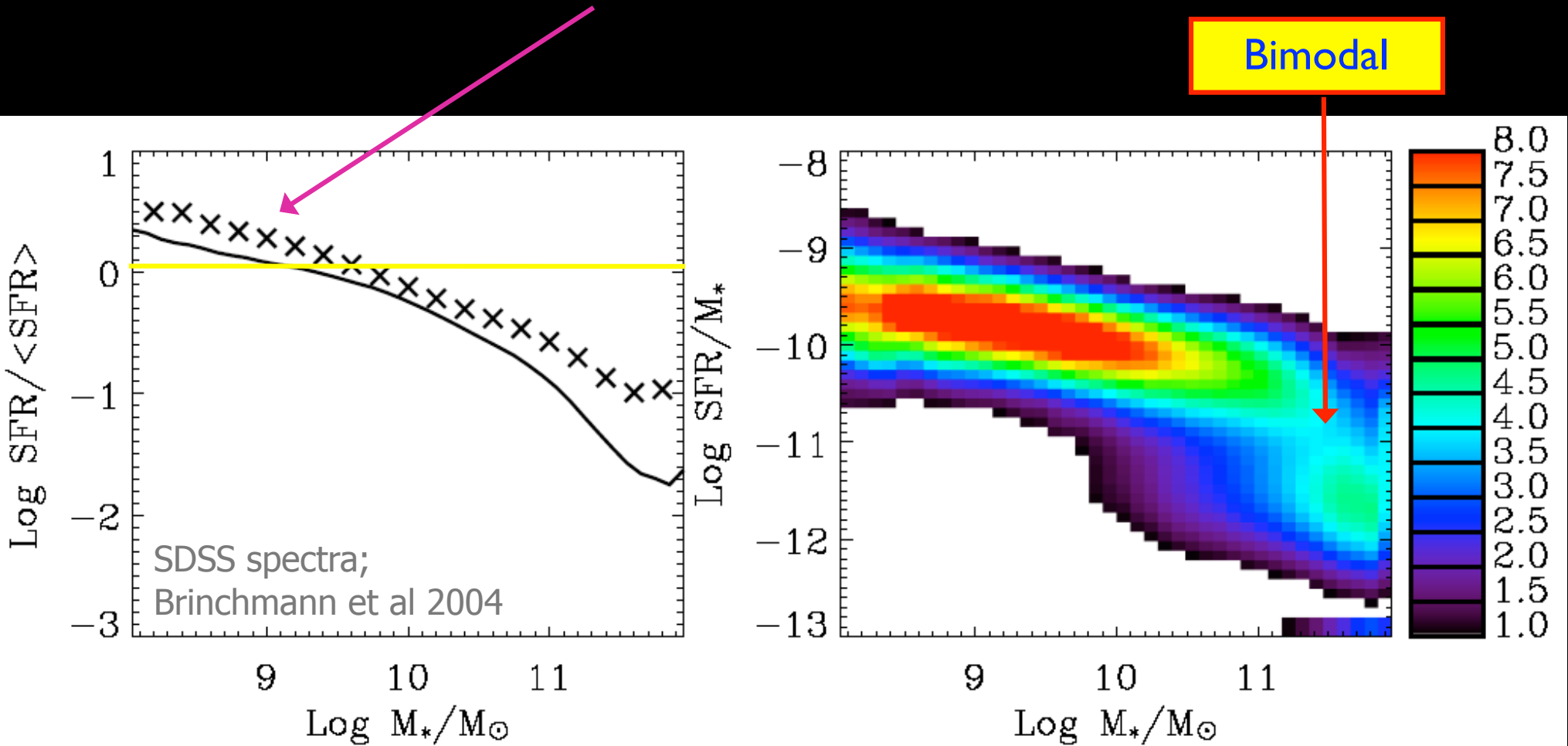


**Figure 24.** Similar to Figure 23 but this time showing  $b$  as a function of the stellar mass.

**Figure 23.** The specific SFR as a function of concentration. The left panel contrasts  $b^g$  with  $b^V$ . The continuous line in this plot shows the median of the unweighted  $b^g$  (right panel) and the crosses show  $b^V$  calculated from the data in Figure 20. The right hand panel shows the (log of the) observed likelihood distribution of  $r\text{SFR}$  with respect to the concentration parameter,  $R_{90}/R_{50}$ , calculated as described in the text. The shading shows the conditional likelihood distribution (volume corrected) given a value for  $R_{90}/R_{50}$ . The contributions to the likelihood distributions below the plotted range have been put in the two lowest bins in  $r\text{SFR}$ .

# 2. Specific SFR:Warning. H $\alpha$ can be stochastic in low mass galaxies

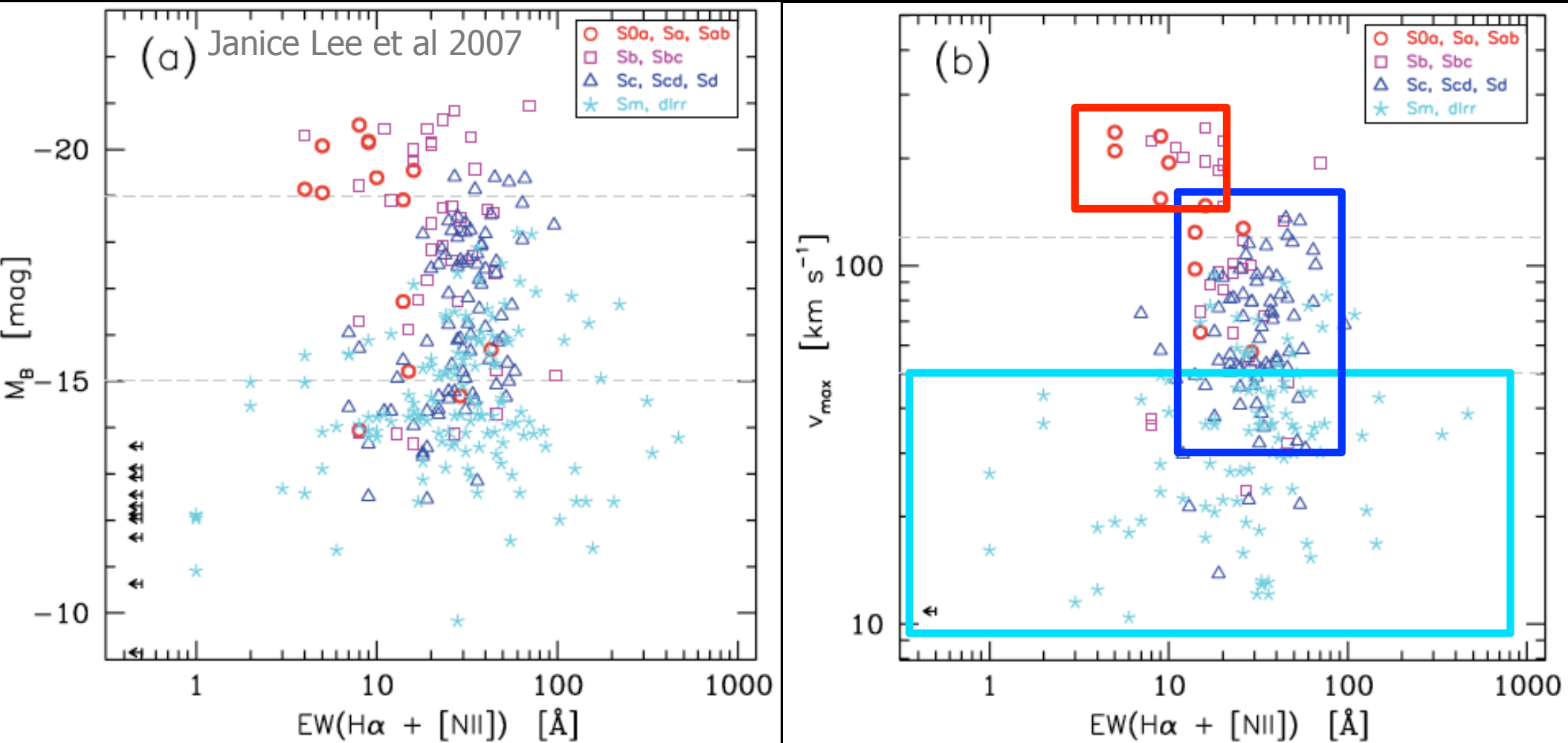
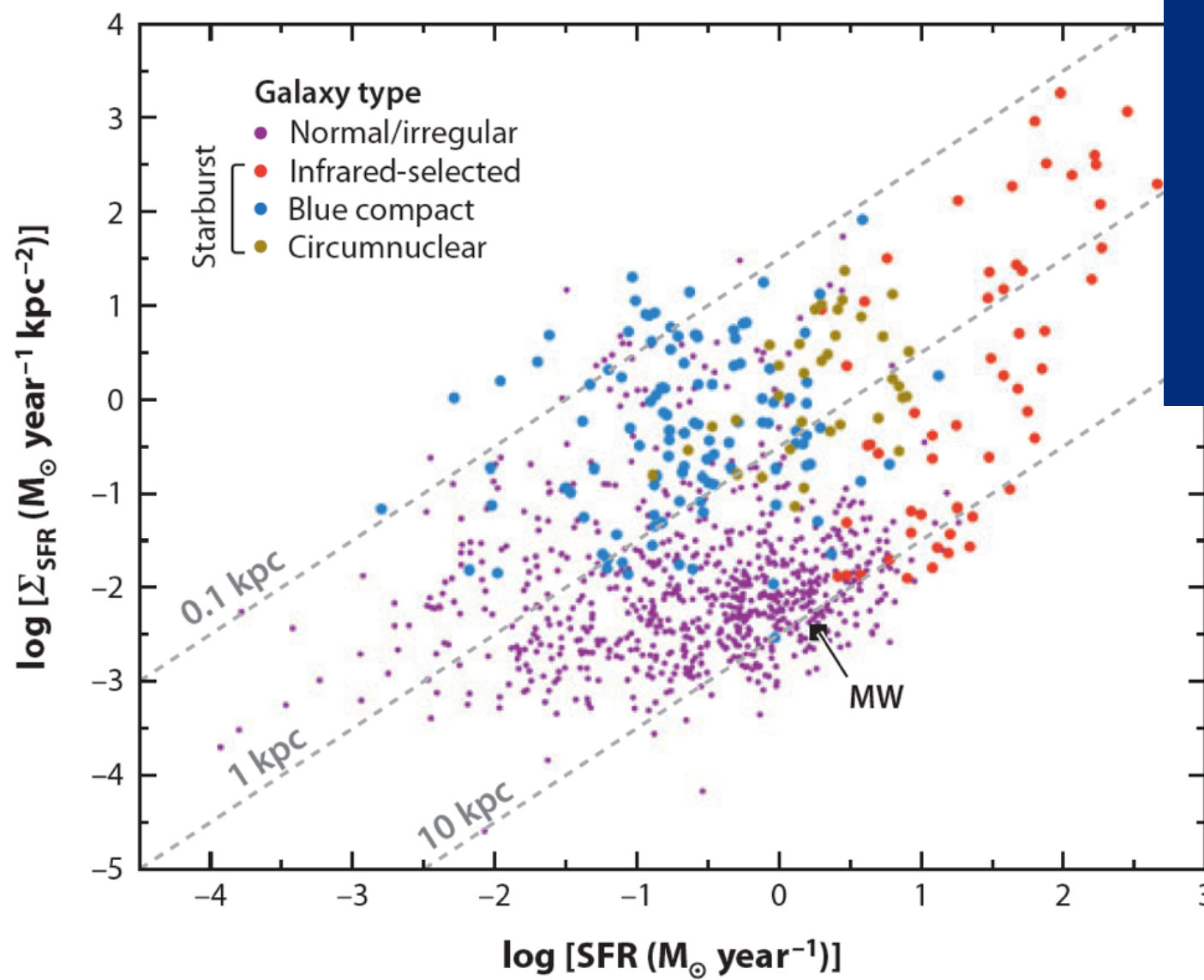


FIG. 1.—The Local Volume star-forming galaxy sequence in the (a)  $M_B$ -EW and the (b) rotational velocity-EW planes. Galaxies in the core sample of 11HUGS (i.e., those with  $T \geq 0$ ,  $D < 11$  Mpc, and  $|b| > 20^\circ$ ) are shown. Gray dashed lines are drawn at  $M_B = -19$  and  $V_{\max} = 120 \text{ km s}^{-1}$ , and  $M_B = -15$  and  $V_{\max} = 50 \text{ km s}^{-1}$  to indicate the two transition regions discussed in the text.

### 3. Star formation rate intensity ( $\Sigma_{\text{SFR}}$ )



SFR Intensity:  
star formation  
rate per unit  
area

Best proxy for local physical conditions,  
particularly in disks

# 4: SFR Efficiency: $SFR / M_{\text{gas}}$

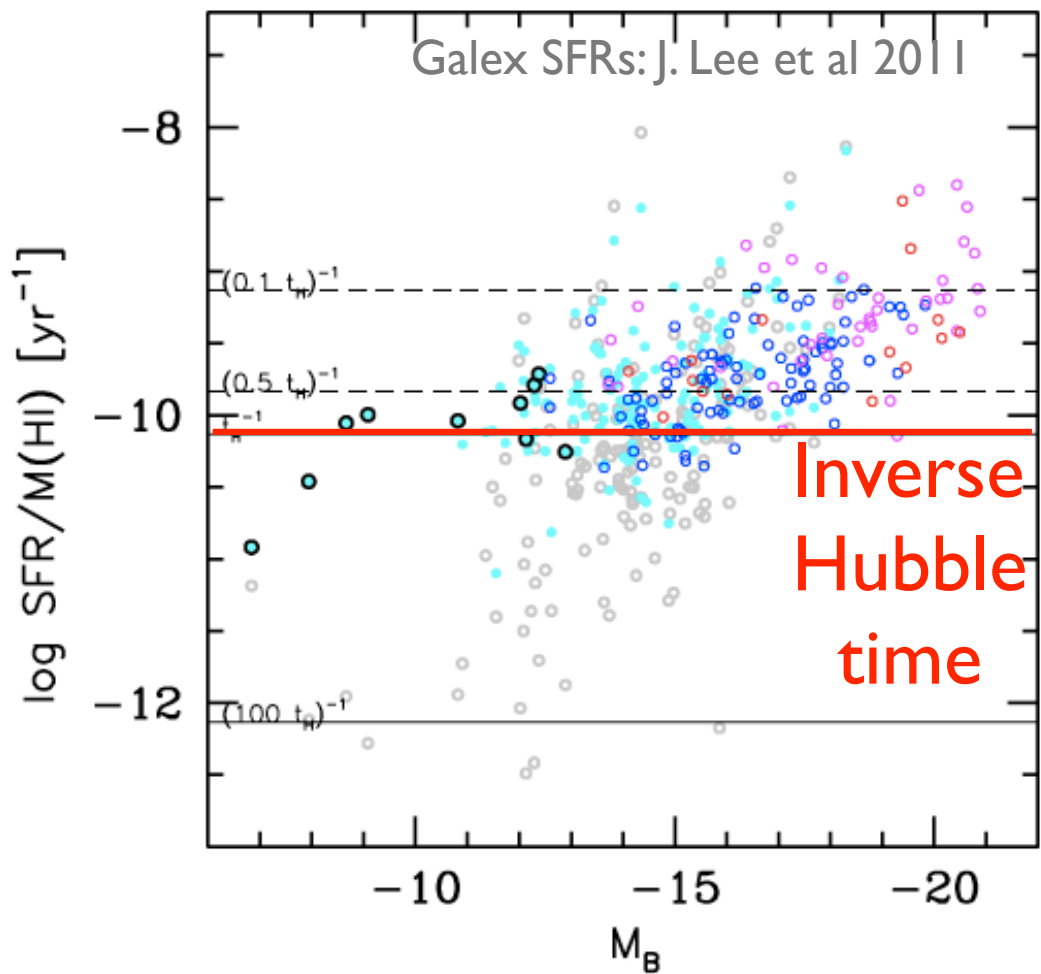
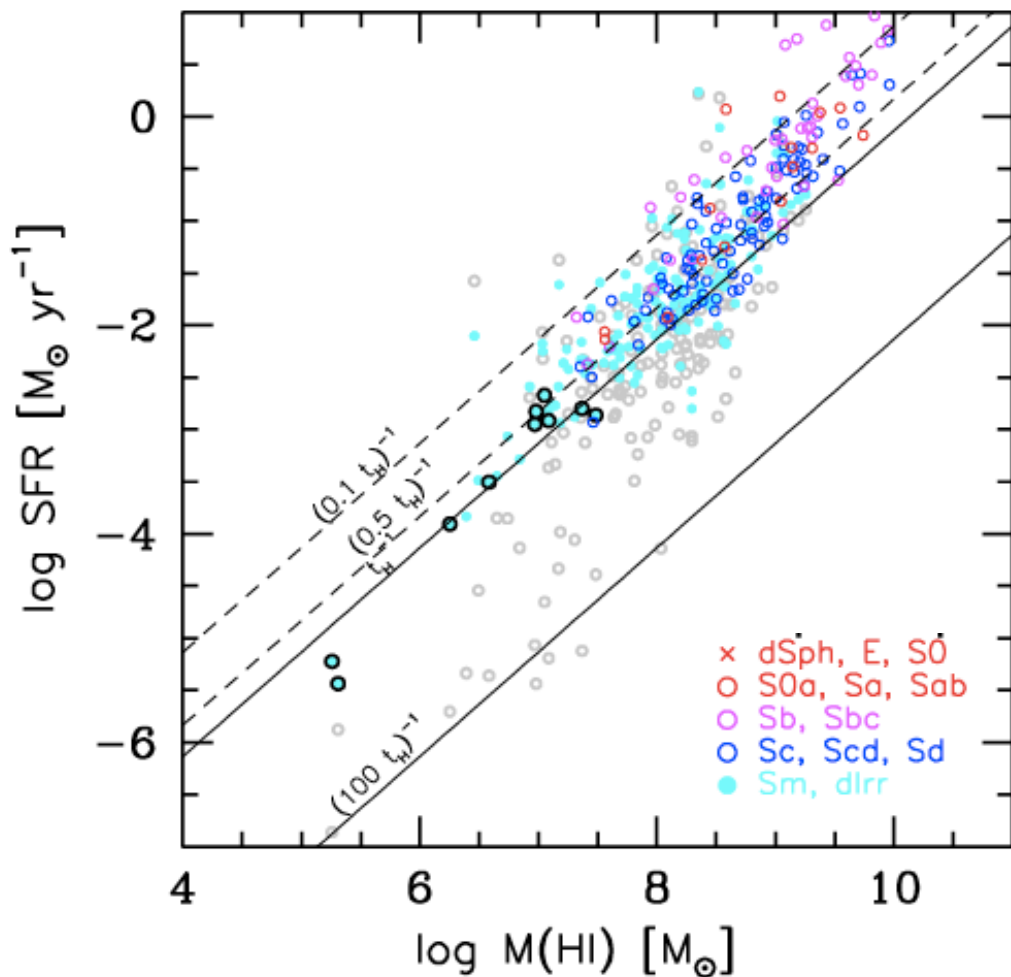


Figure 4. Comparison between star formation efficiencies, as measured by the SFR per unit H<sub>I</sub> mass, when the FUV emission (colored symbols) is used as the star formation tracer, instead of H $\alpha$  (gray symbols). Different symbols and colors are used to distinguish between morphological types as in Figure 3. Only galaxies that have both FUV and H $\alpha$  measurements are shown. Best-effort attenuation corrections are applied before computing the SFR as in Lee et al. (2009b).

Measure of timescale to consume all gas  
(Inverse = “gas consumption timescale”)

# 4. SFR Efficiency: SFR / $M_{\text{gas}}$

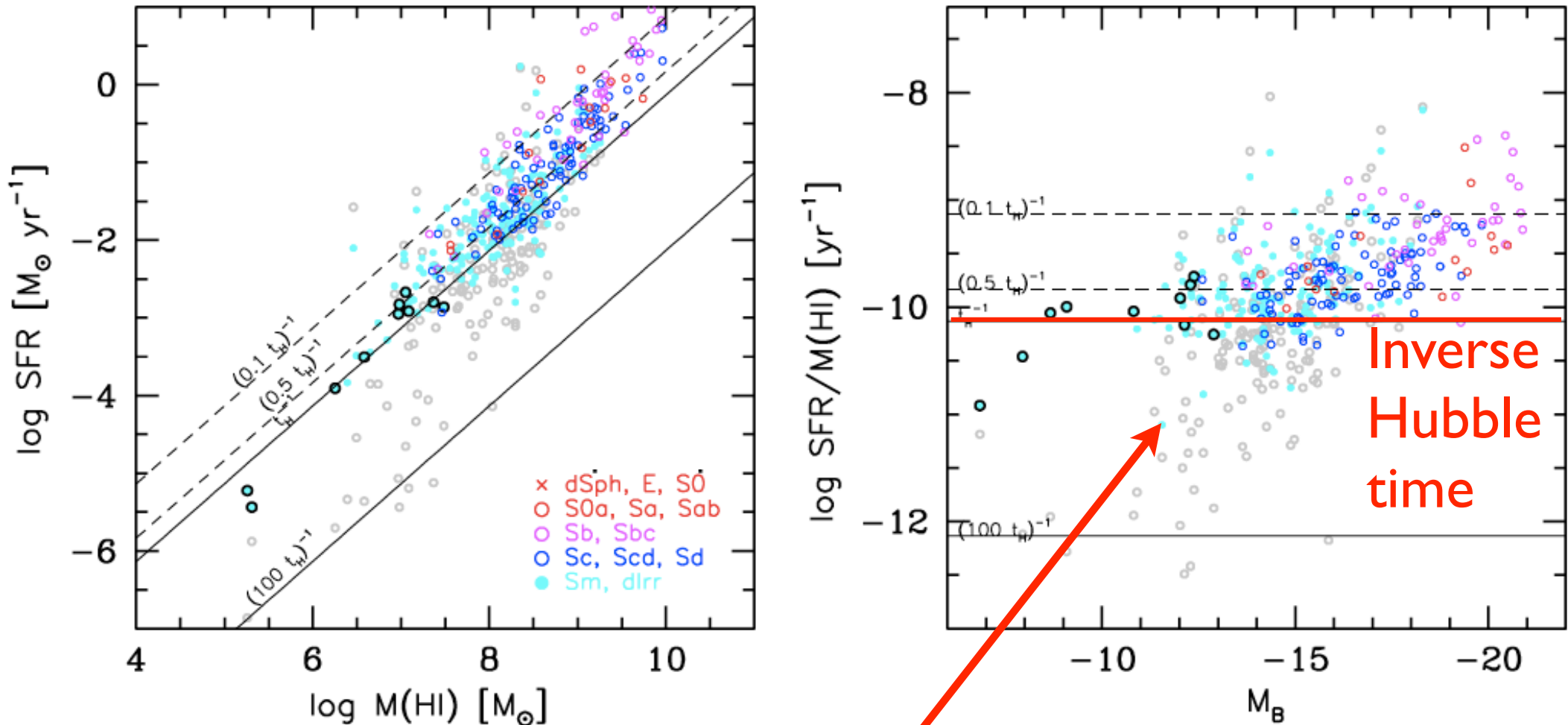


Figure 4. Comparison between star formation efficiencies, as measured by the SFR per unit HI mass, when the FUV emission (colored symbols) is used as the star formation tracer, instead of  $H\alpha$  (gray symbols). Different symbols and colors are used to distinguish between morphological types as in Figure 3. Only galaxies that have both FUV and  $H\alpha$  measurements are shown. Best-effort attenuation corrections are applied before computing the SFR as in Lee et al. (2009b).

- dIrrs would take close to a Hubble time to consume their gas
- Higher mass galaxies close to finished, if not resupplied

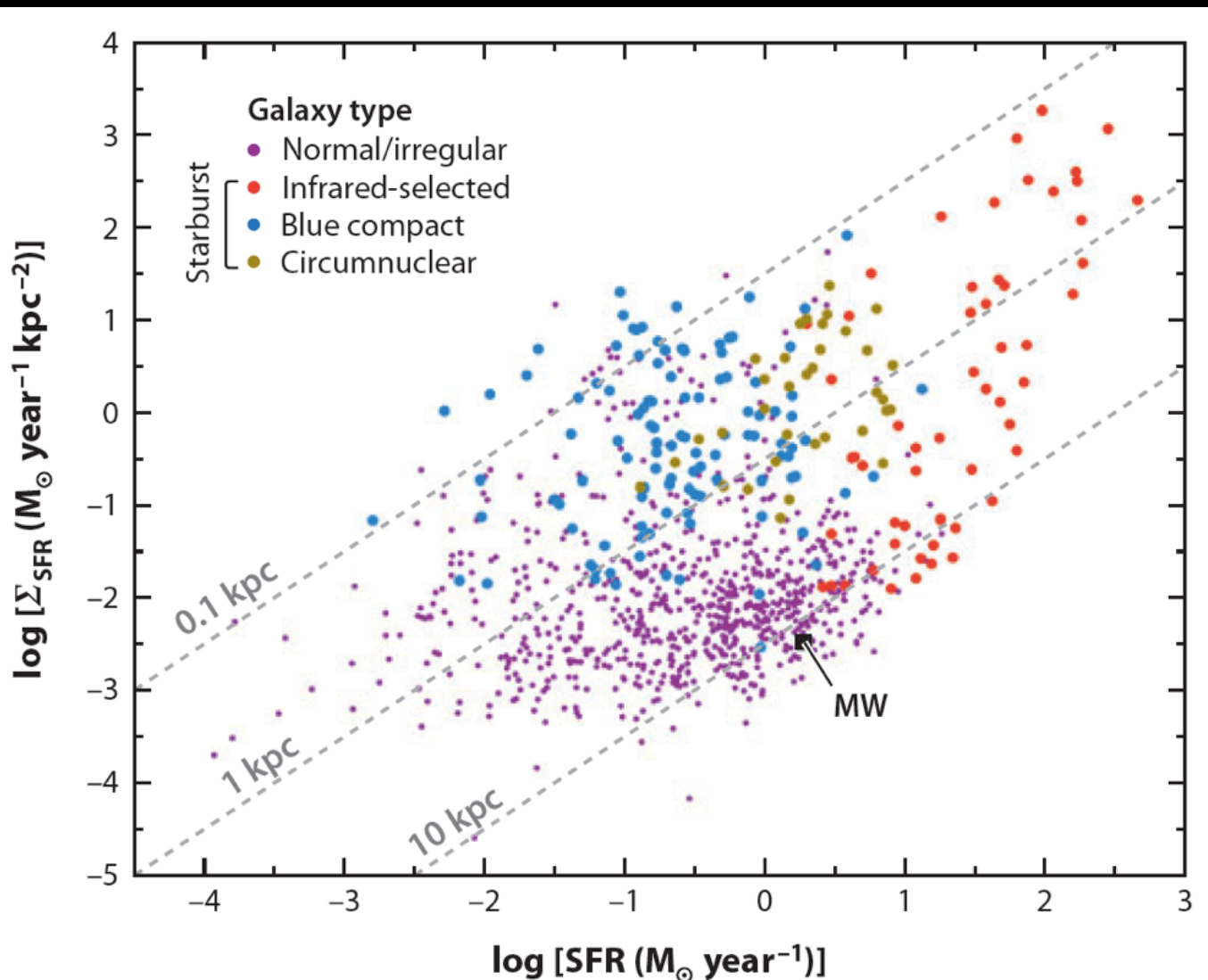
# Systems with High Star Formation

1. Useful as probes of extreme conditions
2. Important phases in build-up of stars

# High in what way?

- High Star formation rates (SFR)
- High Star Formation intensity ( $\Sigma_{\text{SFR}}$ )
- High Specific star formation rates (sSFR)

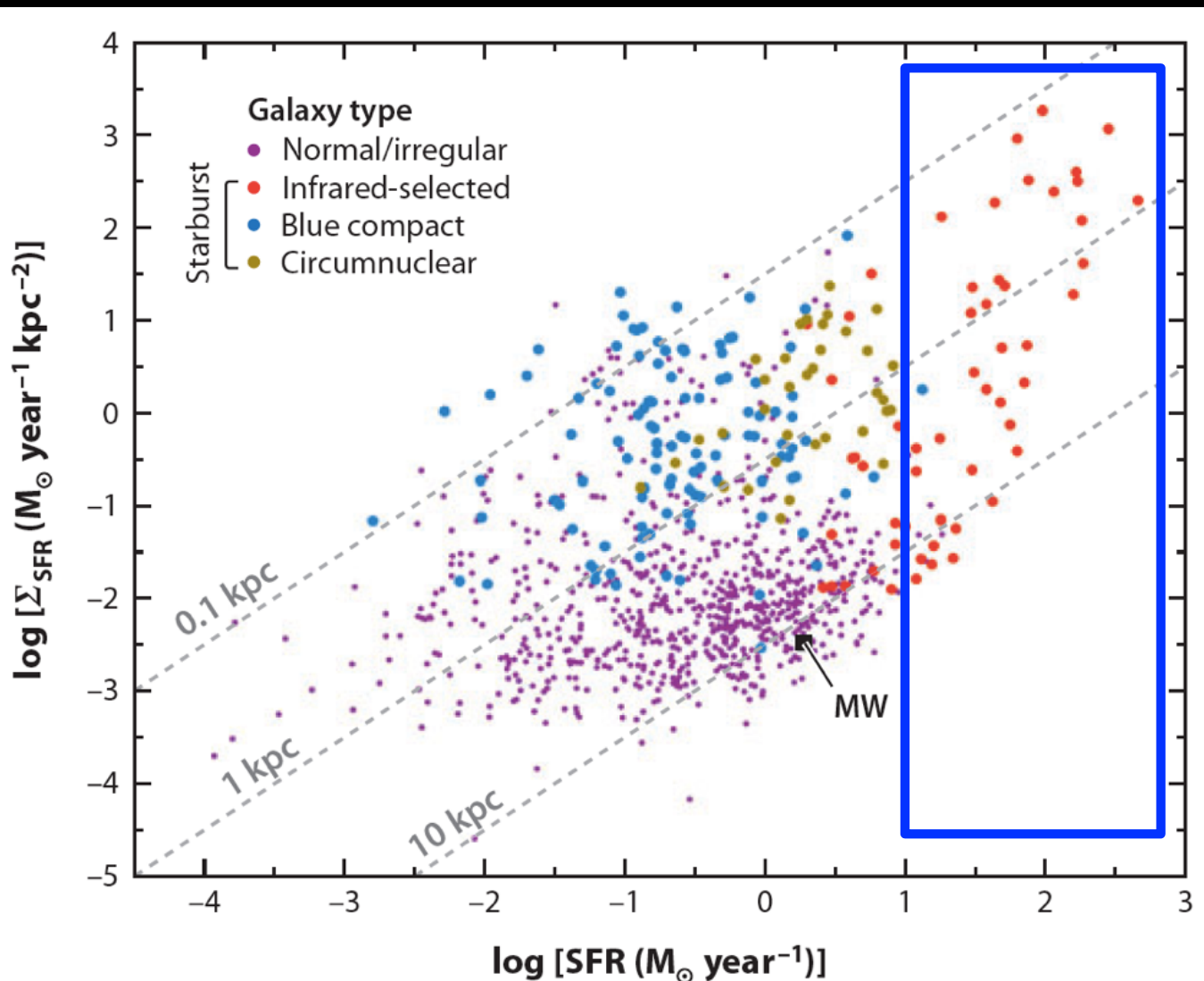
# The High SFR End



Possible Definitions of “High”

- High absolute SFRs
- High SFR intensities
- High SFRs compared to past average

# The High SFR End



Possible Definitions of “High”

- High absolute SFRs
- High SFR intensities
- High SFRs compared to past average

# “ULIRGS” (ultraluminous infrared galaxies) Highest SFRs (10-1000 M<sub>0</sub>/yr)

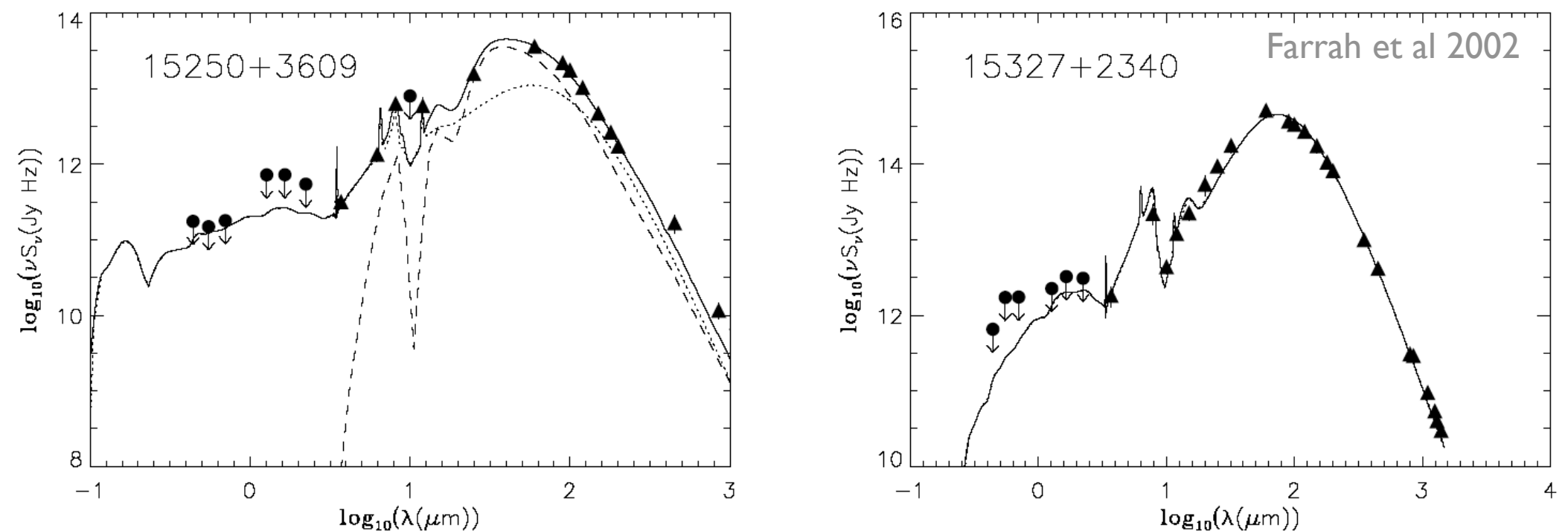
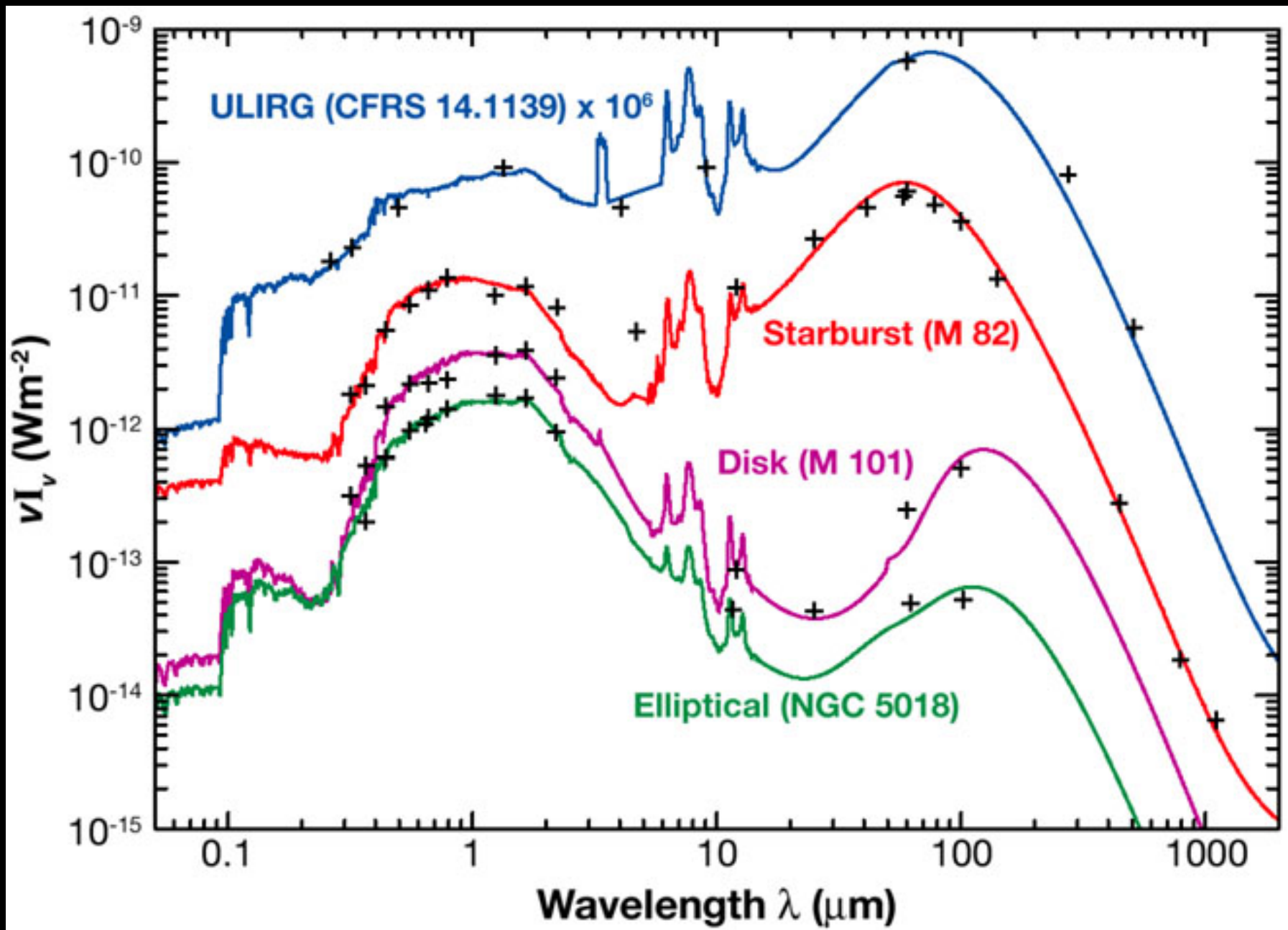


Figure 1. Best fit Spectral Energy Distributions for the 41 ULIRGs in our sample. In each case the solid line is the combined best-fit model, the dotted line is the Starburst component and the long dashed line is the AGN component.

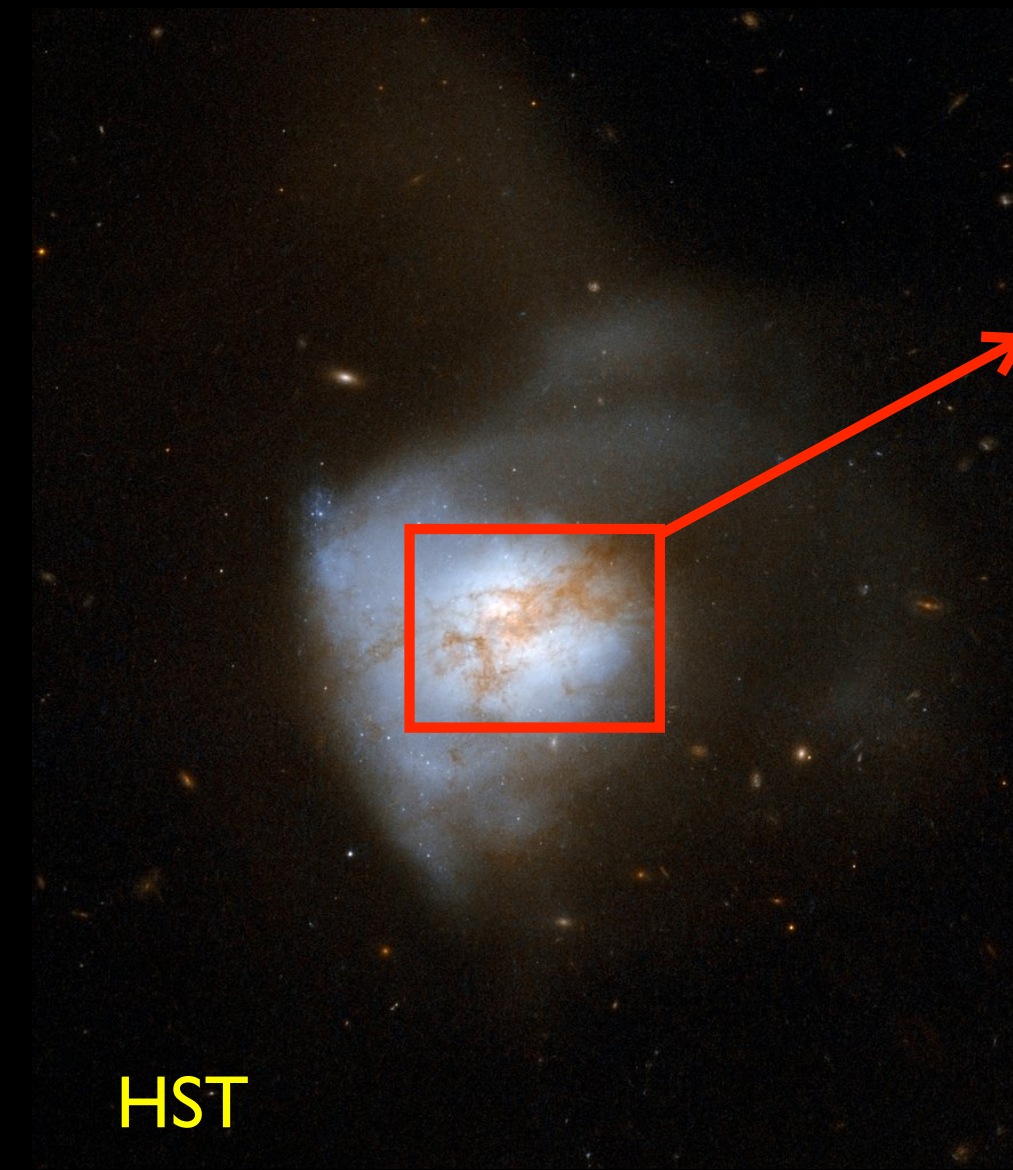
- Majority of their enormous luminosity is reprocessed to FIR.
- Can be inconspicuous in optical because highly obscured.

# ULIRGS vs normalish-galaxies

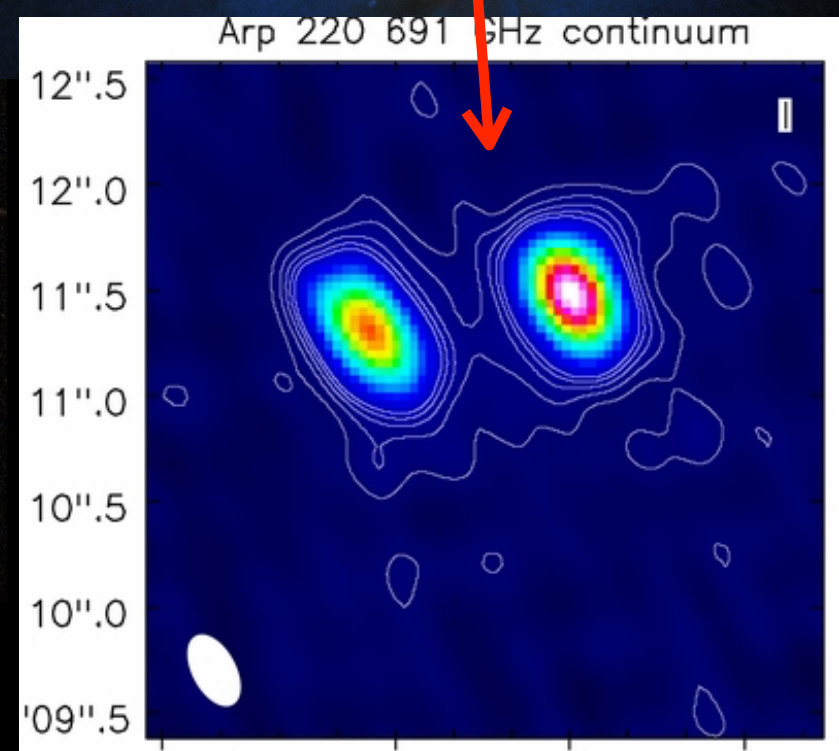


# Arp 220 is the local prototype

HST+ALMA Band 5 (2.6mm)



HST



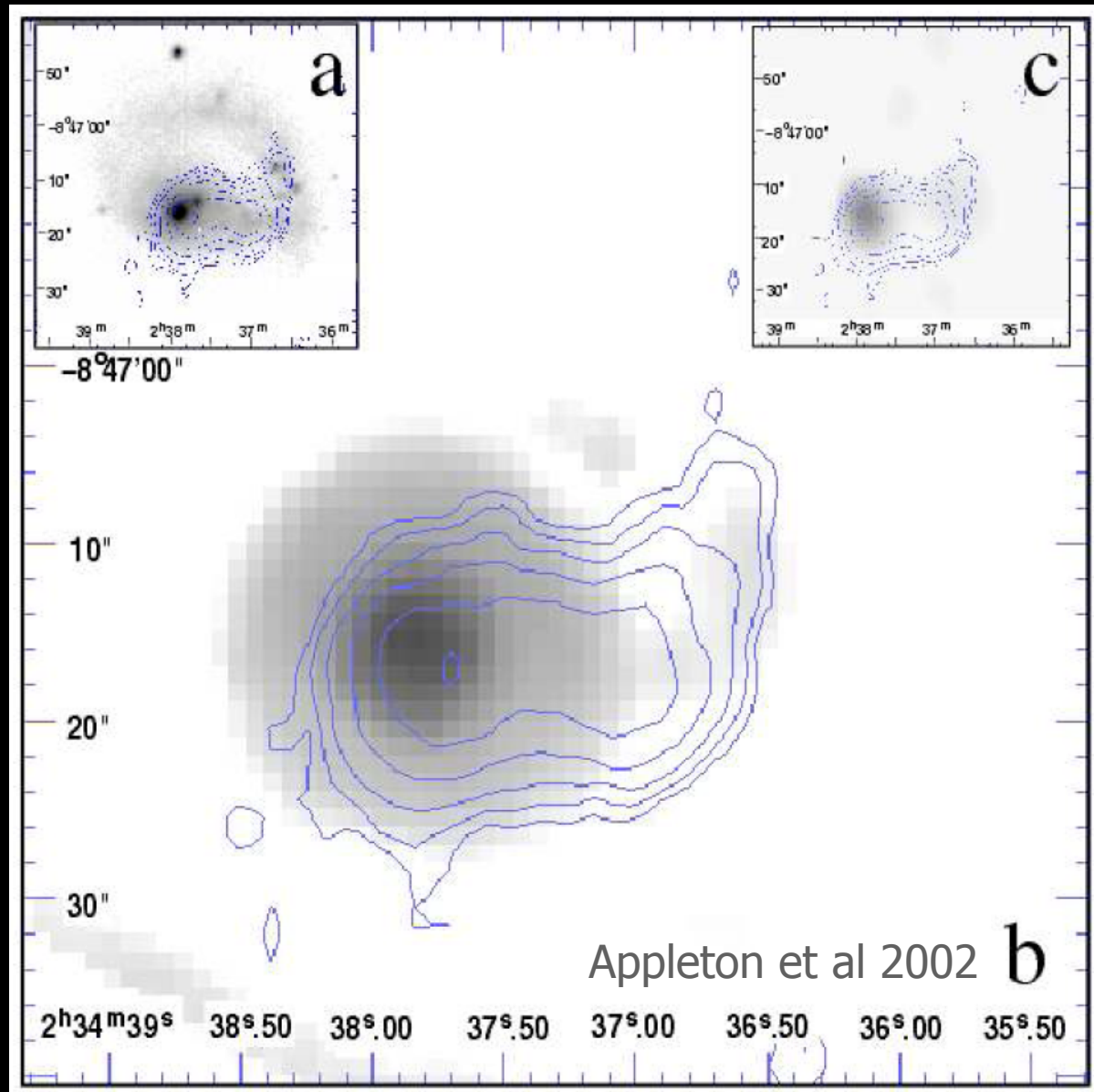
Wilson et al 2014

# ULIRGS are almost universally massive major mergers



- Probably good local analogs of the formation of ellipticals at high redshift.
- These rare systems may actually dominate the star formation rate locally (1 galaxy w/  $10^3 M/\text{yr} = 10^3$  galaxies w/  $1 M/\text{yr}$ )

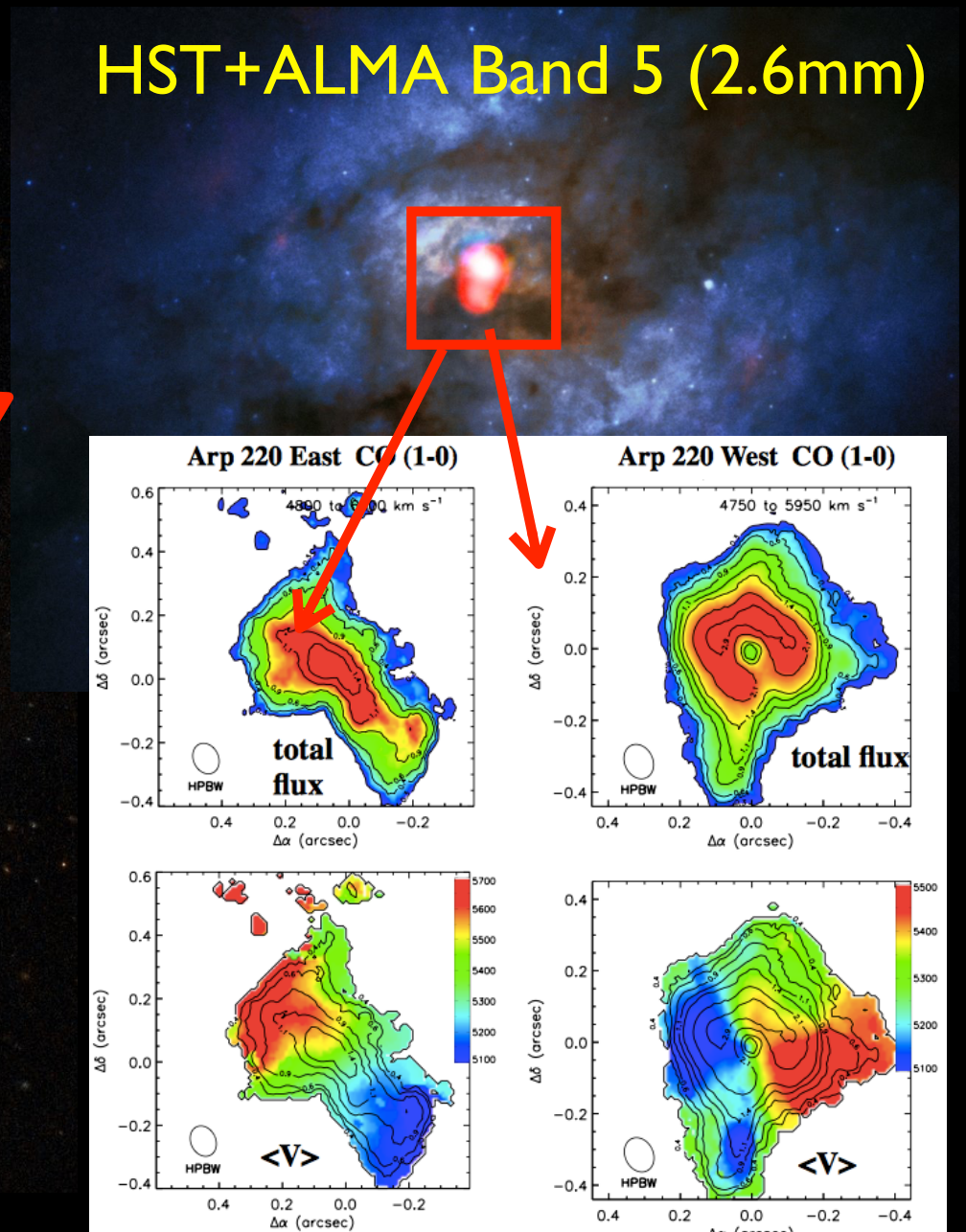
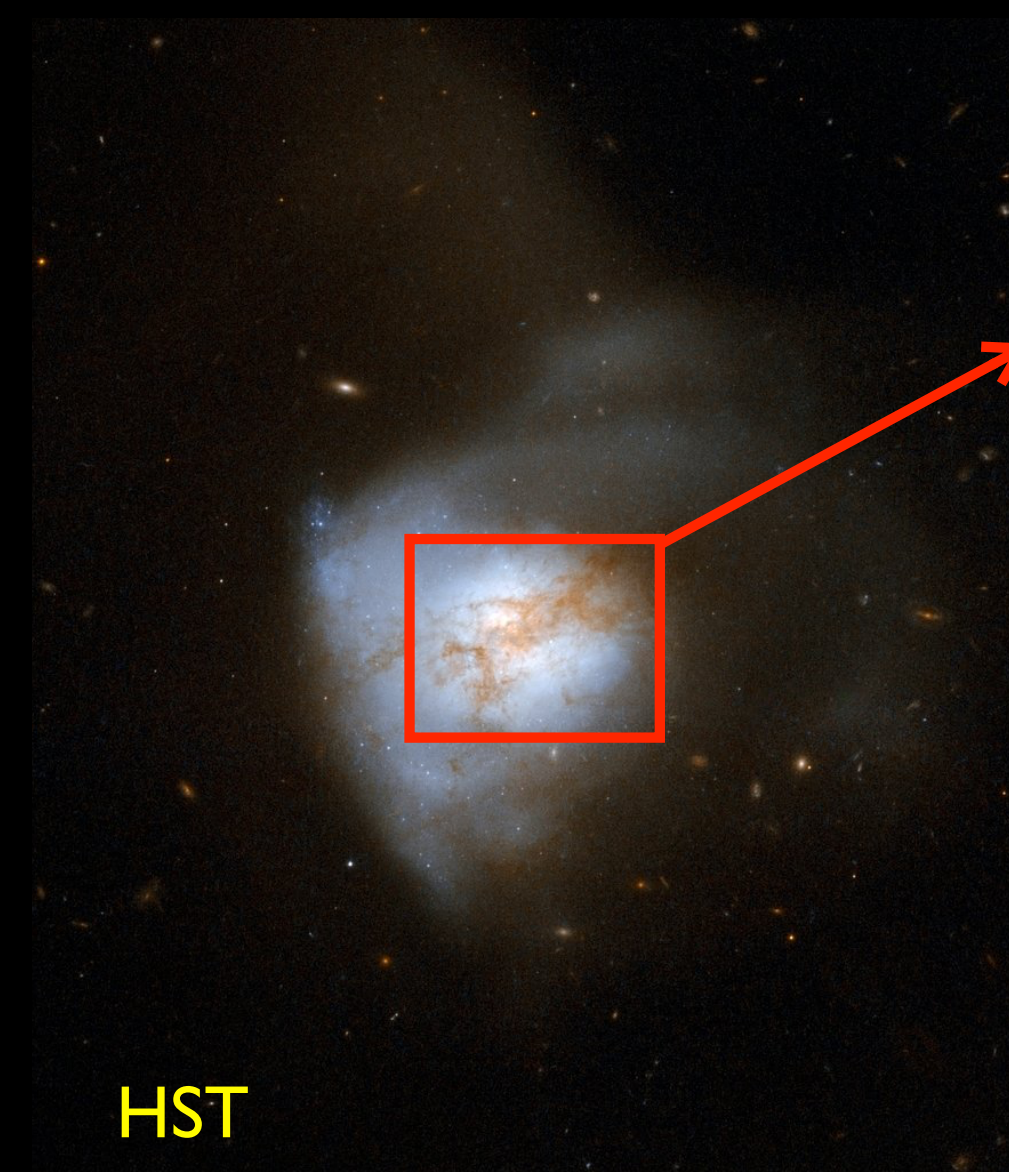
# ULIRGs have extremely high gas surface densities ( $10^2$ - $10^5$ $M_\odot/\text{pc}^2$ within $R < 0.1$ - $1$ kpc)



- Equivalent to a galaxy's whole ISM funnelled into the center.
- Possibly associated with AGN activity (lots of gas dumping onto central BH)
- SFR is near maximum possible ( $\text{SFR}_{\text{max}} \sim M_{\text{gas}} / t_{\text{dyn}}$ )

FIG. 5.— a) The integrated  $^{12}\text{CO}(1-0)$  emission in contours, over the optical R-band image of NGC 985. The contour levels are 4.0, 5.2, 6.8, 8.8, 11.5 and 15.0  $\text{Jy beam}^{-1} \text{km s}^{-1}$ . b) Same as in a) but the background is the 15  $\mu\text{m}$  image of the galaxy. c) Same as in a) but the background is the 3.5 cm (X-band) radio continuum map.

# Resolved in CO w/ ALMA: $10^{26}$ H<sub>2</sub> cm<sup>-2</sup>



$>10^9 M_\odot$  in  $<100$  pc

### (c) Interaction/"Merger"



- now within one halo, galaxies interact & lose angular momentum
- SFR starts to increase
- stellar winds dominate feedback
- rarely excite QSOs (only special orbits)

### (b) "Small Group"



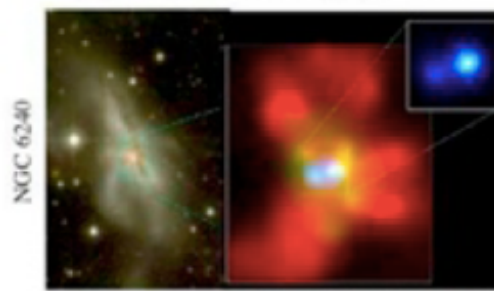
- halo accretes similar-mass companion(s)
- can occur over a wide mass range
- $M_{halo}$  still similar to before: dynamical friction merges the subhalos efficiently

### (a) Isolated Disk



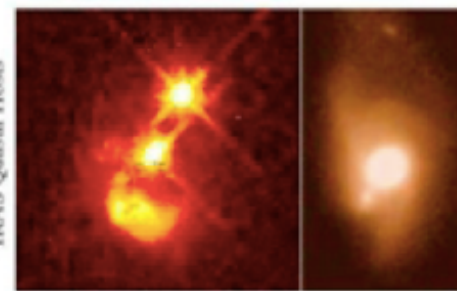
- halo & disk grow, most stars formed
- secular growth builds bars & pseudobulges
- "Seyfert" fueling (AGN with  $M_{*} > -23$ )
- cannot redden to the red sequence

### (d) Coalescence/(U)LIRG



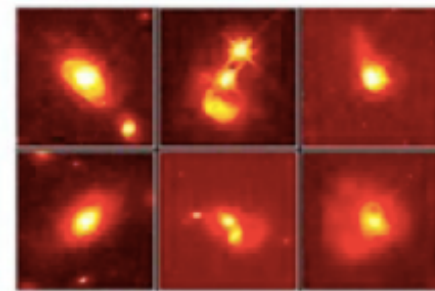
- galaxies coalesce: violent relaxation in core
- gas inflows to center: starburst & buried (X-ray) AGN
- starburst dominates luminosity/feedback, but, total stellar mass formed is small

### (e) "Blowout"



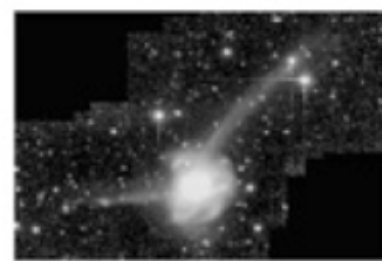
- BH grows rapidly: briefly dominates luminosity/feedback
- remaining dust/gas expelled
- get reddened (but not Type II) QSO: recent/ongoing SF in host; high Eddington ratios
- merger signatures still visible

### (f) Quasar



- dust removed: now a "traditional" QSO
- host morphology difficult to observe: tidal features fade rapidly
- characteristically blue/young spheroid

### (g) Decay/K+A



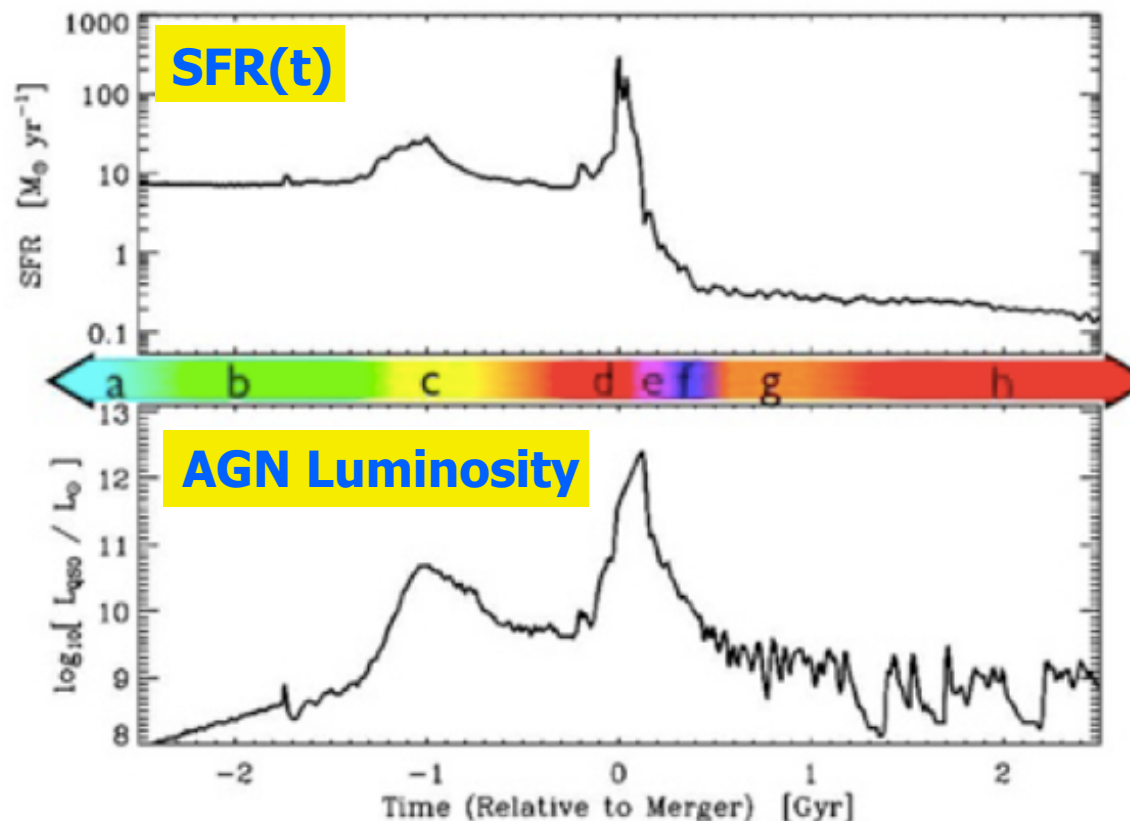
- QSO luminosity fades rapidly
- tidal features visible only with very deep observations
- remnant reddens rapidly (E+A/K+A)
- "hot halo" from feedback
- sets up quasi-static cooling

### (h) "Dead" Elliptical

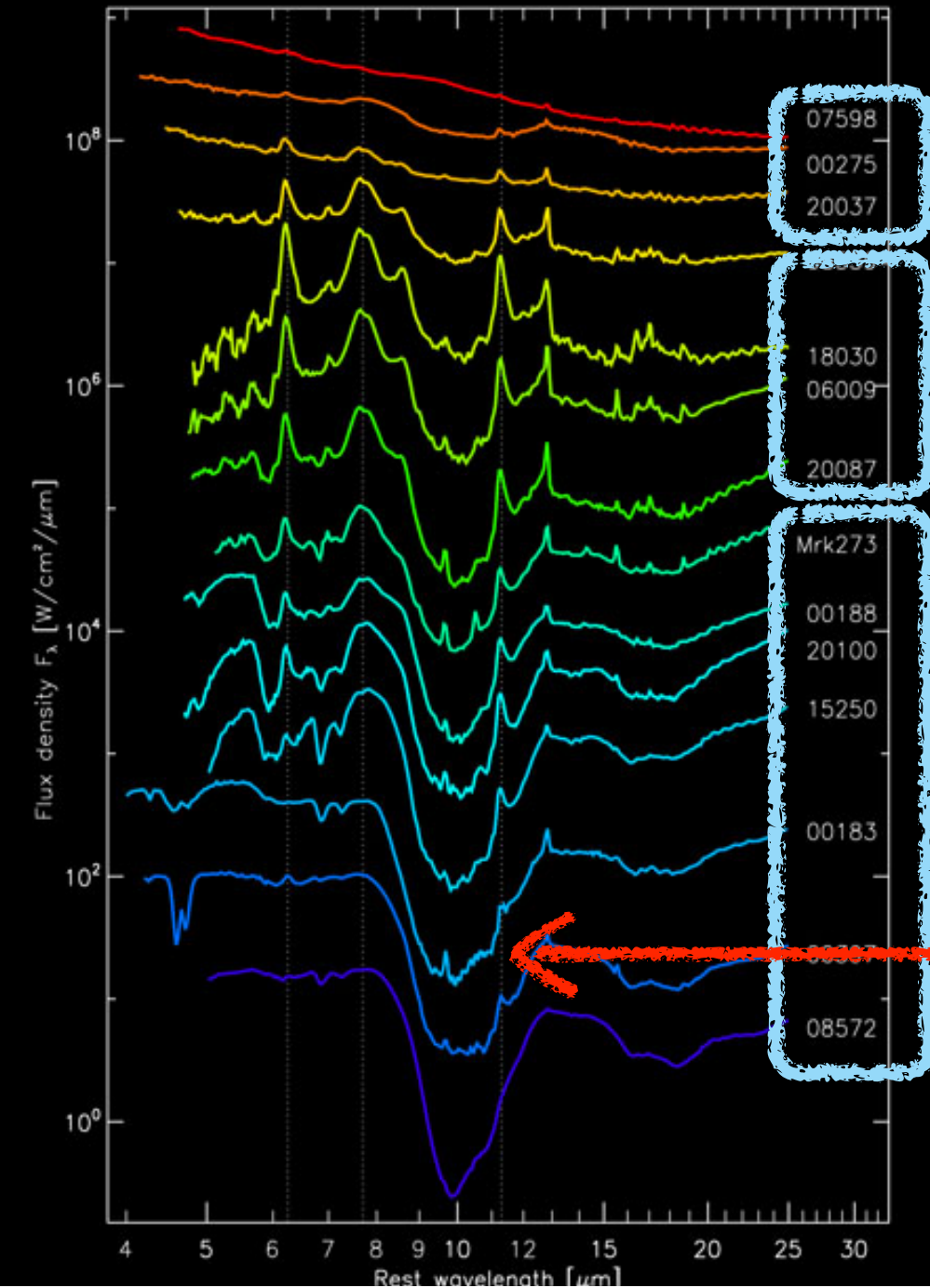


- star formation terminated
- large BH/spheroid - efficient feedback
- halo grows to "large group" scales: mergers become inefficient
- growth by "dry" mergers

Simulation w/ AGN Feedback: Hopkins et al



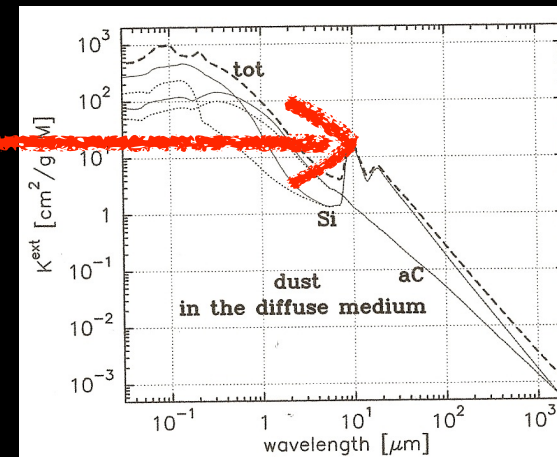
# Separating ULIRGs from AGN



AGN Dominated  
(no PAHs)

Starburst Dominated

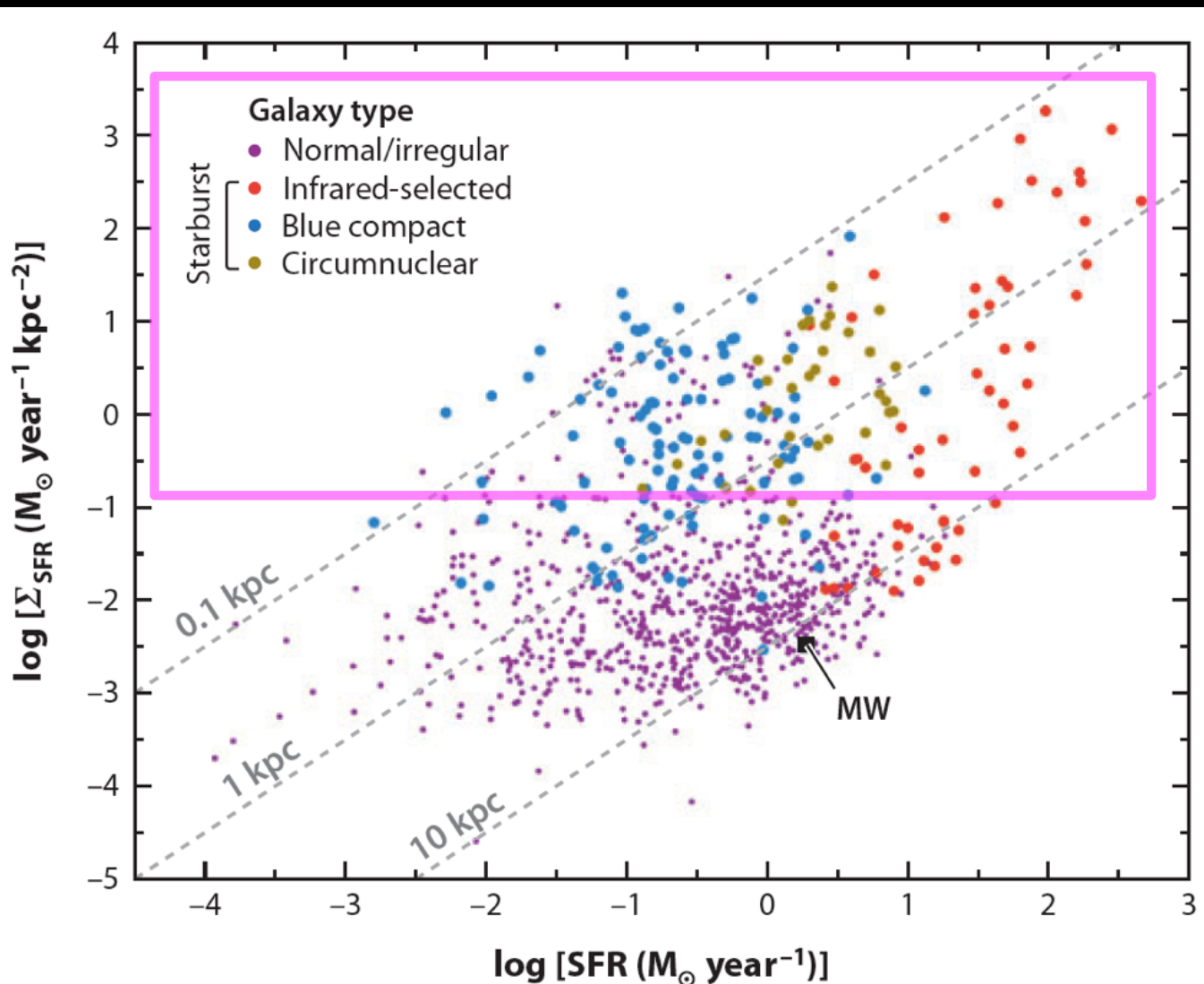
“Buried” nuclei (high  
 $A_\lambda$  even in mid-IR)



Silicate  
Features

# The High SFR End

Possible Definitions of “High”



- High absolute SFRs
- High SFR intensities
- High SFRs compared to past average

# Blue Compact Dwarfs (BCDs)

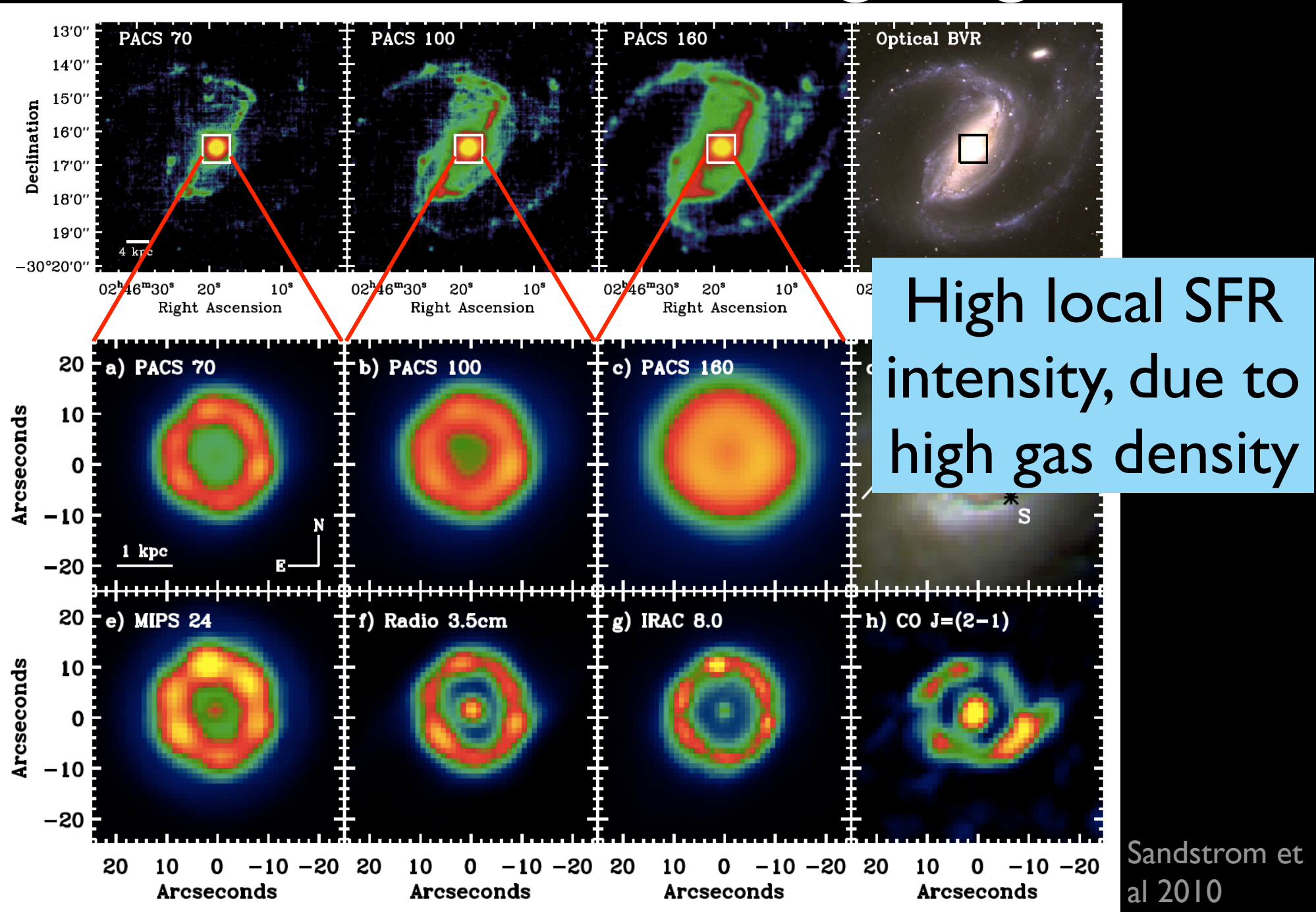


I Zw 18

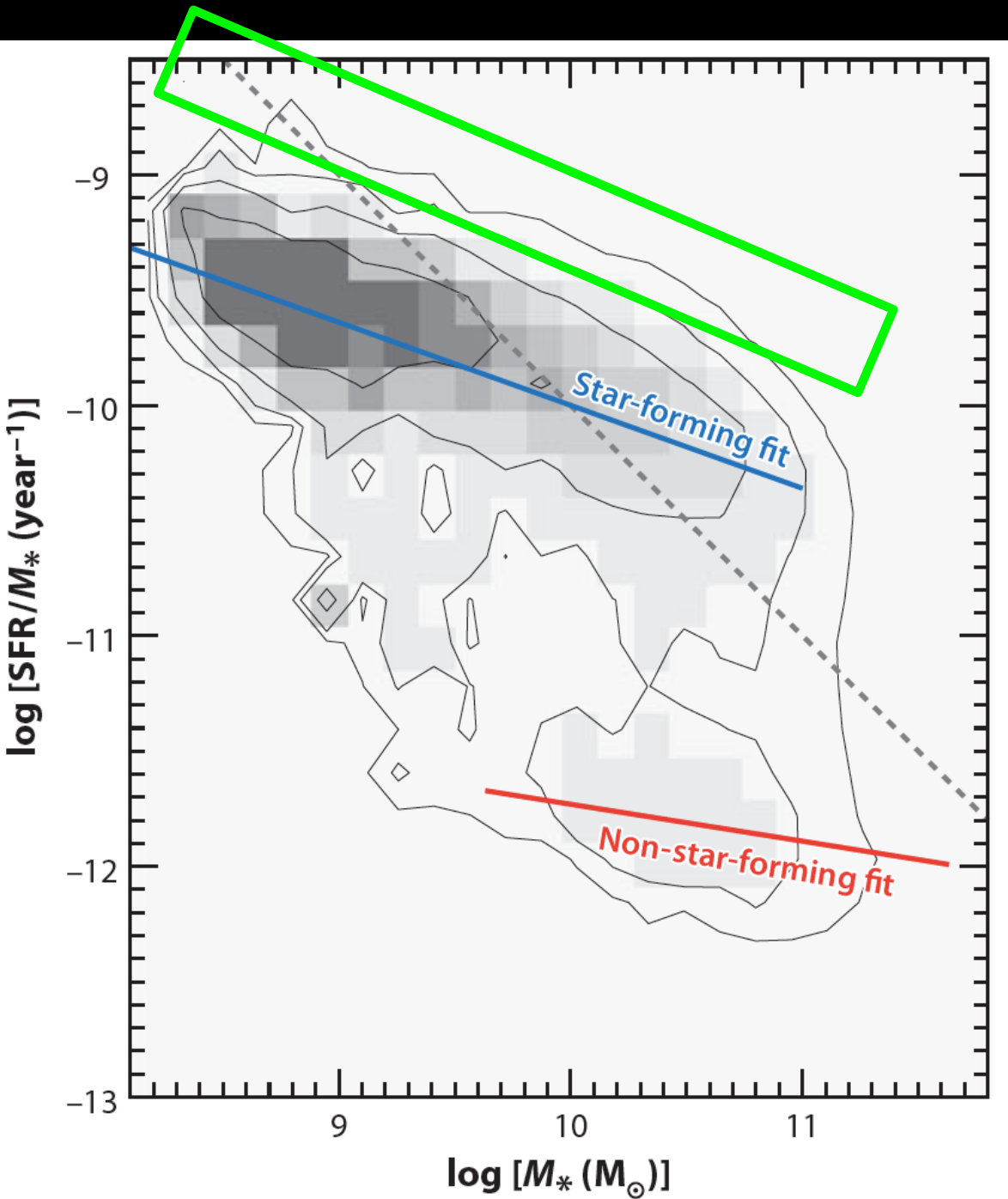
- Very high SFR intensity
- Very low mass
- Among lowest metallicity galaxies known

Well represented  
in Zwicky catalog,  
Markarian catalog

# Nuclear Star Forming Regions



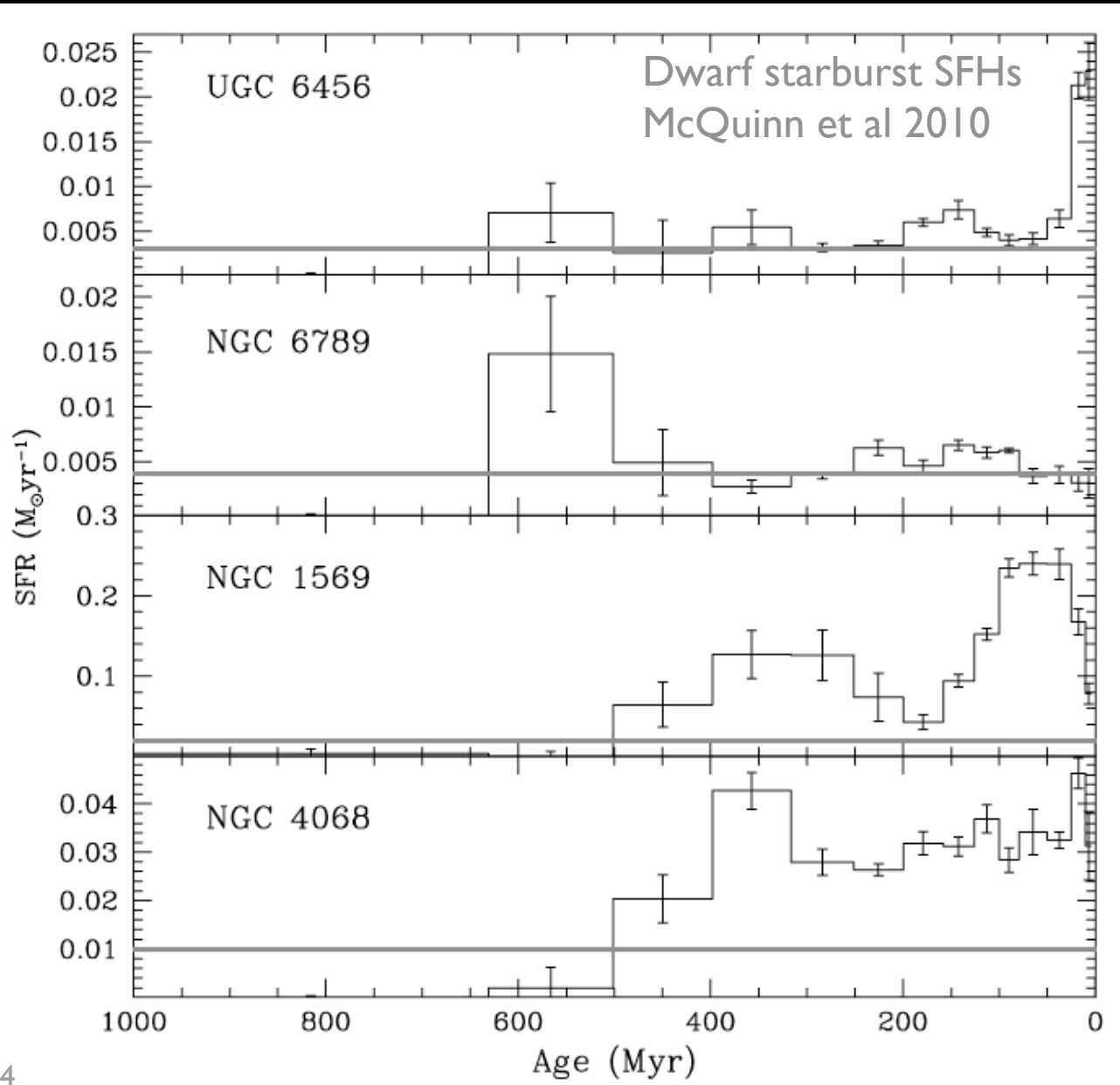
# The High SFR End



Possible  
Definitions of  
“High”

- High absolute SFRs
- High SFR intensities
- High SFRs compared to past average

# Starbursts: Usually defined as >2-3 times past average SFR



Possible  
Triggers?

- Interactions?
- Gas accretion?